NASA CONTRACTOR REPORT

NASA CR-2402

NASA CR-2402

TM SURFACE WAVE DIFFRACTION BY A TRUNCATED DIELECTRIC SLAB RECESSED IN A PERFECTLY CONDUCTING SURFACE

by P. H. Pathak and R. G. Kouyoumjian

Prepared by
THE OHIO STATE UNIVERSITY
ELECTROSCIENCE LABORATORY
Columbus, Ohio 43212
for Langley Research Center

NATIONAL AERONAUTICS AND SPACE ADMINISTRATION • WASHINGTON, D. C. • MAY 1974

1. Report No. NASA CR-2402	2. Government Accession No.	3. Recipient's Catalog No.
4. Title and Subtitle TM SURFACE WAVE DIFFRACTION BY A TRUNCATED DIELECTRIC SLAB RECESSED IN A PERFECTLY CONDUCTING SURFACE		5. Report Date May 1974 6. Performing Organization Code
7. Author(s) P. H. Pathak and R. G. Kouyoumjian		8. Performing Organization Report No. TR 3001-4
9. Performing Organization Name and Address The Ohio State University ElectroScience Laboratory Columbus, Ohio 43212		10. Work Unit No. 502-33-13-02 11. Contract or Grant No. NGR 36-008-144
12. Sponsoring Agency Name and Address National Aeronautics and Space Administration Washington, D.C. 20546		13. Type of Report and Period Covered Contractor Report 14. Sponsoring Agency Code

15. Supplementary Notes

The material contained in this report was also used as a dissertation submitted to the Department of Electrical Engineering, The Ohio State University as partial fulfillment for the degree Doctor of Philosophy. Topical Report

16. Abstract

The diffraction of a TM_0 surface wave by a terminated dielectric slab which is flush mounted in a perfectly-conducting surface is studied. The incident surface wave gives rise to waves reflected and diffracted by the termination; these reflected and diffracted fields may be expressed in terms of the geometrical theory of diffraction by introducing surface wave reflection and diffraction coefficients which are associated with the termination. In this investigation, the surface wave reflection and diffraction coefficients have been deduced from a formally exact solution to this canonical problem. The solution is obtained by a combination of the generalized scattering matrix technique and function theoretic methods. Expressions for the reflection and diffraction coefficients contain integrals which can be evaluated numerically. Calculated values for the TM_0 surface wave reflection and diffraction coefficients and presented, and compared with approximate values obtained from a surface reactance model and from a variational solution of the canonical problems; the accuracy and shortcomings of these approximations are discussed. The relevance of the results obtained here to the design of a phased array of slots radiating through a flush mounted dielectric cover, and to the design of surface wave antennas is discussed. It is noted that spacecraft antennas may consist of such dielectric covered slot arrays.

17. Key Words (Suggested by Author(s))	18. Distribution Statement
Antennas, Spacecraft and Aircraft Antennas Applied Electromagnetic Theory	Unclassified - Unlimited STAR Category 09

19. Security Classif. (of this report)	20. Security Classif. (of this page)	21. No. of Pages	22. Price*
Unclassified	Unclassified	128	$4.75

*For sale by the National Technical Information Service, Springfield, Virginia 22151

Page Intentionally Left Blank

CONTENTS

LIST OF TABLES

LIST OF ILLUSTRATIONS

Page Intentionally Left Blank

CHAPTER I
INTRODUCTION

Flush mounted antennas for the space shuttle vehicle will generally consist of dielectric covered slots in a metallic surface where the dielectric cover is employed as a protective heat shield for the re-usable space vehicle. A typical local antenna geometry is illustrated in Fig. 1 where the truncated dielectric cover is shown recessed and flush mounted in a perfectly-conducting surface. The work described in this report deals with the analysis of the electromagnetic radiation from such an antenna configuration. In particular, it is the purpose of this analysis to assess the effects of the structural discontinuity caused by the truncation of the dielectric cover (at A and B in Fig. 1) with a view towards providing analytical and numerical results which may be useful in the design of such antennas.

In the present work, the configuration illustrated in Fig. 1 is two dimensional, and the infinitely long axial slot excites only TM type electromagnetic fields; here TM implies that the magnetic field intensity is entirely parallel to the axial slot (i.e., it is directed normal to the plane of the paper). This configuration supports surface waves excited by the slot (in addition to the fields directly radiated by the slot). In the present analysis, the thickness, b and the relative permitivity, ε_r of the dielectric cover are chosen so that only the dominant TM_0 surface wave is excited for a given operating frequency. The radiation pattern of this antenna can be conveniently calculated via the geometrical theory of diffraction[1]; however, the diffraction and reflection coefficients associated with the truncation of the dielectric cover must be found. Expressions for these coefficients are derived in this report.

In terms of the geometrical theory of diffraction, the total far-zone field is composed of a geometrical optics field, and a diffracted field. The geometrical optics and diffracted fields are indicated in Fig. 1. The geometrical optics field for this configuration is the direct radiation from the slot to the field point P along the ray path s_0; whereas, the surface waves excited by the slot impinge on the terminations at A and B to produce singly diffracted waves which arrive at P via the ray paths s_1 and s_2. The surface waves excited by the slot also produce reflected waves at the terminations. These reflected surface waves are in turn incident on the opposite terminations thereby producing additional reflected waves, and also diffracted waves which arrive at P along the ray paths s_1 and s_2, and so on. The diffracted field at P is therefore the sum of the fields associated with the singly diffracted and multiply reflected-diffracted rays arriving at P. The latter contribution can be summed into a closed form using a

self-consistent method. The geometrical optics field and the field of the surface waves (incident on the terminations) are obtained from the solution to the problem of a narrow slot radiating through a dielectric covered ground plane of infinite extent. .The diffracted and reflected fields produced by the terminations at A and B are described in terms of the appropriate surface wave diffraction and reflection coefficients just mentioned.

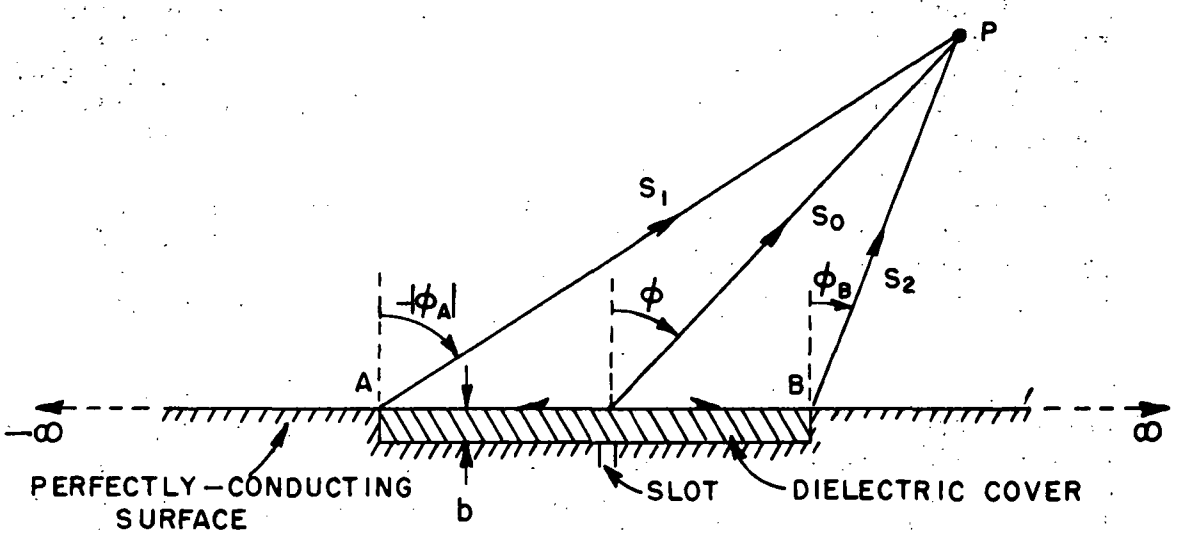

Fig. 1--A typical antenna configuration involving a dielectric covered slot in a perfectly conducting surface.

It is apparent that the superposition principle can be used to extend this analysis for the single narrow slot directly to an array of slots radiating in the presence of a dielectric cover, or to an extended aperture in the presence of a dielectric cover.

Figure 2 illustrates the canonical problem pertinent to the analysis of the terminated dielectric cover shown in Fig. 1. The semi-infinite dielectric slab recessed in a perfectly-conducting surface is excited by a TM_0 surface wave which is incident from the left on the dielectric termination at z = 0. In this report, three methods are employed to solve the above canonical problem; they are:

1. a formally exact solution using the generalized scattering matrix technique combined with function theoretic methods,

2. an approximate solution using the variational technique, and

3. an exact solution of an approximate model wherein the boundary conditions pertaining to the grounded dielectric slab are replaced by an equivalent surface reactance for $x = 0$ and $z < 0$ as illustrated in Fig. 3. One notes that this model also approximately describes the diffraction of a surface wave on the complementary structure of Fig. 4. It is conjectured that the terminated surface impedance model (Fig. 3) is a better approximation for the dielectric slab on the ground plane (Fig. 4) than for the recessed dielectric slab configuration of Fig. 2, because the latter structure has an additional discontinuity in the form of the step in the ground plane. This is evident by noting that as the relative permittivity of the dielectric slab approaches unity, the former structure reduces to the smooth ground plane, whereas a residual step is present in the latter structure. In Chapter IV it is shown that this conducting step significantly affects the reflection coefficient quite apart from the terminated dielectric slab.

The boundary value problems associated with the configurations shown in Figs. 2 and 3 are not ammenable to solutions by the separation of variables technique due to the complicated nature of the boundary conditions. The configuration in Fig. 3 is identifiable as the junction of two semi-infinite sub regions thereby suggesting a solution based on the Wiener-Hopf type factorization procedure. Thus, the two-part boundary value problem of Fig. 3 is formulated in terms of dual integral equations that can be solved exactly using the method of factorization. The factorization for this problem is achieved via an appropriate limiting operation on the Wiener-Hopf factors associated with a related closed region boundary value problem (a closed region problem is one for which no radiation takes place); this technique was originally used by Bates and Mittra[2] in their Wiener-Hopf solution to the problem of waveguide excitation of dielectric and plasma slabs. Such a factorization procedure allows one to obtain factorization functions which are generally far more convenient for numerical processing than those obtained by a formal factorization scheme. The details of this solution are presented in Chapter II. This solution yields the expressions for the surface wave reflection and diffraction coefficients for the approximate configuration in Fig. 3. Several authors have treated two-part boundary value problems whose solutions contain the solution to this problem as a special case; however, most of these authors do not provide numerical results, and where numerical results are given, they are only for the magnitudes of the quantities of interest. One of the reasons for this is the

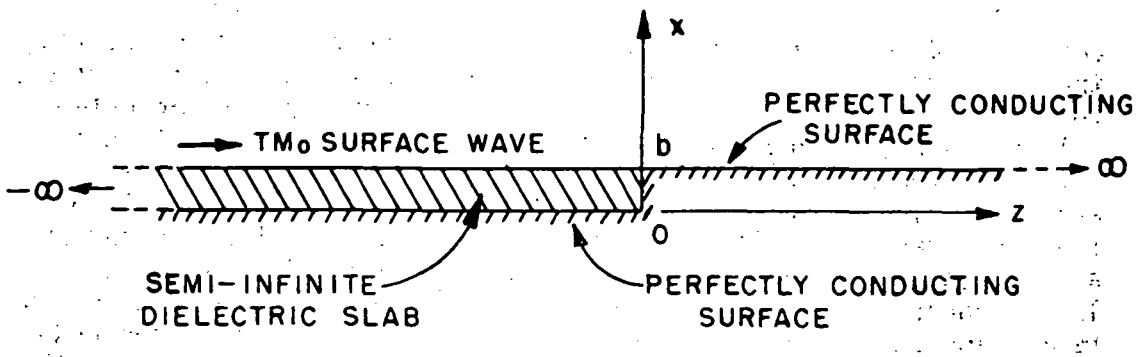

Fig. 2 --Geometry of the canonical problem for analyzing the configuration of Fig. 1.

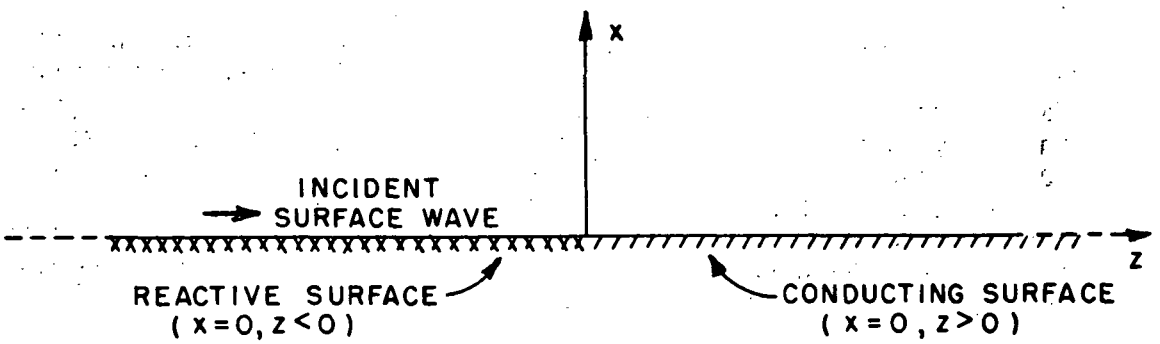

Fig. 3 --An approximation of the configurations shown in Figs. 2 and 4.

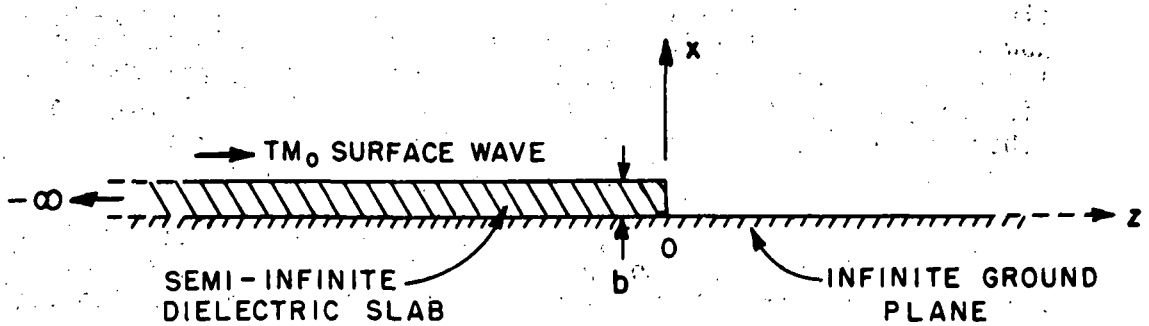

Fig. 4 --A configuration related to that in Fig. 2.

complicated nature of their solutions. Our primary aim in treating the two-part boundary value problem of Fig. 3 is to obtain solutions to quantities of interest in a form which is convenient for calculation and subsequent application to antenna design. Only one reference (Weinstein[5]) appears to provide analytical results which are tractable for calculation; in this case, the values obtainable from the present results and from those in [5] (which are based on a different factorization scheme) provide a valuable mutual check. There appears to be an error in the expressions for the surface wave reflection and diffraction coefficients given in [5]; if one changes the final results in Reference [5] to make them consistent with the development which preceeds the final results, it is found that the numerical results calculated via [5] agree well with the calculations based on the results derived in this report. In particular, the values for the magnitudes of the reflection and diffraction coefficients calculated by these two methods agree perfectly; whereas, there is only a slight difference in the corresponding values for the phase of these coefficients.

The complexity of the solutions and expressions for the parameters of interest which are given by Kay [3] and Maliuzhinets[4] appear to be fairly representative of what one might encounter when consulting references dealing with two part boundary value problems; their expressions for the phase of the reflection and diffraction coefficients contain integrals which appear intractable for numerical computations; in fact, the results for both the amplitude and the phase of these coefficients available in Reference [4] appear intractable for numerical computations (when the results are specialized to our case).

Angulo[6] has given an approximate solution to the problem illustrated in Fig. 4. Using the continuity of the tangential component of the magnetic field in the aperture $z = 0$, $x \geq 0$, Angulo obtained an integral equation for the equivalent magnetic current. He employed the variational method to obtain a stationary expression for the aperture impedance of the incident surface wave. However, in his solution, he approximated the aperture distribution (magnetic current) with only the surface wave field. In related problems treated here we show that such a trial function is too crude to obtain accurate values of the surface wave reflection coefficient. It is clear that the radiation pattern can be calculated from this single term trial function without using the variational method; these patterns are found to be reasonably accurate, except at the lower power levels.

The configuration in Fig. 2 has a transverse discontinuity (due to the step) in addition to the longitudinal discontinuity which defines the junction of two semi-infinite sub regions (in the longitudinal direction); hence, this problem gives rise to a modified Wiener-Hopf equation. Instead of solving the modified Wiener-Hopf problem, the solution to the problem in Fig. 2 is built up from the solutions to two simpler problems which can be treated via the Wiener-Hopf technique. Specifically, the solution to this

problem is formulated using a generalized scattering matrix[7], in which the elements of the generalized scattering matrix are deduced from the Wiener-Hopf solutions to two appropriate auxiliary canonical problems. Both auxiliary problems give rise to identical Wiener-Hopf factorization functions. It was indicated previously in the discussion dealing with the solution to the problem in Fig. 3 that the Wiener-Hopf factors for the open region could be found from a limiting operation on the Wiener-Hopf factors for the related closed region, and that this is to be generally preferred over the formal factorization procedure for reasons of convenience in calculating the factors; unfortunately, the Wiener-Hopf factorization function associated with these auxiliary canonical problems do not yield a convergent representation for the factors obtained via the limiting procedure (see Appendix I, Section III). It is therefore necessary to resort to a formal scheme in order to factorize the Wiener-Hopf Kernel for the auxiliary canonical problems (for details, see Appendix II). It should be noted the generalized scattering matrix formulation leads to a formally exact solution for the boundary value problem corresponding to Fig. 2. The results for the reflection and diffraction coefficients obtained from this solution are expressed in terms of appropriate scattering matrices which are of infinite order; however, accurate computations are possible by truncating the size of the matrices so that one deals with finite order matrices. For a given dielectric constant, operating frequency, and slab thickness, the size of the finite order matrices is determined by the accuracy desired. Numerical calculations indicate that in most practical cases, sufficiently accurate results may be obtained by dealing with a relatively small matrix. A discussion of the auxiliary canonical problems, their solutions, and the manner in which these are used to determine the generalized scattering coefficients appearing in the expressions for reflection and diffraction coefficients, is presented in Chapter III. In addition, an approximate solution to this canonical problem which is based on the variational technique is given in Chapter III.

The use of the surface wave diffraction and reflection coefficients to analyze the radiation from the antenna configuration of Fig. 1 via the GTD is described in Chapter IV. Chapter IV also contains numerical results for the reflection and diffraction coefficients which are derived in Chapters II and III. By a comparison of the numerical results, it is concluded that the approximate physical model in Fig. 3 is not adequate for analyzing the configuration in Fig. 2 unless the conducting step in Fig. 2 is extremely small (much less than $1/50\ \lambda_d$, where λ_d = the wavelength in the dielectric); hence, the formally exact solution given in Chapter III is to be preferred even for relatively thin dielectric slabs. The technological relevance of this research to the design of arrays radiating in the presence of a dielectric cover and to the design of surface wave antennas is pointed out in Chapter IV.

An $e^{-i\omega t}$ time convention is used in this report; this time convention is generally employed by physicists; whereas, the electrical engineers prefer an $e^{i\omega t}$ time dependence. The $e^{-i\omega t}$ time dependence is employed here because it is commonly used for solving problems by the Wiener-Hopf method, and the notation and definitions employed are directly connected with this time convention.

The authors have benefitted from the helpful discussions with Professors H. D. Colson, J. H. Richmond and L. Peters, Jr. Special thanks are due to Professor D. C. Chang of the University of Colorado for pointing out the utility of the generalized scattering matrix technique to the authors.

CHAPTER II
TM_0 SURFACE WAVE DIFFRACTION BY A REACTIVE SURFACE WHICH IS TERMINATED IN A PERFECTLY-CONDUCTING SURFACE

This chapter deals with the solution to the canonical problem illustrated in Fig. 3. As noted in the previous chapter, the boundary value problems described by Figs. 2 and 4 are approximated by the boundary value problem indicated in Fig. 3 where the grounded dielectric cover is replaced by a reactive surface; one expects such an approximation to be valid when the dielectric cover is sufficiently thin. This technique of replacing the original boundary conditions by the approximate impedance boundary conditions for the purpose of simplifying the analysis is not new; it has been employed extensively in the past for analyzing corrugated surfaces, surfaces with finite conductivity, and for thin, grounded, dielectric slabs (a discussion on the impedance surface approximation for the grounded dielectric slab is available in Reference [8]). The main advantage of utilizing the impedance surface is that it simplifies the original problem to an approximate problem which can be solved exactly via function theoretic methods; the exact solution for the original problem is much more difficult as will be seen. The impedance surface for this problem is inductively reactive since the thin dielectric cover is assumed to be lossless. The normal surface impedance, z_s associated with the impedance boundary (for $x=0$, $z<0$) for an assumed $e^{-i\omega t}$ time dependence is

$$(1) \qquad z_s = -i\, x_s$$

The surface reactance, x_s is given by

$$(2) \qquad x_s = z_o\, k_x\, (\tan k_x b)\, (\sqrt{\varepsilon_r}\, k_d)^{-1}$$

where z_o is the free space impedance and ε_r is the relative permittivity of the dielectric slab. The quantity k_x is found from the TM surface wave dispersion relation given by

$$k_x \tan k_x b = \varepsilon_r \sqrt{(\varepsilon_r+1)k^2 - k_x^2}.$$

The quantities k and b are the free space wave number and the thickness of the dielectric slab, respectively. Finally, $k_d = \sqrt{\varepsilon_r}\, k$ in (2). When $k_x b \ll 1$, $x_s \approx z_o\, ((\varepsilon_r - 1)/\varepsilon_r) kb$.

Only a single component of the magnetic field intensity exists for the TM excitation; for our problem, this component of the magnetic field is $\hat{y}$-directed, and will be denoted by $u(x,z)$. Let

$u^i(x,z)$ denote the y component of the magnetic field intensity of the incident surface wave; this surface wave is incident from the left as indicated in Fig. 3. In the analysis, $u^i(x,z)$ is allowed to exist even for $z>0$ as the "unperturbed" incident field so that the y component of the scattered magnetic field intensity, $u^s(x,z)$ accounts for the effects of the perturbation arising from the surface impedance discontinuity at $z=0$, and $x=0$. The total field is thus given by a superposition of $u^i(x,z)$ and $u^s(x,z)$, or

$$u(x,z) = u^i(x,z) + u^s(x,z). \tag{3}$$

The form of the incident surface wave field $u^i(x,z)$ is known:

$$u^i(x,z) = e^{-\alpha x} e^{i\beta z} \quad , \quad \text{for } |z|<\infty \text{ and } 0\leq x<\infty \tag{4}$$

where

$$\alpha \equiv i\omega\varepsilon_o z_s = \omega\varepsilon_o x_s \quad , \tag{5}$$

and

$$\beta = (\alpha^2 + k^2)^{1/2} \tag{6}$$

with

$$k = \omega\sqrt{\mu_o\varepsilon_o} \tag{7}$$

= free space wave number (μ_o and ε_o are the free space permeability and permittivity, respectively, and ω is the angular frequency $2\pi f$).

α and β are the usual surface wave attenuation and propagation constants, respectively. The total field, $u(x,z)$ satisfies the two dimensional (2-D) reduced, scaler wave equation

$$\left(\frac{\partial^2}{\partial x^2} + \frac{\partial^2}{\partial z^2} + k^2\right)u(x,z) = 0, \tag{8}$$

and the following boundary conditions

$$\frac{\partial u}{\partial x} + \alpha u = 0; \quad \text{for } x=0, \text{ and } z<0, \tag{9}$$

and

$$\frac{\partial u}{\partial x} = 0; \quad \text{for } x=0, \text{ and } z>0. \tag{10}$$

In addition, (4) gives

$$\frac{\partial u^i}{\partial x} + \alpha u^i = 0; \quad \text{for } x=0 \text{ and } |z| < \infty \tag{11}$$

and one requires that

(12) u^s satisfy the radiation condition as $|(x^2+z^2)^{1/2}|\to\infty$ for an $e^{-i\omega t}$ time dependence.

One next defines the following Fourier transformations

$$(13)\qquad \hat{u}(x,s) \equiv \frac{1}{\sqrt{2\pi}} \int_{-\infty}^{\infty} u(x,z)e^{isz}\, dz = \hat{u}_+(x,s) + \hat{u}_-(x,s)$$

where

(14a,14b)

$$\hat{u}_+(x,s) \equiv \frac{1}{\sqrt{2\pi}} \int_0^{\infty} u(x,z)e^{isz}\, dz; \quad \hat{u}_-(x,s) \equiv \frac{1}{\sqrt{2\pi}} \int_{-\infty}^{0} u(x,z)e^{isz}\, dz,$$

$$(15)\qquad \hat{u}^s(x,s) \equiv \frac{1}{\sqrt{2\pi}} \int_{-\infty}^{\infty} u^s(x,z)e^{isz}\, dz = \hat{u}^s_+(x,s) + \hat{u}^s_-(x,s),$$

with

(16a,16b)

$$\hat{u}^s_+(x,s) \equiv \frac{1}{\sqrt{2\pi}} \int_0^{\infty} u^s(x,z)e^{isz}\, dz; \quad \hat{u}^s_-(x,s) \equiv \frac{1}{\sqrt{2\pi}} \int_{-\infty}^{0} u^s(x,z)e^{isz}\, dz,$$

and

$$(17)\qquad \hat{u}^i_+(x,s) \equiv \frac{1}{\sqrt{2\pi}} \int_0^{\infty} u^i(x,z)e^{isz}\, dz = \frac{i\, e^{-\alpha x}}{\sqrt{2\pi}(s+\beta)}$$

(one uses (4) in obtaining the R.H.S. of (17)). The incident field, u^i satisfies the 2-D reduced wave equation so it follows from (8) that

$$(18)\qquad \left(\frac{\partial^2}{\partial x^2} + \frac{\partial^2}{\partial z^2} + k^2\right)u^s(x,z) = 0.$$

Fourier transforming (18) and using (15) one obtains

$$(19) \qquad \left(\frac{\partial^2}{\partial x^2} + \lambda_x\right)\hat{u}^s(x,s) = 0$$

where

$$(20) \qquad \sqrt{\lambda_x} \equiv \sqrt{k^2 - s^2} \ .$$

The general solution to (19) is given by

$$(21) \qquad \hat{u}^s(x,s) = \hat{u}^s_+ + \hat{u}^s_- = C(s)e^{i\sqrt{\lambda_x}\,x} + D(s)e^{-i\sqrt{\lambda_x}\,x}$$

In order to simplify some of the analysis, one introduces a small loss in the medium above x=0; i.e., one lets k (and λ_x) be complex

$$(22) \qquad k = k_1 + i\,k_2, \quad (k_2 << k_1; \ k_1 > 0, \ k_2 > 0).$$

This loss may be set equal to zero once the analysis is completed. From (12) one notes that u^s must satisfy the radiation condition as $x \to \infty$ so that $D(s) = 0$. Thus

$$(23) \qquad \hat{u}^s(x,s) = C(s)e^{i\sqrt{\lambda_x}x}$$

with

$$(24) \qquad \sqrt{\lambda_x} = \sqrt{k^2 - s^2} = +i\sqrt{s^2 - k^2} \ ,$$

where the choice of the branch of $\sqrt{\lambda_x}$ is the one for which $\mathrm{Im}\sqrt{\lambda_x} > 0$. One notes that $u^i(x,z)$ already satisfies the impedance boundary condition; therefore

$$(25) \qquad \frac{\partial u^s}{\partial x} + \alpha\, u^s = 0; \quad \text{for} \quad x = 0, \text{ and } z < 0 \ .$$

Furthermore, (10) indicates that

$$(26) \qquad \frac{\partial u^s}{\partial x} = -\frac{\partial u^i}{\partial x} \ ; \text{ for } x = 0, \text{ and } z > 0 \ .$$

In order to apply (25) and (26) to $u^s(x,z)$, one takes the inverse Fourier transform of (23) to obtain

$$u^s(x,z) = \frac{1}{\sqrt{2\pi}} \int_{-\infty}^{\infty} \hat{u}^s(x,s) e^{-isz}\, ds$$

or

$$u^s(x,z) = \frac{1}{\sqrt{2\pi}} \int_{-\infty}^{\infty} C(s) e^{i\sqrt{\lambda_x}x}\, e^{-isz}\, ds \,. \tag{27}$$

Substituting the result on the R.H.S. of (27) into (25) and (26) leads to the following pair of integral equations

$$\int_{-\infty}^{\infty} (\sqrt{\lambda_x} - i\alpha)\, C(s) e^{-isz}\, ds = 0, \quad z < 0 \tag{28}$$

$$\int_{-\infty}^{\infty} \sqrt{\lambda_x}\, C(s) e^{-isz}\, ds = -i\alpha\sqrt{2\pi}\, e^{i\beta z}, \quad z > 0 \tag{29}$$

It is convenient to define

$$\phi(s) \equiv \sqrt{\lambda_x}\, C(s) \tag{30}$$

and

$$L(s) \equiv \frac{\sqrt{\lambda_x}}{\sqrt{\lambda_x} - i\alpha} = \frac{\sqrt{k^2 - s^2}}{\sqrt{k^2 - s^2} - i\alpha} \tag{31}$$

so that an alternate set of dual integral equations is obtained by substituting (30) and (31) into (28) and (29); thus

$$\int_{-\infty}^{\infty} L^{-1}(s)\, \phi(s) e^{-isz} ds = 0, \quad z < 0 \tag{32}$$

$$\int_{-\infty}^{\infty} \phi(s) e^{-isz} ds = -i\sqrt{2\pi}\, \alpha e^{i\beta z}, \quad z > 0 \tag{33}$$

One may now solve for $\phi(s)$ given in (32) and (33) via a factorization procedure.

Let

(34) $$s = \sigma + i\tau ,$$

The region in the complex s plane for $\tau > -k_2$ will be denoted by U.H.P. (upper half s plane), and the region in the complex s plane for $\tau < k_2$ will be denoted by L.H.P. (lower half s plane). Initially, one assumes that $L^{-1}(s)\ \phi(s) \to 0$ in the U.H.P. as $|s| \to \infty$ there, and one also requires that $\phi(s) \to 0$ in the L.H.P. as $|s| \to \infty$ there. It will be indicated aposteriori that these assumptions are true. Under these assumptions, one may employ Jordon's lemma to close the contour of integration in the U.H.P. for (32) and similarly close the contour of integration in the L.H.P. for (33) so that

(35) $$\int_{\text{U.H.P.}} L^{-1}(s)\ \phi(s) e^{-isz} ds = 0, \qquad z < 0$$

and

(36) $$\int_{\text{L.H.P.}} \phi(s) e^{-isz} ds = -i\sqrt{2\pi}\ \alpha e^{i\beta z}, \qquad z > 0$$

From (36), one requires that $\phi(s)$ have a pole in the L.H.P. to provide a residue contribution corresponding to $-i\sqrt{2\pi}\ \alpha e^{i\beta z}$. From (35) one may write

(37) $$L^{-1}(s)\ \phi(s) \equiv A_+(s)$$

where $A_+(s)$ is as yet an unknown analytic function in the U.H.P. Similarly, one may define another as yet unknown analytic function, $A_-(s)$ in the L.H.P. such that

(38) $$\frac{\alpha}{\sqrt{2\pi}}\ \frac{A_-(s)}{A_-(-\beta)(s+\beta)} \equiv \phi(s)$$

If one employs (38) in the L.H.S. of (36), one then obtains the value on the R.H.S. of (36) via the Cauchy Residue Theorem. Eliminating $\phi(s)$ between (37) and (38) yields

$$(39) \qquad L(s) = \frac{\alpha}{\sqrt{2\pi}} \frac{A_-(s)}{A_-(-\beta)} \frac{1}{(s+\beta)} \frac{1}{A_+(s)}$$

The unknowns $A_+(s)$ and $A_-(s)$ can be found by factorizing $L(s)$ into $L_+(s)$ $L_-(s)$ (where $L_+(s)$ is analytic in the U.H.P. and $L_-(s)$ is analytic in the L.H.P.; $L_\pm(s)$ are referred to as the Wiener-Hopf factors). Clearly $L_-(s)$ is proportional to $A_-(s)/A_-(-\beta)$; hence

$$(40) \qquad \frac{L_-(s)}{L_-(-\beta)} = \frac{A_-(s)}{A_-(-\beta)}$$

(The proportionality constant in the above equation is unity since the R.H.S. equals unity where $s = -\beta$). Thus, it follows that

$$(41) \qquad A_+(s) = \frac{\alpha}{\sqrt{2\pi} L_-(-\beta) L_+(s)(s+\beta)}$$

The explicit forms of the functions $L_+(s)$ and $L_-(s)$ are derived in Section II of Appendix I. These $L_\pm(s)$ functions are deduced from an appropriate limiting procedure on the factorization function for a related closed region boundary value problem; this technique leads to factors which are convenient for numerical processing. One notes that if the boundary conditions (25) and (26) were employed in the transformed domain (x,s-domain) instead of in the spatial domain (x,z-domain) as done in this analysis, one would have obtained a Wiener-Hopf equation for the unknown $\phi(s)$. However, the solution to the Wiener-Hopf equation requires decomposition functions in addition to factorization; thus, by formulating this problem in terms of the dual integral equations one avoids any decomposition. The solution to the Wiener-Hopf equation also requires an analytic continuation argument which is not essential for the solution of dual integral equations by the factorization procedure. Some author's prefer to use the analytic continuation argument even to solve dual integral equations by the factorization method; in contrast, the procedure outlined above allows one to by-pass the analytic continuation argument to solve for $A_\pm(s)$. Incorporating (41) in (30) via (37) yields

$$(42) \qquad C(s) = \frac{\alpha}{\sqrt{2\pi}} \frac{L_-(s)}{L_-(-\beta)} \frac{1}{\sqrt{k^2-s^2}(s+\beta)}$$

One may next utilize (42) in (23) to obtain

$$(43)\qquad \hat{u}^s(x,s) = \frac{\alpha}{\sqrt{2\pi}} \frac{L_-(s)}{L_-(-\beta)} \frac{e^{i\sqrt{k^2-s^2}x}}{\sqrt{k^2-s^2}(s+\beta)}$$

Inverse Fourier transforming (43) leads to a formal solution for $u^s(x,z)$ in terms of an inversion integral with known terms in the integrand;

$$(44)\qquad u^s(x,z) = \frac{1}{2\pi} \int_{-\infty}^{\infty} \alpha \frac{L_-(s)e^{i\sqrt{k^2-s^2}\,x}}{L_-(-\beta)\sqrt{k^2-s^2}(s+\beta)} e^{-isz}\, ds\ .$$

An evaluation of the integral in (44) leads to the complete solution of our problem. Before proceding further, one may check aposteriori if the assumptions concerning the behavior of $\phi(s)$ in the L.H.P., and of $L^{-1}(s)\phi(s)$ in the U.H.P., have all been satisfied. From the asymptotic behavior of the factors $L_\pm(|s|\to\infty)$ as given in Appendix I (Section II), one notes that $L_\pm(s) \sim$ (constant). Hence, from (41), $A_+(s) \sim O(s^{-1})$, so that $L^{-1}(s)\phi(s) \sim O(s^{-1})$ and $\phi(s) \sim O(s^{-1})$. It is now easily verified from these asymptotic behaviors that all the previous assumptions are indeed true. The contour of integration in (44) may be closed in the U.H.P., and the Cauchy residue theorem applied to obtain the fields which exist in the region $z < 0$, $x \geq 0$; whereas one may close the contour of integration in the L.H.P. to obtain fields which exist in the region $z > 0$, and $x \geq 0$. The singularities of the integrand of (44) in the complex s plane and the deformed paths of integration are indicated in Fig. 5. One notes that $L_-(s)$ contributes the pole at $s = -\beta$ (see (44)). The original contour may be deformed to one in the L.H.P. as follows

$$(45)\qquad \int_{-\infty}^{\infty} = -\left[\int_{C_{z>0}} + \int_{C_{br.\,1}+C_{br.\,2}} + \oint_{C_\beta}\right], \text{ for } z > 0\ .$$

Similarly, the deformation into the U.H.P. is given by

$$(46)\qquad \int_{-\infty}^{\infty} = -\left[\int_{C_{z<0}} + \int_{C'_{br.\,1}+C'_{br.\,2}} + \oint_{C'_\beta}\right], \text{ for } z < 0.$$

The contributions to the integral from

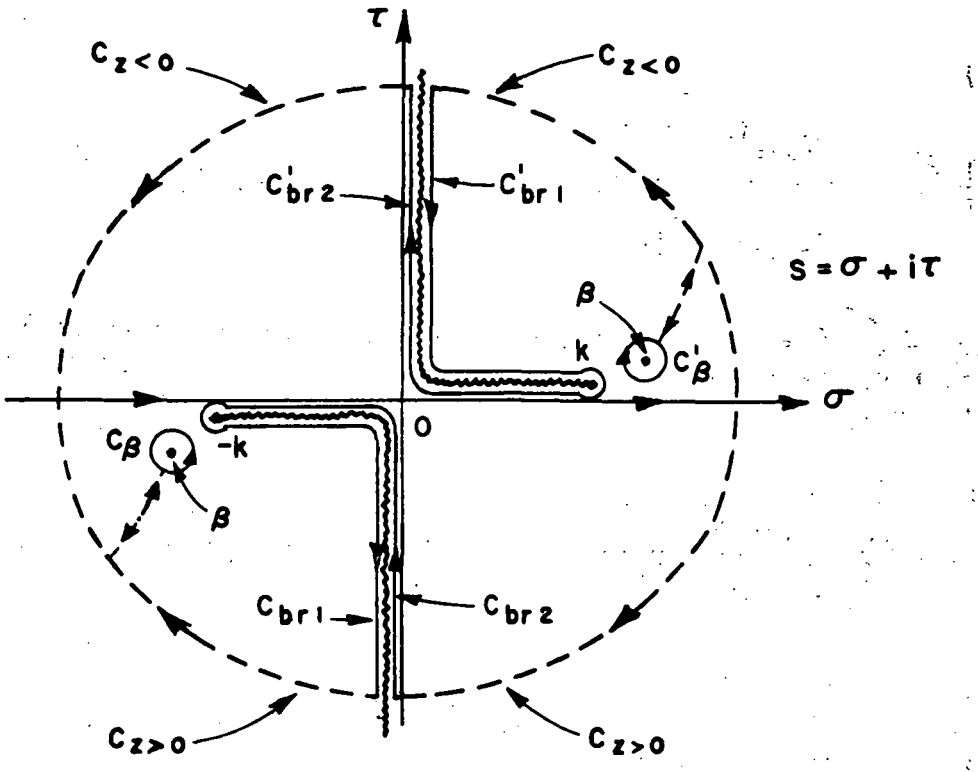

Fig. 5 --Contours of integration in the complex s-plane which occur in the solution to the problem in Fig. 3.

$$\int_{C_{z<0}} \quad \text{and} \quad \int_{C_{z<0}}$$

vanish. The integrals over $C_{br.\,1}+C_{br.\,2}$ and $C'_{br.\,1}+C'_{br.\,2}$ yield the radiation field which may be asymptotically evaluated in closed form via the saddle point method; whereas, the integrals over C_β and C'_β yield the transmitted and reflected surface waves, respectively. There can be no transmitted surface wave above the perfectly conducting surface ($x=0$, $z>0$); however, the transmitted surface wave arising from the integration over the circular contour C_β exactly cancels the incident surface wave field which was assumed to exist for $z>0$ in the analysis. The transmitted surface wave field for $z>0$ is given by the residue at $s=-\beta$ as:

(47)

$$\frac{-1}{2\pi}\oint_{C_\beta}\frac{\alpha L_-(s)e^{i\sqrt{k^2-s^2}x}}{L_-(-\beta)\sqrt{k^2-s^2}(s+\beta)}e^{-isz}ds = -2\pi i\,\frac{\alpha L_-(-\beta)}{L_-(-\beta)i\alpha\,2\pi}e^{-\alpha x}e^{i\beta z} = -u^i$$

(Note: $\sqrt{k^2-\beta^2} = i\alpha$ has been used in deriving the above result)
Similarly, the reflected surface wave for $z<0$ is given by the residue at $s=\beta$ as:

(48)

$$-\frac{1}{2\pi}\oint_{C'_\beta}\alpha\frac{L_-(s)e^{i\sqrt{k^2-s^2}x}}{L_-(-\beta)\sqrt{k^2-s^2}(s+\beta)}e^{-isz}ds = 2\pi i\frac{\alpha\mathcal{L}_-(\beta)e^{-\alpha x}}{L_-(-\beta)i\alpha(2\pi)(2\beta)}e^{-i\beta z}$$

where

(49)

$$L_-(s) = \left(\frac{k}{k-i\alpha}\right)^{1/2}\frac{\left(1-\frac{s}{k}\right)^{1/2}}{\left(1-\frac{s}{\beta}\right)}e^{\frac{1}{\pi}\text{P.V.}\int_0^\infty\left\{\ln\left(1-\frac{s}{\sqrt{k^2-q^2}}\right)\right\}\frac{\alpha}{q^2+\alpha^2}dq}$$

from Appendix I (Section II). The symbol P.V. in front of the integral denotes the principal value of the integral. The quantity $\mathcal{L}_-(\beta)$ may be identified as

(50) $$\mathcal{L}_-(\beta) = -\text{ Residue of } L_-(\beta) = -\lim_{s\to\beta}(s-\beta)\,L_-(s)$$

i.e.,

(51)

$$\mathcal{L}_-(\beta) = -\left(\frac{k}{k-i\alpha}\right)^{1/2}\beta\left(1-\frac{\beta}{k}\right)^{1/2}e^{\frac{1}{\pi}\text{P.V.}\int_0^\infty\left\{\ln\left(1-\frac{\beta}{\sqrt{k^2-q^2}}\right)\right\}\frac{\alpha}{q^2+\alpha^2}dq}$$

Since the value of the surface wave field at $x=0$, $z=0$ is unity, the reflected surface wave denoted by $u^r(x,z)$ for $z<0$ may be expressed as

(52) $$u^r(x,z) = R_1\,e^{-\alpha x}\,e^{-i\beta z},$$

where R_1 denotes the surface wave reflection coefficient for this canonical problem. From (48), (49) and (50), R_1 is explicitly given by

$$(53) \qquad R_1 = -i\left(\frac{\beta-k}{\beta+k}\right)^{1/2} \frac{1}{e^{\pi}} P.V.\int_0^{\infty} \ln\left\{\frac{\sqrt{k^2-q^2}-\beta}{\sqrt{k^2-q^2}+\beta}\right\} \frac{\alpha}{q^2+\alpha^2}\, dq \ .$$

The radiation fields obtainable from $C_{br.\,1} + C_{br.\,2}$ and $C'_{br.\,1} + C'_{br.\,2}$ via an asymptotic evaluation are the fields diffracted by the impedance discontinuity at (x=0, z=0). It is sufficient to evaluate the branch cut integral either in the U.H.P. or in the L.H.P. by the saddle point method (both lead to the same result). Instead of asymptotically evaluating the integrals by deforming the contours $C_{br.\,1} + C_{br.\,2}$ into a steepest descent contour which passes through the saddle point in the s-plane, it appears to be more convenient to employ a polar transformation in the integral of (44) and later evaluate the transformed integral via the saddle point method. The use of polar transformations is a common procedure for evaluating integrals of the type given in (44) (see [8,9] for example). The polar transformations are

$$(54) \qquad s = k \sin \xi; \sqrt{s^2-k^2} = -ik \cos \xi$$

$$(55) \qquad x = \rho \cos \phi \text{ and } z = \rho \sin \phi \ .$$

Figure 6 illustrates the quantities ρ and ϕ; these correspond to the polar coordinates at the field point. The polar transformation yields a single valued integrand in the transformed plane (complex ξ-plane). The new contour in the ξ-plane may be deformed into the steepest descent path denoted by C_{SDP} in order to obtain the saddle point contribution to the integral. The saddle point contribution gives the diffracted field contribution; whereas, the residues corresponding to the poles which may be crossed in deforming the original contour in the ξ-plane to the C_{SDP} contour give rise to surface wave contributions to the field. In this problem, these pole contributions in the ξ-plane are identical to the pole contributions arising from contours C_β and C'_β in the s-plane as given by (47) and (48); hence, these will not be calculated again. The complex s-plane representation appears more suitable for calculating surface wave contributions to the field; whereas, the ξ-plane representation appears to be more convenient for calculating the diffracted field. The details of the transformation of the integral in (44) from the s-plane to the ξ-plane, and the complex ξ-plane topology will not be presented for the sake of brevity. The final expression for the integral over the steepest descent path is denoted by u^d, where

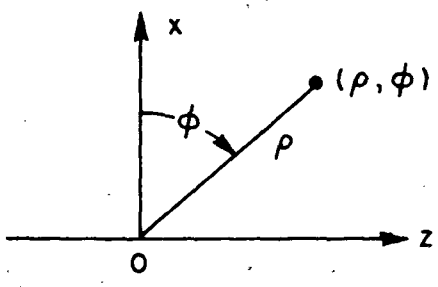

Fig. 6 --Polar coordinates for the field point.

$$(56) \qquad u^d(\rho,\phi) = \frac{\alpha}{2\pi} \int_{C_{SDP}} \frac{L_-(k \sin \xi)}{L_-(-\beta)(\beta+k \sin \xi)} e^{ik\rho \cos(\xi+\phi)} d\xi$$

The above integral is evaluated asymptotically by the saddle point method; and the leading term in the resulting asymptotic solution for large $k\rho$ is

$$(57) \qquad u^d(\rho,\phi) \sim \frac{\alpha e^{-i\frac{\pi}{4}}}{\sqrt{2\pi k}} \frac{L_-(-k \sin \phi)}{L_-(-\beta)(\beta-k \sin \phi)} \frac{e^{ik\rho}}{\sqrt{\rho}} .$$

Since the value of the incident surface wave field at x=0, and z=0 is unity, one may express u^d as

$$(58) \qquad u^d \sim D_1(\phi) \frac{e^{ik\rho}}{\sqrt{\rho}}$$

where D_1 represents the surface wave diffraction coefficient for this canonical problem. From (57) and (58) D_1 is thus given by

$$(59) \qquad D_1(\phi) \equiv \frac{\alpha e^{-i\frac{\pi}{4}}}{\sqrt{2\pi k}} \frac{L_-(-k \sin \phi)}{L_-(-\beta)(\beta-k \sin \phi)}$$

Substituting for $L_-(s)$, $D_1(\phi)$ becomes

$$(60)\quad D_1 = e^{-i\frac{\pi}{4}} \frac{2\alpha\beta(1+\sin\phi)^{1/2}}{\sqrt{2\pi k}\left(1+\frac{\beta}{k}\right)^{1/2}(\beta^2-k^2\sin^2\phi)} \cdot$$

$$\cdot \frac{1}{e^{\pi}} \text{P.V.} \int_0^{\infty} \ln\left\{\frac{\sqrt{k^2-q^2}+k\sin\phi}{\sqrt{k^2-q^2}+\beta}\right\} \frac{\alpha}{q^2+\alpha^2}\, dq \cdot$$

The derivations for the surface wave reflection and diffraction coefficients given above complete the solution to the canonical problem of Fig. 3.

CHAPTER III
TM_0 SURFACE WAVE DIFFRACTION BY A RECESSED SEMI-INFINITE DIELECTRIC SLAB WHICH IS FLUSH MOUNTED IN A PERFECTLY CONDUCTING SURFACE

This chapter deals with the solution to the canonical problem illustrated in Fig. 2. Two approaches for solving this boundary value problem are explored. One approach is based on the generalized scattering matrix technique (henceforth denoted by GSMT) which was recently developed by Pace and Mittra[7] for analysing a class of waveguide discontinuity problems; the generalized scattering matrix approach leads to a formally exact solution for the problem. The scattering matrices involved are found from the solution of associated problems by the Wiener-Hopf method. The second approach is based on the variational technique which leads to an approximate solution. The details pertaining to the solution of this canonical problem via the GSMT is indicated in section A of this chapter; whereas, section B of this chapter describes the variational solution to the same problem.

A. Solution Based on the GSMT

The GSMT was originally developed for analyzing the effects of discontinuities in closed waveguide regions [7]; however, more recently, Lee and Mittra[10] extended the application of this technique by solving an open region problem involving the diffraction of a plane wave by a thick conducting half plane (they actually considered plane wave diffraction by a dielectric loaded parallel plate waveguide which reduces to the case of a thick conducting half plane when the relative dielectric constant tends to infinity). Kashyap and Hamid [11] later extended the results of Lee and Mittra to treat the diffraction by a slit in a thick-conducting screen via the GSMT. The concept of the generalized scattering matrix is closely connected with the scattering matrix theory used for describing microwave networks. The basic difference between the ordinary scattering matrix and the generalized scattering matrix is that the former considers only propagating modes; whereas, the latter considers both evanescent as well as propagating modes. As a result of the extension to include evanescent modes, the generalized scattering matrix is of infinite order, and is non-symmetric (the symmetry in the ordinary scattering matrix results from the normalization on the propagating modes such that they carry unit power; such a normalization cannot be applied to evanescent modes). In general, boundary value problems whose geometrical configurations can be identified as being composed of two or more junctions can be solved via the GSMT, provided that the generalized scattering matrices associated with these junctions can be found. In the GSMT, the formally exact

solution to the boundary value problem is obtained by systematically summing up field contributions arising from the multiple scattering between these junctions. The multiple scattering process between the junctions can be described by a convergent Neumann series whose terms contain these generalized scattering matrices [7]; however, one can directly arrive at the same result via a self consistent method for multiple interactions. The latter viewpoint will be employed in our analysis. The formal solution arising from the multiple interactions contains infinite order matrices. In most practical cases it is possible to obtain accurate results by truncating the matrices to a reasonably small size as seen from [10] and from the results obtained in this report.

At first glance, the canonical problem illustrated in Fig. 2 does not appear to be composed of two junctions. However, if one assumes that the dielectric slab is extended by an "infinitesimal" distance, δ into the conducting region (i.e., into the region $0 \leq z < \delta$; $0 < x \leq b$), one creates physically identifiable junctions ① and ② as indicated in Fig. 7. When $\delta \to 0$, the problem illustrated in Fig. 7 becomes identical to the canonical problem illustrated in Fig. 2. For later convenience, one defines the regions Ⓐ, Ⓑ and Ⓒ surrounding junction ① such that region Ⓐ exists for $(x > b;\ |z| < \infty)$, region Ⓑ exists for $(0 < x < b;\ z < 0)$, and region Ⓒ exists for $(0 < x < b;\ 0 < z < \delta)$. These regions are also indicated in Fig. 7. The geometries of junctions ① and ② are indicated indicated in Figs. 8a and 8b, respectively. The properties of junctions ① and ② may now be described in terms of their respective generalized scattering matrices.

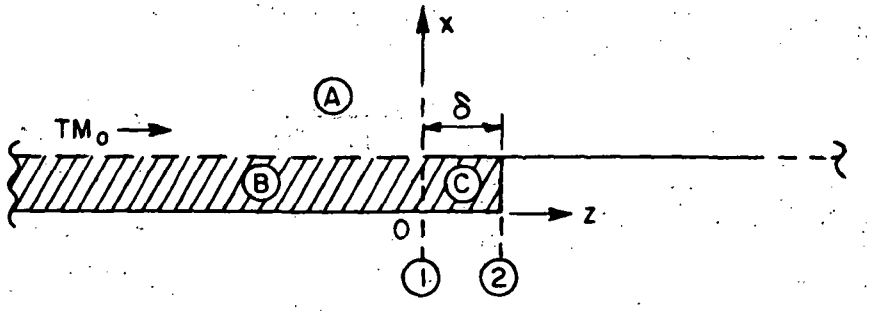

Fig. 7 --Junctions ① and ② for the recessed slab in Fig. 2.

In order to introduce the generalized scattering matrices for junction ①, one begins by considering the geometry for this junction alone as shown in Fig. 8a. Junction ① is excited by the TM_0 surface wave which is incident from the left as in Fig. 7. This incident surface wave is scattered by ① such that a part of it is scattered into region Ⓒ and the rest is scattered into regions Ⓐ and Ⓑ. The fields transmitted into region Ⓒ are described by the generalized scattering matrix denoted by S_{21}; whereas, the fields scattered into regions Ⓐ and Ⓑ may be described by the generalized scattering matrix denoted by S_{11}. The scattering processes described by S_{21} and S_{11} are indicated in Fig. 9a. The field transmitted into region Ⓒ impinges on junction ② from which it is reflected towards ①. The field in region Ⓒ is represented by a sum of TM_{0n} waveguide modes (for $n = 0, 1, 2, \cdots \infty$). Thus, any TM_{0n} mode which is incident at ① after reflection at ② is partly scattered back into the waveguide region Ⓒ, and the rest is scattered into regions Ⓐ and Ⓑ. The field scattered back into Ⓒ is described by the generalized scattering matrix denoted by S_{22}; whereas, the corresponding scattered fields in regions Ⓐ and Ⓑ are described by the generalized scattering matrix denoted by S_{12}. The scattering processes described by S_{22} and S_{12} are shown in Fig. 9b. It is clear that the matrices S_{11} and S_{21} may be obtained from the solution to the problem illustrated in Fig. 9a; whereas, the matrices S_{22} and S_{12} may be obtained from the solution to the problem illustrated in Fig. 9b. The problems illustrated in Figs. 9a and 9b may be regarded as auxiliary problems associated with the original canonical problem; the solutions to these auxiliary canonical problems are instrumental to the solution of the original canonical problem illustrated in Fig. 2. The generalized scattering matrix for junction ② is denoted by Γ. Γ corresponds to the reflection coefficients of the TM_{0n} modes which are reflected at ②; it is easily seen that Γ is an identity matrix of infinite order.

The explicit forms of the generalized scattering matrices S_{11}, S_{12}, S_{21} and S_{22} are derived next. The derivations for S_{11} and S_{21} are indicated first; these are followed by the derivations for S_{12} and S_{22}. It is a trivial matter to determine Γ, and hence the derivation for Γ is not presented here for the sake of brevity. The surface wave reflection and diffraction coefficients are then constructed from these scattering matrices by considering interactions between the junctions ① and ②.

Derivation of S_{11} and S_{21}:

The generalized scattering matrices S_{11} and S_{21} are obtained from the solution to the auxiliary problem illustrated in Fig. 9a as mentioned before. The excitation for this problem is a TM_0 surface wave incident at ① from the left as shown in Fig. 7. For the TM case, the magnetic field intensity is $\hat{y}$-directed;

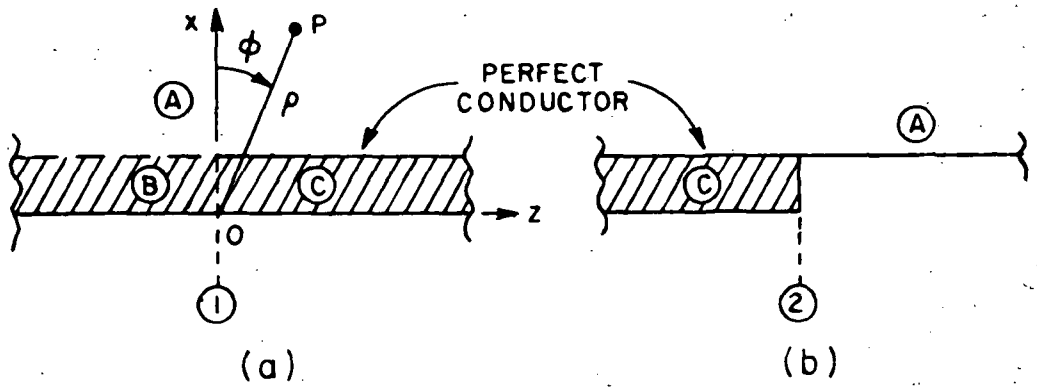

Fig. 8 -- Geometries associated with the individual junctions.

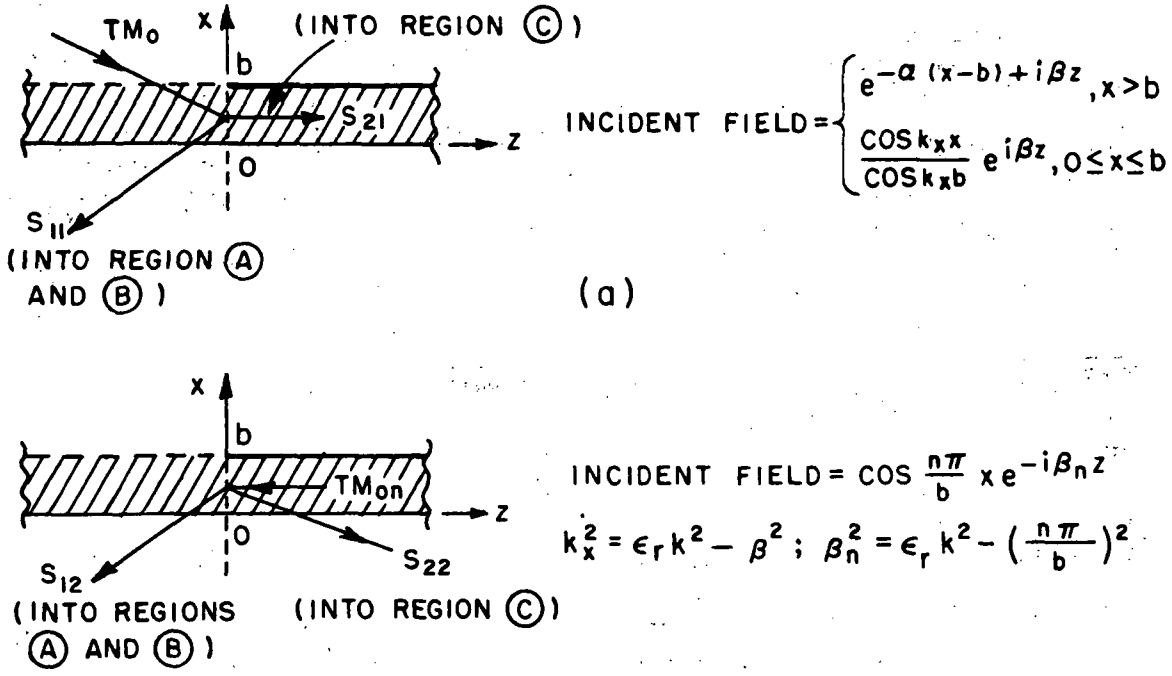

Fig. 9 -- Auxiliary canonical problems associated with the recessed slab problem.

hence, in the following analysis one defines the scaler fields Φ^i, Φ, and Φ^t to respectively correspond to the y-directed components of the incident, scattered and the total magnetic field intensities. For the purposes of anlaysis, it is convenient to assume that Φ^i exists even for $z > 0$. The final solution will contain a contribution to Φ which exactly cancels the incident field for $z > 0$. The form of the incident field Φ^i is

$$(61) \qquad \Phi^i \equiv \begin{cases} e^{-\alpha(x-b)+i\beta z} & ; \quad x \geq b, \ |z| < \infty \\ \dfrac{\cos k_x x}{\cos k_x b} e^{i\beta z} & ; \quad 0 \leq x \leq b, \ |z| < \infty \end{cases}$$

with

$$(62) \qquad -k_x^2 + k_d^2 = \beta^2 ,$$

$$(63) \qquad \alpha^2 + k^2 = \beta^2 ,$$

where α and β are the TM_0 surface wave attenuation and propagation constants which are found from the TM surface wave dispersion relation

$$(64) \qquad k_x \tan k_x b = \varepsilon_r \alpha \quad .$$

k and k_d are the wave numbers in the regions $x > b$, and $0 < x < b$, respectively. Thus,

$$(65) \qquad k_d = \sqrt{\varepsilon_r}\, k,$$

where ε_r is the relative permittivity of the dielectric in $0<x<b$. The total field Φ^t is a superposition of Φ^i and Φ.

$$(66) \qquad \Phi^t = \Phi^i + \Phi.$$

Φ^t, Φ^i, and Φ satisfy the homogeneous, 2-D, reduced wave equation.

$$(67) \qquad \left(\frac{\partial^2}{\partial x^2} + \frac{\partial^2}{\partial z^2} + k^2\right) \Phi(x,z) = 0; \quad x \geq b, \ |z| < \infty$$

and

$$(68)\qquad \left(\frac{\partial^2}{\partial x^2}+\frac{\partial^2}{\partial z^2}+k_d^2\right)\Phi(x,z)=0;\quad 0\le x\le b,\ |z|<\infty$$

In addition, Φ must satisfy the following boundary conditions and the radiation condition.

$$(69)\qquad \left.\frac{\partial\Phi}{\partial x}\right|_{x=0}=0;\quad \text{for } |z|<\infty$$

$$(70)\qquad \frac{\partial}{\partial x}\{\Phi+\Phi^i\}\Big|_{x=b_+}=0=\frac{1}{\varepsilon_r}\frac{\partial}{\partial x}\{\Phi+\Phi^i\}\Big|_{x=b_-};\ \text{for } z>0$$

$$(71)\qquad \Phi\Big|_{x=b_+}=\Phi\Big|_{x=b_-};\ \text{for}\quad z<0$$

$$(72)\qquad \left.\frac{\partial\Phi}{\partial x}\right|_{x=b_+}=\frac{1}{\varepsilon_r}\left.\frac{\partial\Phi}{\partial x}\right|_{x=b_-};\quad \text{for } z<0$$

(73) Φ satisfies the radiation condition as $|(x^2+z^2)^{1/2}|\to\infty$ for an $e^{-i\omega t}$ time dependence.

One defines the following Fourier transformations:

$$(74)\qquad \hat{\Phi}(x,s)\equiv\frac{1}{\sqrt{2\pi}}\int_{-\infty}^{\infty}\Phi(x,z)e^{isz}dz=\hat{\Phi}_+(x,s)+\hat{\Phi}_-(x,s)$$

where

(75a,75b)

$$\hat{\Phi}_+(x,s)\equiv\frac{1}{\sqrt{2\pi}}\int_0^{\infty}\Phi(x,z)e^{isz}dz;\quad \hat{\Phi}_-(x,s)\equiv\frac{1}{\sqrt{2\pi}}\int_{-\infty}^{0}\Phi(x,z)e^{isz}dz$$

and $s = \sigma + i\tau$ as in Chapter II. Also

(76a,76b)

$$\hat{\Phi}_+^i(x,s) \equiv \frac{1}{\sqrt{2\pi}}\int_0^\infty \Phi^i(x,z)e^{isz}dz; \qquad \hat{\Phi}_+^{i'}(x,s) \equiv \frac{1}{\sqrt{2\pi}}\int_0^\infty \frac{\partial \Phi^i}{\partial x}\, e^{isz}dz$$

From (61) and (76a), one easily obtains

$$(77) \qquad \hat{\Phi}_+^i = \begin{cases} \dfrac{e^{-\alpha(x-b)}}{\sqrt{2\pi}} \cdot \dfrac{i}{s+\beta} & , \quad x \geq b \\ \dfrac{1}{\sqrt{2\pi}} \dfrac{\cos k_x x}{\cos k_x b} \dfrac{i}{s+\beta} & , \quad 0 \leq x \leq b \end{cases}$$

and

$$(78) \qquad \Phi_+^{i'} = \begin{cases} -\dfrac{\alpha}{\sqrt{2\pi}} e^{-\alpha(x-b)} \dfrac{i}{s+\beta} , & x \geq b \\ -\dfrac{k_x}{\sqrt{2\pi}} \dfrac{\sin k_x x}{\cos k_x b} \dfrac{i}{s+\beta}, & 0 \leq x \leq b \end{cases}$$

Fourier transforming (67) and (68) w.r.t. z yields

$$(79) \qquad \left\{\frac{\partial^2}{\partial x^2} - (s^2-k^2)\right\} \hat{\Phi}(x_>,s) = 0$$

and

$$(80) \qquad \left\{\frac{\partial^2}{\partial x^2} - (s^2-k_d^2)\right\} \hat{\Phi}(x_<,s) = 0$$

Where $x_>$ and $x_<$ denote values of x for $x \geq b$ and $0 \leq x \leq b$, respectively; thus, $x_> \to b_+$ and $x_< \to b_-$ as $x \to b$. General solutions to (79) and (80) are

$$(81) \qquad \hat{\Phi}(x_>,s) = A(s)e^{-\gamma x} + B(s)e^{\gamma x}$$

$$(82) \qquad \hat{\Phi}(x_<,s) = C(s) \cosh \gamma_1 x + D(s) \sinh \gamma_1 x$$

where

$$\gamma \equiv \sqrt{s^2 - k^2} = -i\sqrt{k^2 - s^2} \tag{83}$$

and

$$\gamma_1 \equiv \sqrt{s^2 - k_d^2} \tag{84}$$

Here, the choice of the branch of γ is the one for which Re $\gamma > 0$. For ease of analysis, one introduces a small loss into the regions $x \geq b$ and $0 \leq x \leq b$; i.e., one lets k and k_d be complex.

$$k = k_1 + ik_2, \quad (k_2 << k_1; \quad k_1 > 0, \; k_2 > 0) \tag{85}$$

and

$$k_d = k_3 + ik_4, \quad (k_4 << k_3; \quad k_3 > 0, \quad k_4 > 0) \tag{86}$$

The radiation condition (73) requires that $B(s) = 0$; and (69) requires that $D(s) = 0$. Thus,

$$\Phi(x_>) = A(s)e^{-\gamma x} = \hat{\Phi}_+(x_>) + \hat{\Phi}_-(x_>) \tag{87}$$

$$\Phi(x_<) = C(s) \cosh \gamma_1 x = \hat{\Phi}_+(x_<) + \hat{\Phi}_-(x_<) \tag{88}$$

Employing (71) in (87) and (88) yields

$$\hat{\Phi}_+(b_+) - \hat{\Phi}_+(b_-) = A(s)e^{-\gamma b} - C(s) \cosh \gamma_1 b \tag{89}$$

Similarly, from (72), (87) and (88) one obtains

$$\varepsilon_r \hat{\Phi}'_+(b_+) - \hat{\Phi}'_+(b_-) = -\varepsilon_r \gamma A(s)e^{-\gamma b} - \gamma_1 C(s) \sinh \gamma_1 b \tag{90}$$

where primes indicate differentiation w.r.t. x. Employing (70), and (78) in (90), one arrives at the following result after some manipulations (and the use of (64))

$$(91) \qquad \varepsilon_r \gamma A(s) e^{-\gamma b} = -\gamma_1 \, C(s) \sinh \gamma_1 b$$

One next defines

$$(92) \qquad J_+(s) \equiv \hat{\Phi}_+(b_-) - \hat{\Phi}_+(b_+)$$

Utilizing (91) and (92) into (89) gives

$$(93) \qquad -J_+(s) = \gamma A(s) e^{-\gamma b} \, G^{-1}(s)$$

where

$$(94) \qquad G(s) \equiv (\gamma\gamma_1 \sinh \gamma_1 b)(\gamma_1 \sinh \gamma_1 b + \varepsilon_r \gamma \cosh \gamma_1 b)^{-1}$$

From the fact that

$$(95) \qquad \hat{\Phi}'_+(b_+) + \hat{\Phi}'_-(b_+) = -\gamma A(s) e^{-\gamma b},$$

and

$$(96) \qquad \hat{\Phi}'_+(b_+) = -\hat{\Phi}^{i\,\prime}_+(b_+) \, ,$$

one obtains

$$(97) \qquad -\hat{\Phi}^{i\,\prime}_+(b_+) + \hat{\Phi}'_-(b_+) = -\gamma A(s) e^{-\gamma b} \, .$$

Finally, incorporating (97) into (93) and using (78) allows one to obtain a Wiener-Hopf equation

$$(98) \qquad J_+(s)\,G(s) = \hat{\Phi}'_-(b_+) + \frac{i\alpha}{\sqrt{2\pi}\,(s+\beta)}$$

From the behavior of $\phi(x,z)$ and $\partial\phi(x,z)/\partial x$ as $|z| \to \infty$, it is evident that the transform $\Phi(x_>)$ is analytic in $|\tau| < k_2$; whereas, $\Phi(x_<)$ is analytic in $|\tau| < k_4$. Also, $J_+(s)$ is analytic for $\tau > -[\text{Min}(k_2,k_4)]$. $G(s)$ is analytic for $|\tau| < \text{Min}(k_2,k_4)$, and $\hat{\Phi}'_-(b_+)$ is analytic for $\tau < k_2$. Thus, (98) is analytic in the strip $|\tau| < \text{Min}(k_2,k_4)$. One begins solving (98) by factorizing $G(s)$, i.e.

$$(99) \qquad G(s) = G_+(s)\,G_-(s)$$

Where G_+ is analytic in the U.H.P. (i.e., for $\tau > -\text{Min}(k_2,k_4)$) and G_- is analytic in the L.H.P. (i.e, for $\tau < \text{Min}(k_2,k_4)$). The factorization functions $G_\pm(s)$ for this problem are derived in Appendix II via a formal factorization procedure since the limiting type factorization scheme indicated in Appendix I is shown to cause convergence problems in the integral representations for the factors $G_\pm(s)$ (see section III of Appendix I for these details). The use of (99) in (98) yields

$$(100) \qquad G_+(s)J_+(s) = \frac{\hat{\Phi}'_-(b_+)}{G_-(s)} + \frac{i\alpha}{\sqrt{2\pi}G_-(s)(s+\beta)}$$

The R.H.S. of (100) is analytic in L.H.P. except at $s=-\beta$. It is convenient to put the preceeding equation into the form

$$(101) \qquad G_+(s)J_+(s) - \frac{i\alpha}{\sqrt{2\pi}G_-(-\beta)(s+\beta)} = \frac{\hat{\Phi}'_-(b_+)}{G_-(s)} + \frac{i\alpha}{\sqrt{2\pi}(s+\beta)}\,[G_-^{-1}(s) - G_-^{-1}(-\beta)]$$

The L.H.S. of (101) is analytic in the U.H.P.; whereas, the R.H.S. of (101) is now analytic in the L.H.P. Hence, the R.H.S. and the L.H.S. of (101) together define an entire function denoted by $P(s)$. Since $G(s) \sim O(s)$ as $|s| \to \infty$ in the strip of analyticity, $G_\pm(s) \sim O(s^{1/2})$ as $|s| \to \infty$, in their regions of analyticity. The edge condition for this problem dictates that the magnetic field intensity must behave as $\rho^{+1/2}$ in the neighborhood of the edge as $\rho \to 0$ (ρ = radial distance away from the edge at $x = 0$, $z = 0$), which correspondingly implies that $J_+(s) \sim O(s^{-3/2})$ as $|s| \to \infty$ in the strip (since $J_+(s)$ may be interpreted as the transform of the current density on the plate at $x = b$ for $z > 0$); the edge condition for this problem is deduced by

an application of the technique described in [9]. The entire function P(s) therefore equals zero from the asymptotic conditions for large s. Hence, each side of (101) is zero. It follows that

$$(102) \qquad J_+(s) = \frac{i\alpha}{\sqrt{2\pi}G_+(s)G_-(-\beta)(s+\beta)}$$

Utilizing (102) in (93) gives

$$(103) \qquad A(s) = \frac{-i\alpha e^{\gamma b} G_-(s)}{\sqrt{2\pi}\gamma G_-(-\beta)(s+\beta)}$$

From (103) and (91), one can obtain an expression for C(s) in terms of known quantities. Incorporating this value of C(s) in (87), and the above value of A(s) in (88) one obtains

$$(104) \qquad \hat{\Phi}(x_>,s) = \frac{-i\alpha e^{\gamma b} G_-(s) e^{-\gamma x_>}}{\sqrt{2\pi}\gamma\, G_-(-\beta)(s+\beta)} \quad ,$$

and

$$(105) \qquad \hat{\Phi}(x_<,s) = \frac{i\varepsilon_r\alpha\, G_-(s)\cosh \gamma_1 x_<}{\sqrt{2\pi}\gamma_1 \sinh\gamma_1 b\, G_-(-\beta)(s+\beta)}$$

Finally, inverse transforming (104) and (105) yields

$$(106) \qquad \Phi(x_>,z) = \frac{1}{2\pi}\int_{-\infty}^{\infty} \frac{-i\alpha G_-(s) e^{-\gamma(x_>-b)}}{\gamma G_-(-\beta)(s+\beta)}\, e^{-isz} ds$$

and

$$(107) \qquad \Phi(x_<,z) = \frac{1}{2\pi}\int_{-\infty}^{\infty} \frac{i\varepsilon_r\alpha G_-(s)\cosh \gamma_1 x_<}{\gamma_1 \sinh\gamma_1 b\, G_-(-\beta)(s+\beta)}\, e^{-isz} ds$$

thereby completing the formal solution to this canonical problem. One may close the integration contours along the real axis in (106) and (107) by semi-circular contours at infinity (except for the deformations around the branch cuts) so that the fields represented by $\Phi(x_>,z)$ and $\Phi(x_<,z)$ may be calculated via Cauchy's residue theorem. The semi-circular contours at infinity provide vanishing contributions to the integral. If one closes these contours defined along the real axis by a semi-circular contour at infinity in the U.H.P., the fields for the region $z < 0$ are obtained; whereas, if one closes the path of integration defined on the real axis by a semi-circular contour at infinity in the L.H.P., the fields for the region $z > 0$ are obtained. The pertinent contours in the complex s-plane are shown in Fig. 10. Clearly, the residue at the pole $s = -\beta$ in the L.H.P. which is obtained by closing the contour of integration in the L.H.P. exactly cancels the incident field for $z > 0$, as was anticipated.

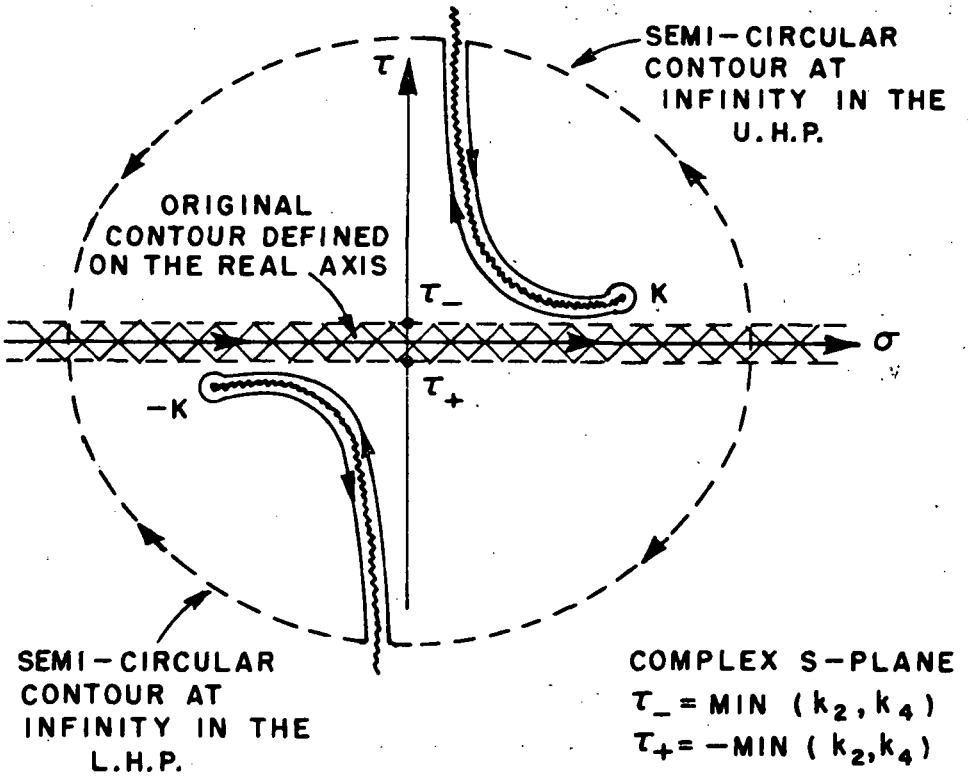

Fig. 10 -- Contours of integration in the complex s-plane which occur in the solution to the auxiliary canonical problems.

The diffracted field in region Ⓐ may be obtained from (106) via an asymptotic approximation to the integral. This diffracted field arises from the branch cut contributions to (106). One begins by introducing the usual polar transformations

$$(108a) \qquad s = k \sin \hat{\alpha}, \quad \sqrt{k^2-s^2} = k \cos \hat{\alpha}$$

and

$$(108b) \qquad x = \rho \cos \phi, \quad z = \rho \sin \phi \ .$$

Incorporating the above transformations into (106) leads to the following integral along the contour $C_{\hat{\alpha}}$ in the complex $\hat{\alpha}$-plane

$$(109) \qquad \Phi(\rho,\phi) = \frac{\alpha}{2\pi} \int_{C_{\hat{\alpha}}} \frac{G_-(k \sin \hat{\alpha}) e^{ik\rho\cos(\hat{\alpha}+\phi)}}{G_-(-\beta)(k \sin \hat{\alpha} + \beta)} \, e^{-ikb \cos \hat{\alpha}} d\hat{\alpha} \ .$$

The quantities ρ and ϕ are indicated in Fig. 8a. The contour $C_{\hat{\alpha}}$ may be deformed into the steepest descent contour for the above integral in the $\hat{\alpha}$-plane, and the resulting integral may then be asymptotically evaluated for large $k\rho$ by the saddle point method, to give the result for the diffracted field denoted by Φ^d as

$$(110) \qquad \Phi^d(\rho,\phi) \sim F^A(\phi) \frac{e^{ik\rho}}{\sqrt{\rho}}$$

where

$$(111) \qquad F^A(\phi) \equiv \frac{\alpha G_-(-k \sin \phi) e^{-ikb \cos \phi}}{\sqrt{2\pi k} \, G_-(-\beta)(\beta - k \sin \phi)} \, e^{-i\frac{\pi}{4}} \ .$$

Since the surface wave incident on the discontinuity at $z = 0$ in Fig. 8a has unit amplitude, it is apparent that $F^A(\phi)$ is a diffraction coefficient for this auxiliary problem. It is interesting that it has the same form as the diffraction coefficient D_1 for the diffraction of a surface wave by a discontinuity in surface reactance (see (59)) except for the factor $e^{-ikb \cos \phi}$ which is due to a difference in the origin of the coordinates for the two problems.

The TM_0 surface wave which is reflected from ① is obtained from the residue at the pole $s = \beta$ of $G_-(s)$ in (106) for the reflected surface wave in the region $x \geq b$ and $z < 0$ (i.e., for the part of region Ⓐ for which $z < 0$), or from the residue at the pole $s = \beta$ of $G_-(s)$ in (107) for the reflected surface wave in region Ⓑ (i.e., $0 \leq x \leq b$; $z < 0$). The result for the reflected surface wave field in region Ⓐ (for $z < 0$) which is denoted by Φ^r is indicated below; it is obtained in a straightforward manner by closing the contour of integration in (106) by a semi-circular contour at infinity in the U.H.P. and evaluating the residue at $s = \beta$, and by replacing $G_-(s)$ in (106) by $G(s)/G_+(s)$ for convenience.

$$\Phi^r = \frac{\mathcal{R}_0\, e^{-\alpha(x-b)}\, e^{-i\beta z}}{G_-(-\beta)G_+(\beta)2\beta} \qquad ;\ x \geq b,\ z < 0 \tag{112}$$

where

$$\mathcal{R}_0 \equiv \text{Residue of } G(\beta) = \lim_{s\to\beta} (s-\beta)\, G(s) \tag{113a}$$

Using (94), $\mathcal{R}_0$ is found to be

$$\mathcal{R}_0 = \frac{-\varepsilon_r \alpha (\alpha\sqrt{k_d^2 - \beta^2})^2}{\beta[\varepsilon_r(k_d^2-k^2)+\alpha b(k_d^2-\beta^2+\varepsilon_r^2\alpha^2)]} \tag{113b}$$

One may now express Φ^r above as

$$\Phi^r = R^{SW}\, e^{-\alpha(x-b)} e^{-i\beta z} \qquad ;\ x \geq b,\ z < 0 \tag{114}$$

where R^{SW} is the TM_0 surface wave reflection coefficient at ①.

$$R^{SW} \equiv \frac{\mathcal{R}_0}{2\beta G_-(-\beta)G_+(\beta)} = \frac{\mathcal{R}_0}{2\beta\, G_+^2(\beta)} \tag{115}$$

(since $G_-(-s) = G_+(s)$ as indicated in Appendix II).

The fields transmitted into region Ⓒ are given by the residues at the poles of $(\gamma_1 \sinh \gamma_1 b)^{-1}$ in the integrand of (107). Before evaluating this contribution it is convenient to re-write (107) as

$$(116) \qquad \Phi(x_<,z) = \frac{-1}{2\pi} \int_{-\infty}^{\infty} \frac{i\varepsilon_r \alpha G_-(s)\cos\sqrt{k_d^2-s^2}\,x_< \; e^{-isz}}{\sqrt{k_d^2-s^2}\,\sin\sqrt{k_d^2-s^2}\,b\; G_+(\beta)(s+\beta)}\, ds$$

The zeros of $\sqrt{k_d^2-s^2}\,\sin\sqrt{k_d^2-s^2}\,b$ corresponding to the fields for $z>0$ occur at $s = -\beta_m$. β_m is given by

$$(117) \qquad \beta_m = \sqrt{k_d^2 - \left(\frac{m\pi}{b}\right)^2} \; ; \quad m = 0, 1, 2, \cdots .$$

The fields transmitted into the waveguide region Ⓒ are thus obtained by closing the contour for (116) in the L.H.P. and by summing up the residues contributions arising from the poles of

$$(\sqrt{k_d^2-s^2}\,\sin\sqrt{k_d^2-s^2}\,b)^{-1} \text{ at } s = -\beta_m.$$

Let the transmitted field in region Ⓒ be denoted by Φ^t.

$$(118) \qquad \Phi^t = -\varepsilon_r \alpha \sum_{m=0}^{\infty} \frac{G_-(-\beta_m)\cos\frac{m\pi}{b}\,x_< \; e^{i\beta_m z}}{\left\{\frac{d}{ds}\left(\sqrt{k_d^2-s^2}\,\sin\sqrt{k_d^2-s^2}\,b\right)\right\}_{s=-\beta_m} G_+(\beta)(\beta-\beta_m)}$$

or

$$(119) \qquad \Phi^t = \begin{cases} -\dfrac{\varepsilon_r \alpha G_+(k_d) e^{ik_d z}}{2bk_d G_+(\beta)(\beta-k_d)} \;, & \text{for } m = 0 \\[2ex] -\varepsilon_r \alpha \displaystyle\sum_{m=1}^{\infty} \dfrac{G_-(-\beta_m)\cos\frac{m\pi}{b}\,x\; e^{i\beta_m z}}{(-1)^m b\beta_m G_+(\beta)(\beta-\beta_m)} \;, & \text{for } m\neq 0 \\ & \text{and } m=1,2,3,\cdots \end{cases}$$

Φ^t may be expressed as

$$(120) \qquad \Phi^t = \sum_{m=0}^{\infty} T_m \cos\frac{m\pi}{b}\,x_< \; e^{i\beta_m z} \quad ; \text{ for } 0 \leq x \leq b \text{ and } z > 0$$

where T_m denote the modal coefficients of the fields transmitted into region Ⓒ. From (119) and (120) one may define T_m as

$$(121) \qquad T_m \equiv - \frac{\varepsilon_r \, \alpha G_+(\beta_m)}{\Delta_m (-1)^m \beta_m b \; G_+(\beta)(\beta - \beta_m)}$$

with

$$\Delta_m = \begin{cases} 2 & \text{for } m = 0 \\ 1 & \text{for } m \neq 0 \end{cases}$$

The generalized scattering matrix s_{11} for junction ① describes the fields scattered in regions Ⓐ and Ⓑ when a TM_0 surface wave is incident at junction ①; this scattered field is composed of a reflected TM_0 surface wave field and a diffracted field contribution. If one is interested in the reflected surface wave calculation, one defines s_{11} to be R^{SW} of (115); on the other hand, if one is interested in calculating the diffracted field in region Ⓐ, one defines s_{11} to be $F^A(\phi)$ of (111). Thus,

$$(122) \qquad s_{11} \equiv \begin{cases} R^{SW}, & \text{for reflected surface wave field calculations in regions Ⓐ (for } z<0), \text{ and Ⓑ} \\ F^A(\phi), & \text{for diffracted field calculations in region Ⓐ.} \end{cases}$$

The generalized scattering matrix s_{21} represents the modal coefficients of the field transmitted into the waveguide region Ⓒ when a TM_0 surface wave is incident at ① from the left. The field transmitted into Ⓒ is given by (120). Hence, s_{21} may be conveniently represented by a matrix whose elements are T_0, T_1, T_2, $\cdots$ T_m $\cdots$, where T_m is defined in (121). Thus, one defines s_{21} as

$$(123) \qquad s_{21} \equiv [T_0 \; T_1 \; T_2 \cdots T_m \cdots]^T_{1 \times M}$$

where T is the transpose operator. s_{21} is an M x 1 matrix in which $M \to \infty$.

Derivation of s_{12} and s_{22}

The generalized scattering matrices s_{12} and s_{22} are obtained from the solution of the auxiliary problem illustrated in Fig. 9b. The excitation for this problem is a TM_{on} waveguide mode which is incident at ① from the waveguide region ⓒ (i.e., from the right). One denotes the y-component of the incident, scattered and the total magnetic field intensities by Φ_n^i, Φ_n and Φ_n^t, respectively. Then $\Phi_n = \Phi_n^t - \Phi_n^i$ where the incident field, Φ_n^i is assumed to exist even for $z < 0$ for convenience of analysis. The final solution will contain a contribution to Φ_n which exactly cancels the incident field for $z < 0$. The form of the incident field Φ_n^i is

$$\Phi_n^i = \cos \frac{n\pi}{b} x \, e^{-i\beta_n z} \; ; \quad \text{for } 0 \leq x \leq b \text{ and } |z| < \infty \tag{124}$$

where

$$\beta_n = \sqrt{k_d^2 - \left(\frac{n\pi}{b}\right)^2} \; ; \quad n = 0, 1, 2 \cdots \tag{125}$$

and k_d has been defined in (65). Bates and Mittra [2], and Angulo and Chang [15], have solved the problem illustrated in Fig. 9b for the special case when the structure is excited by a TEM waveguide mode; this corresponds to the $n = 0$ case in our problem. Φ_n^i satisfies the 2-D, reduced wave equation

$$\left(\frac{\partial^2}{\partial x^2} + \frac{\partial^2}{\partial z^2} + k_d^2\right) \Phi_n^i = 0; \quad 0 \leq x \leq b, \; |z| < \infty \tag{126}$$

$\Phi_n^i = 0$ everywhere else. Also, Φ_n^t satisfies the 2-D, reduced wave equation; hence, Φ_n must satisfy

$$\left(\frac{\partial^2}{\partial x^2} + \frac{\partial^2}{\partial z} + k^2\right) \Phi_n(x,z) = 0; \quad \text{for } x \geq b, \; |z| < \infty \tag{127}$$

and

$$\left(\frac{\partial^2}{\partial x^2} + \frac{\partial^2}{\partial z^2} + k_d^2\right) \Phi_n(x,z) = 0; \quad \text{for } 0 \leq x \leq b, \; |z| < \infty \tag{128}$$

In addition, Φ_n satisfies the following boundary conditions and the radiation condition.

(129) $$\left.\frac{\partial \Phi_n}{\partial x}\right|_{x=b} = 0, \text{ for } z > 0$$

(130) $$\left.\frac{\partial \Phi_n}{\partial x}\right|_{x=0} = 0, \text{ for } |z| < \infty$$

(131) $$\Phi_n|_{x=b_+} = (\Phi_n^i + \Phi_n)|_{x=b_-}, \quad \text{for } z < 0$$

(132) $$\left.\frac{\partial \Phi_n}{\partial x}\right|_{x=b_+} = \frac{1}{\varepsilon_r}\frac{\partial}{\partial x}(\Phi_n^i + \Phi_n)|_{x=b_-}, \quad \text{for } z < 0$$

(133) Φ_n satisfies the radiation condition as $|(x^2+z^2)^{1/2}| \to \infty$ for an $e^{-i\omega t}$ time dependence.

As before, one defines

(134) $$\hat{\Phi}_n(x,s) \equiv \frac{1}{\sqrt{2\pi}}\int_{-\infty}^{\infty} \Phi_n(x,z)e^{isz}\,dz = \hat{\Phi}_n^+(x,s) + \hat{\Phi}_n^-(x,s)$$

where

(135)
$$\hat{\Phi}_n^+(x,s) \equiv \frac{1}{\sqrt{2\pi}}\int_0^{\infty} \Phi_n(x,z)e^{isz}dz; \quad \hat{\Phi}_n^-(x,s) \equiv \frac{1}{\sqrt{2\pi}}\int_{-\infty}^{0} \Phi_n(x,z)e^{isz}dz$$

Similarly,

(136) $$\hat{\Phi}_n^{i-}(x,s) \equiv \frac{1}{\sqrt{2\pi}}\int_{-\infty}^{0} \Phi_n^i(x,z)e^{isz}dz = \cos\left(\frac{n\pi x}{b}\right)\left\{\frac{-i}{\sqrt{2\pi}(s-\beta_n)}\right\}$$

and

$$(137)\quad \frac{\partial}{\partial x}\hat{\Phi}_n^{i-}(x,s) = \frac{1}{\sqrt{2\pi}}\int_{-\infty}^{0}\frac{\partial}{\partial x}\Phi_n^{i}(x,z)e^{isz}dz$$
$$= -\frac{n\pi}{b}\sin\frac{n\pi}{b}x\left\{\frac{-i}{\sqrt{2\pi}(s-\beta_n)}\right\}$$

Fourier transforming (127) and (128) w.r.t. z gives

$$(138)\quad \left(\frac{\partial^2}{\partial x^2} - \gamma^2\right)\hat{\Phi}_n(x_>,s) = 0$$

$$(139)\quad \left(\frac{\partial^2}{\partial x^2} - \gamma_1^2\right)\hat{\Phi}_n(x_<,s) = 0$$

where γ and γ_1 are identical to (83) and (84). Also $x_>$ and $x_<$ have the same meaning as before. The general solutions to (138) and (139) are

$$(140)\quad \hat{\Phi}_n(x_>,s) = \hat{\Phi}_n(x_>) = A(s)e^{-\gamma x_>} + B(s)e^{\gamma x_>}$$

$$(141)\quad \hat{\Phi}_n(x_<,s) = \hat{\Phi}_n(x_<) = C(s)\cosh\gamma_1 x_< + D(s)\sinh\gamma_1 x_<$$

$B(s) = 0$ and $D(s) = 0$ from (133) and (130), respectively. Thus,

$$(142)\quad \hat{\Phi}_n(x_>,s) = \hat{\Phi}_n^{+}(x_>) + \hat{\Phi}_n^{-}(x_>) = A(s)e^{-\gamma x}$$

$$(143)\quad \hat{\Phi}_n(x_<,s) = \hat{\Phi}_n^{+}(x_<) + \hat{\Phi}_n^{-}(x_<) = C(s)\cosh\gamma_1 x\ .$$

The steps leading to the final solution for $\Phi_n(x,z)$ are similar to those previously followed in the derivation of s_{11} and s_{21}.

From (129) it follows that

$$(144) \qquad \hat{\Phi}_n^{+\prime}(x=b_{\pm}) = 0$$

Using (132) together with (144) yields

$$(145) \qquad -\varepsilon_\gamma \gamma A(s)e^{-\gamma b} = \gamma_1 C(s)\sinh \gamma_1 b$$

From (131) one obtains

$$(146) \qquad \hat{\Phi}_n^{-}(b_+) = \frac{(-1)^n(-i)}{\sqrt{2\pi}(s - \beta_n)} + \hat{\Phi}_n^{-}(b_-)$$

(Eq. (136) has been used in obtaining (146)). One may re-write (146) via (142) and (143) as

$$(147) \qquad A(s)e^{-\gamma b}\hat{\Phi}_n^{+}(b_+) = \frac{(-1)^n(-i)}{\sqrt{2\pi}(s - \beta_n)} + C(s)\cosh \gamma_1 b - \hat{\Phi}_n^{+}(b_-)$$

It is convenient to define

$$(148) \qquad J^+(s) \equiv \hat{\Phi}_n^{+}(b_-) - \hat{\Phi}_n^{+}(b_+)$$

Equation (147) becomes via (148)

$$(149) \qquad A(s)e^{-\gamma b} - C(s)\cosh\gamma_1 b = \frac{(-1)^n(-i)}{\sqrt{2\pi}(s - \beta_n)} - J^+(s)$$

Eliminating C(s) between (145) and (149) leads to

$$(150) \qquad \gamma A(s)e^{-\gamma b}\, G^{-1}(s) = \frac{(-i)(-1)^n}{\sqrt{2\pi}(s - \beta_n)} - J^+(s)$$

in which G(s) is identical to that in (94). One notes from (142) and (144) that $A(s)e^{-\gamma b}$ is given by

$$(151) \qquad -\gamma A(s)e^{-\gamma b} = \hat{\Phi}_n^{+\prime}(b_+) + \hat{\Phi}_n^{-\prime}(b_+) = \hat{\Phi}_n^{-\prime}(b_+)$$

Utilizing (151) in (150) yields the Wiener-Hopf equation

$$(152) \qquad G^{-1}(s)\,\hat{\Phi}_n^{-\prime}(b_+) = J^+(s) + \frac{i(-1)^n}{\sqrt{2\pi}(s - \beta_n)}$$

From the behavior of ϕ_n and $\partial\phi_n/\partial x$ as $|z| \to \infty$, it is evident that $\hat{\phi}_n^{-\prime}(b_+)$ is analytic for $\tau < k_2$ and $J^+(s)$ is analytic for $\tau > -\mathrm{Min}(k_2,k_4)$. Also G(s) is analytic for $|\tau| < \mathrm{Min}(k_2,k_4)$. Hence, one notes that Eq. (152) is analytic in the strip $|\tau| < \mathrm{Min}(k_2,k_4)$. Factorizing G(s) into $G_+(s)G_-(s)$ leads to

$$(153) \qquad \hat{\Phi}_n^{-\prime}(b_+)G_-^{-1}(s) = J^+(s)G_+(s) + \frac{i(-1)^n G_+(s)}{\sqrt{2\pi}(s - \beta_n)}$$

The L.H.S. of (153) is analytic in the L.H.P.; whereas, the R.H.S. of (153) is analytic in the U.H.P., except at $s = \beta_n$. For convenience, (153) is re-written as

$$(154) \qquad \hat{\Phi}_n^{-\prime}(b_+)G_-^{-1}(s) - \frac{i(-1)^n G_+(\beta_n)}{\sqrt{2\pi}(s - \beta_n)} = J^+(s)G_+(s) + \frac{i(-1)^n}{\sqrt{2\pi}(s - \beta_n)}\{G_+(s) - G_+(\beta_n)\}$$

The L.H.S. of (154) is analytic in the L.H.P.; whereas the R.H.S. is analytic in the U.H.P. Thus, the two sides of (154) together define an entire function Q(s) which can be determined from the asymptotic behavior of (154) as $|s| \to \infty$. As before, $G_\pm(s) \sim O(s^{1/2})$ as $|s| \to \infty$ in their respective regions of analyticity. The edge condition for this problem dictates that the electric field intensity

can become singular no faster than $\rho^{-1/2}$ in the neighborhood of the edge (at $x = 0$, $z = 0$) as $\rho \to 0$; since the transform of the electric field is proportional to $\hat{\phi}_n^{-'}$, the edge condition therefore implies that $\hat{\phi}_n^{-'}(b_+) \sim 0\ (s^{-1/2})$ as $|s| \to \infty$ in the strip. This is also deduced via techniques discussed in [9]. Thus, one concludes that $Q(s) = 0$ from the asymptotic conditions for large s. It follows that the L.H.S. and the R.H.S. of (154) are each equal to zero; hence,

$$(155) \qquad \hat{\Phi}_n^{-'}(b_+) = \frac{i(-1)^n G_+(\beta_n) G_-(s)}{\sqrt{2\pi}(s - \beta_n)}$$

Equation (154) via (151) becomes

$$(156) \qquad -\gamma A(s) e^{-\gamma b} = \frac{i(-1)^n G_+(\beta_n) G_-(s)}{\sqrt{2\pi}(s - \beta_n)}$$

Also using (145) in (156) one gets

$$(157) \qquad \frac{1}{\varepsilon_r} \gamma_1 C(s) \sinh \gamma_1 b = \frac{i(-1)^n G_+(\beta_n) G_-(s)}{\sqrt{2\pi}(s - \beta_n)}$$

Incorporating the values of A(s) and C(s) from (156) and (157) into (142) and (143), respectively leads to

$$(158) \qquad \hat{\Phi}_n(x_>, s) = \frac{-i(-1)^n G_+(\beta_n) G_-(s)}{\sqrt{2\pi}\ \gamma(s - \beta_n)} e^{-\gamma(x_> - b)}$$

and

$$(159) \qquad \hat{\Phi}_n(x_<, s) = \frac{i(-1)^n \varepsilon_r G_+(\beta_n) G_-(s)}{\sqrt{2\pi}(s - \beta_n)\gamma_1 \sinh \gamma_1 b} \cosh \gamma_1 x_<$$

The formal solution to this problem is now complete since $\Phi_n(x_>, z)$ and $\Phi_n(x_<, z)$ are respectively obtained from (158) and (159) by the inverse transformation. Thus,

$$(160)\qquad \Phi_n(x_>,z) = \frac{1}{2\pi}\int_{-\infty}^{\infty} \frac{-i(-1)^n G_+(\beta_n)G_-(s)}{\gamma(s-\beta_n)}\, e^{-\gamma(x_>-b)}\, e^{-isz}\, ds$$

and

$$(161)\qquad \Phi_n(x_<,z) = \frac{1}{2\pi}\int_{-\infty}^{\infty} \frac{i(-1)^n \varepsilon_r\, G_+(\beta_n)G_-(s)}{(s-\beta_n)\,\gamma_1 \sinh \gamma_1 b}\, \cosh \gamma_1 x_<\, e^{-isz}\, ds$$

As before, the integrals in (160) and (161) may be evaluated via the Cauchy Residue theorem after closing the contours defined on the real axis by semi-circular contours at infinity. The semi-circular contours at infinity give vanishing contributions to the integral. The pertinent contours in the U.H.P. and the L.H.P. are indicated in Fig. 10. The fields for $z > 0$ are obtained by closing the contour of integration in the L.H.P. Whereas the fields for $z < 0$ are obtained by closing the contour of integration in the U.H.P.

The field radiated into region Ⓐ is obtained from (160) via an asymptotic approximation to the integral. This radiation field arises from the branch cut contribution to (160). Introducing the polar transformations given by (108a,108b) into (160), and deforming the transformed contour of integration in the $\hat{\alpha}$ plane to the steepest descent path provides one with the necessary form of the integral for a saddle point evaluation. The saddle point result which is valid for large $k\rho$ yields an expression for the radiated field denoted by Φ^{rad} as

$$(162)\qquad \Phi^{rad}(\rho,\phi) \sim F_n^B(\phi)\, \frac{e^{ik\rho}}{\sqrt{\rho}}$$

where

$$(163)\qquad F_n^B(\phi) \equiv \frac{(-1)^{n+1} G_+(\beta_n)G_-(-k\sin\phi)\, e^{-i\left[kb\cos\phi + \frac{\pi}{4}\right]}}{\sqrt{2\pi k}\,(k\sin\phi + \beta_n)}\ ;\ n=0,1,2,\cdots$$

(Figure 8a illustrates the coordinates ρ and ϕ for the observation point.)

The TM_0 surface wave which is launched into regions Ⓑ and Ⓐ (for $z < 0$) due to the TM_{0n} waveguide mode incident at ① (from Ⓒ) may be obtained from the residue at the pole $s = \beta$ of $G_-(s)$ in (160) for region Ⓐ (for $z < 0$), or from the residue at the pole $s = \beta$ of $G_-(s)$ in (161) for region Ⓑ. The residue corresponding to the pole at $s = \beta$ is obtained by closing the

contour of integration in the U.H.P. The result for the TM_0 surface wave launched into region Ⓐ (for $z < 0$) is denoted by Φ_n^{sw}, where

$$(164) \qquad \Phi_n^{sw} = T_n^{sw}\, e^{-\alpha(x-b)}\, e^{-i\beta z} \quad ; \quad x \geq b, \quad z < 0$$

in which T_n^{sw} is the surface wave launching coefficient given by

$$(165) \qquad T_n^{sw} \equiv \frac{(-1)^n G_+(\beta_n)\mathcal{R}_0}{\alpha G_+(\beta)(\beta-\beta_n)} \quad ; \quad n = 0, 1, 2, \cdots$$

and $\mathcal{R}_0$ was defined earlier in (113). One notes that $G_-(s)$ in (160) has been replaced by $G(s)/G_+(s)$ to arrive at (165).

Finally, the fields reflected back into the waveguide region Ⓒ are given by the sum of the residues corresponding to the poles at at $s = -\beta_m$ of $(\gamma_1 \sinh \gamma_1 b)^{-1}$ in the integrand of (161). The residues at these poles are obtained by closing the contour of integration in the L.H.P. Before evaluating these residues, it is convenient to re-write (161) as

$$(166) \qquad \Phi_n(x_<, z) = \frac{-i(-1)^n \varepsilon_r G_+(\beta_n)}{2\pi} \int_{-\infty}^{\infty} \frac{G_-(s)\cos\sqrt{k_d^2-s^2}\, x_<\; e^{-isz}}{\sqrt{k_d^2-s^2}\, \sin\sqrt{k_d^2-s^2}\, b\; (s-\beta_n)}\, ds$$

As indicated earlier, the poles of $(\sqrt{k_d^2-s^2}\, \sin\sqrt{k_d^2-s^2}\, b)^{-1}$ corresponding to fields in the region $z > 0$ occur at $s = -\beta_m$. Thus, the field scattered back into Ⓒ which is denoted by Φ_s is given as

$$(167) \qquad \Phi_s = (-1)^n \varepsilon_r G_+(\beta_n) \sum_{m=0}^{\infty} \frac{G_-(-\beta_m)\cos\frac{m\pi}{b} x_<\; e^{i\beta_m z}}{\left\{\frac{d}{ds}\left(\sqrt{k_d^2-s^2}\, \sin\sqrt{k_d^2-s^2}\, b\right)\right\}_{s=-\beta_m} (\beta_m+\beta_n)}$$

One may therefore express Φ_s in (167) as

$$(168) \qquad \Phi_s = \sum_{m=0}^{\infty} R_{mn} \cos\frac{m\pi}{b} x_<\; e^{i\beta_m z}$$

where R_{mn} denotes the reflection coefficient at ① for an mth waveguide mode reflected back into region ⓒ due to an nth waveguide mode incident at ① . R_{mn} is thus given by

$$(169) \qquad R_{mn} \equiv \frac{(-1)^{n-m}\,\varepsilon_r G_+(\beta_n) G_+(\beta_m)}{\Delta_m(\beta_m+\beta_n)\beta_m b}$$

where

$$(170) \qquad \Delta_m = \begin{cases} 2, & \text{for } m = 0 \\ 1, & \text{for } m \neq 0 \end{cases}$$

(in going from (167) to (169), one again uses the relationship $G_-(-s) = G_+(s)$ which is indicated in Appendix II).

The generalized scattering matrix s_{12} describes the fields produced in regions Ⓐ and Ⓑ by a TM_{on} waveguide mode which is incident at ① from the waveguide region ⓒ (i.e., from the right). The fields produced by the incident TM_{on} mode consist of the radiation field in regions Ⓐ and Ⓑ, and a TM_0 surface wave field which is launched into regions Ⓑ and Ⓐ (for $z < 0$). If one is interested in calculating the radiation field produced in region Ⓐ, then one defines s_{12} to be $F_n^B(\phi)$ of (163); whereas, if one is interested in calculating the TM_0 surface wave field which is launched into regions Ⓐ (for $z < 0$) and Ⓑ, then s_{12} is defined to be T_n^{sw} of (165). Thus,

$$(171) \qquad s_{12} \equiv \begin{cases} T_n^{sw}, & \text{for calculating the surface wave field which is launched into regions Ⓐ (for } z<0) \text{ and Ⓑ} \\ F_n^B(\phi), & \text{for calculating the fields radiated into region Ⓐ.} \end{cases}$$

Clearly, s_{12} may be expressed as a 1 x M matrix where $M \to \infty$. Thus,

$$(172) \qquad s_{12} = \left[T_0^{sw}\; T_1^{sw} T_2^{sw} \cdots T_n^{sw} \cdots\right]_{1xM}; \quad \text{for regions Ⓐ and Ⓑ (when } z<0)$$

or

$$(173) \qquad s_{12} = \left[F_0^B(\phi)\; F_1^B(\phi)\; F_2^B(\phi)\; F_3^B(\phi) \cdots F_n^B(\phi) \cdots\right]_{1xM}; \quad \text{for region Ⓐ}$$

The generalized scattering matrix s_{22} represents the modal coefficients of the fields reflected back into Ⓒ due to a TM_{on} waveguide mode incident at ① from Ⓒ. The field reflected back into the waveguide is given by (168). Hence, it is clear the s_{22} is an MxM matrix ($M \to \infty$) whose elements are R_{mn} of (169). Thus,

$$(174) \qquad s_{22} = [R_{mn}]_{MxM} = \begin{bmatrix} R_{00} & R_{01} & R_{02} & \cdots \\ R_{10} & R_{11} & R_{12} & \cdots \\ \cdot & \cdot & \cdot & \\ \cdot & \cdot & \cdot & \\ \cdot & \cdot & \cdot & \end{bmatrix}_{MxM}$$

Determination of the surface wave diffraction coefficient by the GSMT

Referring to Fig. 9a, it is seen that the incident TM_0 surface wave field is scattered by junction ① to produce a diffracted field in region Ⓐ; one denotes its magnetic field by u_1^d, where u_1^d is given via (122) as

$$(175) \qquad u_1^d = s_{11}\, u^i \frac{e^{ik\rho}}{\sqrt{\rho}} = F^A(\phi) u^i \frac{e^{ik\rho}}{\sqrt{\rho}} \text{ ; in region Ⓐ}$$

u^i in (175) denotes the magnetic field of the incident surface wave evaluated at ①. The part of the incident surface wave field which is scattered by ① into region Ⓒ becomes incident at ②, from which it is reflected; this reflected field is incident back at ① where it undergoes further scattering into regions Ⓐ, Ⓑ and Ⓒ, and so on, thereby giving rise to multiple interactions between junctions ① and ②. The fields resulting from these multiple interactions may be expressed in a convergent Neumann series as done by Pace and Mittra[7]; however, an alternate procedure based on a self consistent method leads directly to the same result. The self consistent method will be used in this analysis; the use of this method is described with the aid of Fig. 11. Let u_{12} represent the value of the magnetic field incident at ① from ② after taking all the multiple interactions into consideration. Similarly, let u_{21} represent the value of the magnetic field intensity incident at ② from ① after taking all the multiple interactions into account. The total diffracted field in region Ⓐ denoted by u^d is thus a superposition of the field u_1^d, and u_m^d, the field diffracted into Ⓐ due to u_{12} incident on ①. Thus,

$$(176) \qquad u^d = u_1^d + u_m^d$$

where u_m^d may be expressed as

(177) $$u_m^d = s_{12}u_{12}\frac{e^{ik\rho}}{\sqrt{\rho}} = [F_n^B]u_{12}\frac{e^{ik\rho}}{\sqrt{\rho}}\ ;\ \text{in region } \textcircled{A}.$$

$s_{12} = [F_n^B]$ in this case and F_n^B is defined in (163). The expressions for u_{12} and u_{21} for $\delta \to 0$ (see Fig. 11) are given in terms of s_{21} and s_{22} as

(178) $$u_{21} = s_{21}u^i + s_{22}u_{12}$$

(179) $$u_{12} = \Gamma\, u_{21}$$

where Γ is the generalized matrix for junction ②; it corresponds to the reflection coefficient at ② and it is an identity matrix of infinite order I as mentioned earlier. Eliminating u_{12} between (178) and (179) yields

$$(I - s_{22})u_{21} = s_{21}u^i$$

Hence it follows that

(180) $$u_{21} = (I - s_{22})^{-1}s_{21}u^i$$

From (179) and (180) u_{12} becomes

(181) $$u_{12} = (I - s_{22})^{-1}s_{21}u^i$$

Incorporating (181) in (177) yields

(182) $$u_m^d = s_{12}\,(I - s_{22})^{-1}s_{21}u^i\,\frac{e^{ik\rho}}{\sqrt{\rho}}$$

Finally, combining (175) and (182) according to (176) yields the expression for the diffracted field u^d as

(183) $$u^d = [s_{11} + s_{12}(I - s_{22})^{-1}s_{21}]u^i\,\frac{e^{ik\rho}}{\sqrt{\rho}}$$

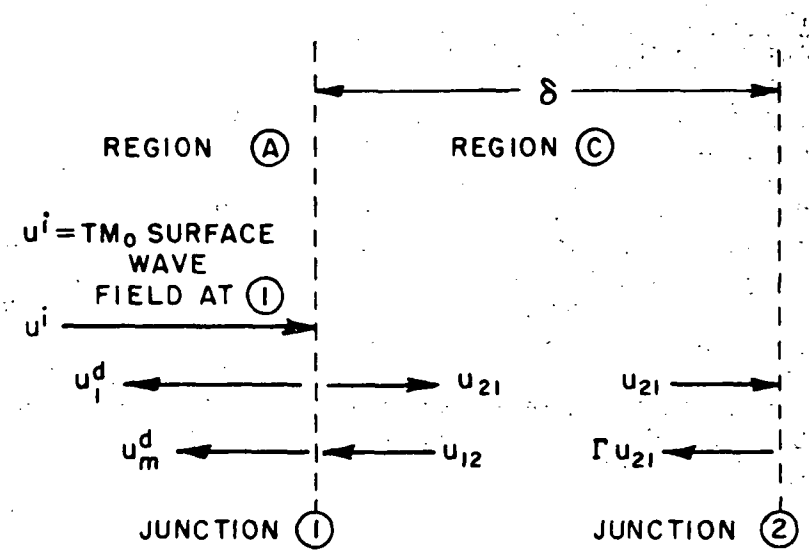

Fig. 11-- Multiple interactions between junctions ① and ② for the calculation of the diffracted field.

Eq. (183) may be written as

$$u^d = D_2\, u^i \frac{e^{ik\rho}}{\sqrt{\rho}} \tag{184}$$

where D_2 is the diffraction coefficient for the canonical problem of the recessed, truncated dielectric cover which is flush mounted in a perfectly-conducting surface (see Fig. 2). Thus, the formal expression for D_2 in terms of the scattering matrices of junctions ① and ② is obtained via (183) and (184).

$$D_2 \equiv s_{11} + s_{12}(I - s_{22})^{-1} s_{21} \tag{185}$$

Since $s_{11} = F^A(\phi)$, and $s_{12} = [F_n^B(\phi)]$, (185) becomes

$$D_2 = F^A(\phi) + [F_n^B(\phi)](I - s_{22})^{-1} s_{21} \tag{186}$$

where s_{22} and s_{21} are given by (174) and (123), respectively.

Determination of the surface wave reflection coefficient by the GSMT

The expression for the surface wave reflection coefficient for the canonical problem illustrated in Fig. 4 is derived in a manner analogous to that for the diffraction coefficient discussed previously. Figure 12 illustrates the self consistent procedure for determining the reflected TM_0 surface wave field for the canonical problem. The reflected TM_0 surface wave field is denoted by u^r. The incident field at ① is denoted by u^i as before. Also, u_{12} and u_{21} used here have the same meaning as in the previous discussion for the diffraction coefficient. The field u^r is a superposition of the field expressible in terms of the scattering matrix s_{11} at ① denoted by u_1^r, and the field contribution due to multiple interactions denoted by u_m^r. Thus

$$u^r = u_1^r + u_m^r \tag{187}$$

where

$$u_1^r = s_{11}\, u^i\, f_{sw} \tag{188}$$

and

$$u_m^r = s_{12} u_{12} f_{sw} \tag{189}$$

The quantity f_{sw} in (188) and (189) is defined by

$$f_{sw} \equiv \begin{cases} e^{-\alpha(x-b)} e^{-i\beta z}, & \text{in region Ⓐ} \quad (\text{for } z<0) \\ \dfrac{\cos k_x x}{\cos k_x b}\, e^{-i\beta z}, & \text{in region Ⓑ}. \end{cases} \tag{190}$$

The quantities α, β and k_x in the expression for f_{sw} are the same as in (62) and (63). Following the procedure for the diffracted field, one may write

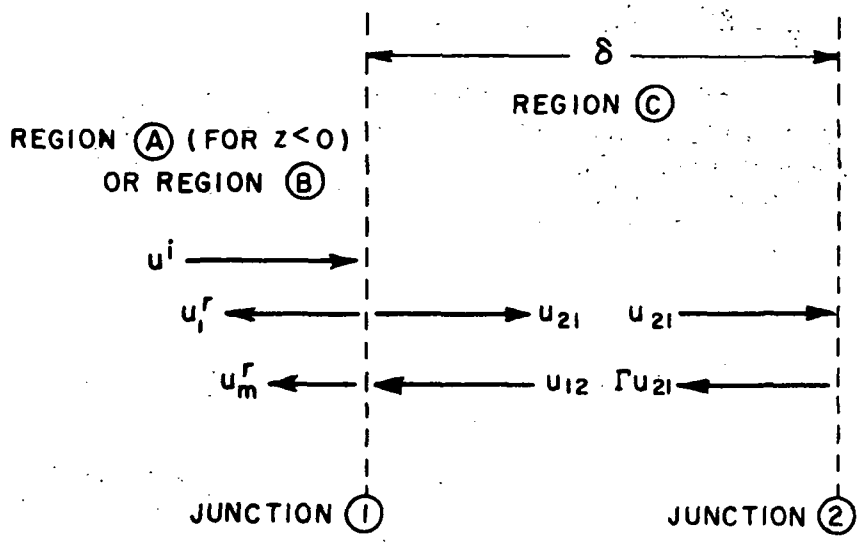

Fig. 12-- Multiple interaction between junctions ① and ② for calculating the reflected surface wave field.

$$u_{12} = (I - s_{22})^{-1} s_{21} u^i \tag{191}$$

so that (189) becomes

$$u_m^r = s_{12}(I - s_{22})^{-1} s_{21} u^i f_{sw} \tag{192}$$

and u^r becomes

$$u^r = \{s_{11} + s_{12}(I - s_{22})^{-1} s_{21}\} u^i f_{sw} \tag{193}$$

The above expression may be written as

$$u^r = R_2 u^i f_{sw} \tag{194}$$

where R_2 is the TM_0 surface wave reflection coefficient for the canonical problem of the recessed, truncated dielectric slab which is flush mounted in a perfectly conducting surface (see Fig. 2). R_2 is given via (193) and (194) as

(195) $$R_2 \equiv R^{SW} + [T_n^{SW}]\,(I - s_{22})^{-1} s_{21}$$

because $s_{11} = R^{SW}$ and $s_{12} = [T_n^{SW}]$ for the surface wave reflection coefficient calculation. R^{SW} and T_n^{SW} are defined in (115) and (165), respectively. The quantities s_{22} and s_{21} are given by (174) and (123), respectively.

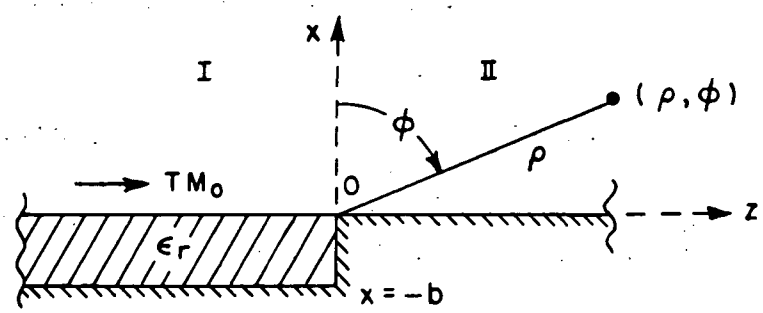

Fig. 13 -- Geometry for the variational solution.

B. Solution Based on the Variational Technique

In this section, a variational solution to the canonical problem is briefly indicated. The geometry for the problem is indicated in Fig. 13 above; it is identical to Fig. 2, except for a shift in the origin of the x-z coordinate system. The region defined by ($x > -b$ and $z < 0$) is denoted as region I; whereas, the region for ($x > 0$, $z > 0$) is denoted as region II. The excitation for this problem is again a TM_0 surface wave incident at ($x = 0$, $z = 0$) from region I (i.e., from the left). The incident and the total magnetic fields are denoted by Φ_I^i and Φ. Here, $\Phi \equiv \Phi_I$ in region I; whereas, $\Phi \equiv \Phi_{II}$ in region II.

(196) $$\Phi_I^i = \begin{cases} e^{-\alpha x} e^{i\beta z} & ; \quad \text{for } x \geq 0 \text{ and } z < 0 \\ \dfrac{\cos k_x(x+b)}{\cos k_x b}\, e^{i\beta z} & ; \quad \text{for } -b \leq x \leq 0, \text{ and } z < 0 \end{cases}$$

where α, β and k_x are identical to those in (62) and (63). One may express the fields Φ_I and Φ_{II} in terms of special Green's functions

G_I and GII for regions I and II, respectively, as

$$(197)\quad \Phi_I(x,z) = \Phi_I^i(x,z) - \int_0^\infty G_I(x,z;x',0)\left.\frac{\partial \Phi_I}{\partial z'}\right|_{z'=0} dx' + (\Phi_I^i(x,z))^*,$$

for region I, and

$$(198)\quad \Phi_{II}(x,z) = \int_0^\infty G_{II}(x,z;x',0)\left.\frac{\partial \Phi_{II}}{\partial z'}\right|_{z'=0} dx' ,$$

for region II. The term $(\Phi_I^i(x,z))^*$ in (197) refers to the complex conjugate of $\Phi_I^i(x,z)$ and is present as a result of the boundary condition given in (200) so that in effect there is a perfectly-conducting wall at $z = 0$, $x > -b$. The special Green's functions G_I and G_{II} satisfy the following differential equations and boundary conditions.

$$(199a)\quad \left(\frac{\partial^2}{\partial x^2} + \frac{\partial^2}{\partial z^2} + k^2\right) G_I(x,z;x',z') = -\delta(x-x')\delta(z-z');$$

for $x \geq 0$, and $z \leq 0$.

$$(199b)\quad \left(\frac{\partial^2}{\partial x^2} + \frac{\partial^2}{\partial z^2} + k_d^2\right) G_I(x,z;x',z') = 0;$$

for $-b \leq x \leq 0$, and $z \leq 0$

$$(200)\quad \left.\frac{\partial G_I}{\partial z}\right|_{z=0} = 0$$

$$(201)\quad \left.\frac{\partial G_I}{\partial x}\right|_{x=-b} = 0$$

$$(202)\quad G_I|_{x=0+} = G_I|_{x=0-}$$

$$(203)\quad \left.\frac{\partial G_I}{\partial x}\right|_{x=0+} = \frac{1}{\varepsilon_r}\left.\frac{\partial G_I}{\partial x}\right|_{x=0-}$$

(204) G_I satisfies the radiation condition as $|(x^2+z^2)^{1/2}|\to\infty$ for an $e^{-i\omega t}$ time dependence.

The quantities, k, k_d and ε_r appearing above are the same as those in (62) and (63). The δ in (199a) symbolizes the Dirac delta function.

$$(205)\qquad \left(\frac{\partial^2}{\partial x^2}+\frac{\partial^2}{\partial z^2}+k^2\right) G_{II}(x,z;x',z') = -\delta(x-x')\delta(z-z');$$

for $x \geq 0$, and $z \geq 0$.

$$(206)\qquad \left.\frac{\partial G_{II}}{\partial z}\right|_{z=0} = 0$$

$$(207)\qquad \left.\frac{\partial G_{II}}{\partial x}\right|_{x=0} = 0$$

(208) G_{II} satisfies the radiation condition as $|(x^2+z^2)^{1/2}|\to\infty$ for an $e^{-i\omega t}$ time dependence.

The derivations for the special Green's functions G_I and G_{II} will not be presented here for the sake of brevity; only the final forms of G_I and G_{II} are given.

$$(209)\qquad G_I = -\frac{1}{2\pi i}\oint_{C_x} G_x(x,x')\, G_z(z,z')\, d\lambda_{xo}$$

where

$$(210)\qquad G_x(x,x') = \frac{\left(e^{-i\sqrt{\lambda_{xo}}x_<} + \hat{R}\, e^{i\sqrt{\lambda_{xo}}x_<}\right) e^{i\sqrt{\lambda_{xo}}x_>}}{-2i\sqrt{\lambda_{xo}}}, \quad x \geq 0$$

and

$$(211)\qquad G_z(z,z') = \frac{e^{-i\sqrt{\lambda_z}z_<}\cos\sqrt{\lambda_z}z_>}{-i\sqrt{\lambda_z}}, \quad \text{for } z \leq 0$$

Here, $x_<$ refers to values of x for which $x < x'$, and the quantities $x_>$, $z_>$ and $z_<$ are defined in the same manner.

$$\lambda_{xo} + \lambda_z = k^2 \tag{212}$$

and

$$\hat{R} \equiv \frac{\varepsilon_r\sqrt{\lambda_{xo}}\cos\sqrt{\lambda_{x1}}\,b + i\sqrt{\lambda_{x1}}\sin\sqrt{\lambda_{x1}}\,b}{\varepsilon_r\sqrt{\lambda_{xo}}\cos\sqrt{\lambda_{x1}}\,b - i\sqrt{\lambda_{x1}}\sin\sqrt{\lambda_{x1}}\,b} \tag{213}$$

with

$$\lambda_{x1} + \lambda_z = k_d^2 \tag{214}$$

The contour C_x in (209) encloses the singularities of $G_x(x,x')$ in the complex λ_{xo} plane. Also,

$$G_{II} = \frac{1}{2\pi i}\int_{-\infty}^{\infty} du\,\frac{e^{iu|x-x'|} + e^{iu(x+x')}}{\sqrt{k^2-u^2}}\,e^{i\sqrt{k^2-u^2}z_>}\cos\sqrt{k^2-u^2}z_< \tag{215}$$

The Green's functions G_I and G_{II} given above have been constructed via the techniques indicated in [12,13]. The integral in (209) may be re-written as a superposition of a pole contribution and a branch cut contribution associated with the singularities of G_x; the pole contribution may be expressed in the form $R'(\Phi_I(x,z))^*$ in which the complex constant R' is unknown at present; whereas, the branch cut contribution has the form (after employing a change of variables $u^2 = \lambda_{xo}$)

$$\frac{1}{2\pi i}\int_0^{\infty} dx'\int_{-\infty}^{\infty} du\,\frac{e^{iu|x-x'|} + \hat{R}\,e^{iu(x+x')}}{\sqrt{k^2-u^2}}\cdot \left\{e^{-i\sqrt{k^2-u^2}z_<}\cos\sqrt{k^2-u^2}z_>\right\}_{z'=0}\cdot \frac{\partial\Phi_I}{\partial z'}\bigg|_{z'=0} \tag{216}$$

Hence, one may rewrite (197) and (198) as

$$(217)\qquad \Phi_I(x,z) = \Phi_I^i(x,z) + (1-R')(\Phi_I^i(x,z))^* - \frac{1}{2\pi i}\int_{-\infty}^{\infty} du \int_0^{\infty} dx' \left\{ \frac{e^{iu|x-x'|} + \hat{R}\, e^{iu(x+x')}}{\sqrt{k^2-u^2}} \right\} \cdot \left[\left(e^{-i\sqrt{k^2-u^2}\, z_<} \cdot \cos\sqrt{k^2-u^2}\, z_> \right) \cdot \frac{\partial \Phi_I}{\partial z'} \right]_{z'=0}$$

and

$$(218)\qquad \Phi_{II}(x,z) = \frac{1}{2\pi i}\int_{-\infty}^{\infty} du \int_0^{\infty} dx' \left\{ \frac{e^{iu|x-x'|} + e^{iu(x+x')}}{\sqrt{k^2-u^2}} \right\} \cdot \left[e^{i\sqrt{k^2-u^2}\, z_>} \cos\sqrt{k^2-u^2}\, z_< \cdot \frac{\partial \Phi_{II}}{\partial z'} \right]_{z'=0}$$

The fields Φ_I and Φ_{II} must be continuous across the aperture defined by $z = 0$ and $x > 0$. Also $\partial\Phi_I/\partial z'|_{z'=0}$ and $\partial\Phi_{II}/\partial z'|_{z'=0}$ must be continuous. Let

$$(219)\qquad \left.\frac{\partial \Phi_I}{\partial z'}\right|_{z'=0} = \left.\frac{\partial \Phi_{II}}{\partial z'}\right|_{z'=0} \equiv K(x')$$

Equating $\Phi_I(x,0)$ to $\Phi_{II}(x,0)$ and utilizing (219) one obtains the following integral equation

$$(220)\qquad (1 + R_3)\Phi_I^i(x,0) = \int_0^{\infty} \Gamma(x,x')K(x')dx'$$

where

(221) $$R_3 \equiv 1 - R'$$

and

(222) $$\Gamma(x,x') \equiv \frac{1}{2\pi i}\int_{-\infty}^{\infty} \frac{2e^{i|x-x'|} + (1+\hat{R})e^{iu(x+x')}}{\sqrt{k^2 - u^2}}\, du$$

The quantities R_3 and $K(x')$ in (220) are unknowns. It is clear from (217), that R_3 as defined by (221) represents the surface wave reflection coefficient which is of interest. Multiplying both sides of (220) by $K(x)$ and integrating on x gives

(223) $$(1 + R_3)\int_0^{\infty} K(x)\Phi_I^i(x,0)dx = \int_0^{\infty}\int_0^{\infty} K(x)\Gamma(x,x')K(x')dx'\, dx$$

One may represent $K(x)$ by a sum of discrete surface wave modes (arising from the discrete spectrum of the integral operator in (220)) and an appropriate integral (pertaining to the continuous spectrum contribution); hence,

(224) $$K(x) = \frac{\partial}{\partial z'}\left[\Phi_I^i(x,z') + R_3\Phi_I^{i*}(x,z')\right]\Big|_{z'=0^+} + \Phi_C(x,0)$$

$$= i\beta(1-R_3)\Phi_I^i(x,0) + \Phi_C(x,0)\ .$$

The present analysis is restricted so that obly the dominant surface wave mode exists. The term $\Phi_C(x,0)$ denotes the contribution to $K(x)$ arising from the continuous spectrum. The surface wave modes are orthogonal to the continuous spectrum; thus (224) when multiplied by $\Phi_I^i(x,0)$ and integrated with respect to x gives

(225a) $$(1-R_3) = \frac{2\alpha}{i\beta}\int_0^{\infty} K(x)\Phi_I^i(x,0)dx$$

in which

(225b) $$\int_0^{\infty}[\Phi_I^i(x,0)]^2dx = \int_0^{\infty}(e^{-\alpha x})^2\, dx = \frac{1}{2\alpha}$$

has been used. From (223) and (225a) one obtains the following stationary form for $(1+R_3)/(1-R_3)$

$$(226a)\qquad \frac{1+R_3}{1-R_3} = \frac{i\beta}{2\alpha}\,\frac{\int_0^\infty\int_0^\infty K(x)\Gamma(x,x')K(x')dx'\,dx}{\left[\int_0^\infty K(x)\,\Phi_I^i(x,0)dx\right]^2}$$

To solve for R_3 in (226a), it is customary to assume that $K(x)$ can be approximated by the incident and reflected dominant surface wave modes, i.e.,

$$K(x) \approx i\beta(1-R_3)\Phi_I^i(x,0)\ .$$

When the above approximation is chosen as the trial field, (226a) becomes

$$(226b)\qquad \frac{1+R_3}{1-R_3} = 2i\alpha\beta\int_0^\infty dx\int_0^\infty dx'\ \Phi_I^i(x,0)\Gamma(x,x')\Phi_I^i(x',0)$$

The integral on the R.H.S. of (226b) can be simplified by performing the integrations on x and x'.

$$(227)\qquad \int_0^\infty dx\int_0^\infty dx'\ e^{-\alpha x}\Gamma(x,x')e^{-\alpha x'} = \frac{1}{2\pi i}\,P.V.\int_{-\infty}^{\infty}$$

$$\left[\frac{2}{\alpha^2+u^2} + \frac{1+\hat{R}}{(\alpha-iu)^2}\right]\frac{du}{\sqrt{k^2-u^2}}$$

The symbol P.V. in front of the integral on the R.H.S. of (227) indicates the principal value of the integral which is evaluated numerically to calculate R_3. The evaluation of the diffracted field is discussed next. The branch cut contribution to

$$\int_0^\infty \left(G_I\,\frac{\partial\Phi_I}{\partial z'}\right)\Big|_{z'=0} dx'$$

gives rise to the diffracted field in region I denoted by Φ_I^d. Thus

$$(228)\qquad \Phi_I^d = -\frac{1}{2\pi i}\int_{-\infty}^{\infty} du\int_0^\infty dx'\left(\frac{e^{iu|x-x'|} + \hat{R}\,e^{iu(x+x')}}{\sqrt{k^2-u^2}}\right)e^{-i\sqrt{k^2-u^2}z}\,K(x')$$

The branch cut contribution to the field Φ_{II} corresponds to the diffracted field in region II; the diffracted field in region II is denoted by Φ^d_{II}. Thus,

(229)
$$\Phi^d_{II} = \frac{1}{2\pi i} \int_{-\infty}^{\infty} du \int_0^{\infty} dx' \left(\frac{e^{iu|x-x'|} + e^{iu(x+x')}}{\sqrt{k^2 - u^2}} \right) e^{i\sqrt{k^2-u^2}z} K(x')$$

Employing $K(x') \overset{\sim}{\sim} i\beta(1-R_3)\Phi^i_I(x',0)$ in (228) and (229), and integrating on x' yields

(230)
$$\Phi^d_I = -\frac{1}{2\pi i} \int_{-\infty}^{\infty} du \frac{e^{iux} e^{-i\sqrt{k^2-u^2}z}}{\sqrt{k^2 - u^2}} \left[i\beta(1-R) \left\{ \frac{1}{\alpha + iu} + \frac{\hat{R}}{\alpha - iu} \right\} \right]$$

and

(231)
$$\Phi^d_{II} = \frac{1}{2\pi i} \int_{-\infty}^{\infty} du \frac{e^{iux} e^{i\sqrt{k^2-u^2}z}}{\sqrt{k^2 - u^2}} \left[i\beta(1-R) \left\{ \frac{2\alpha}{\alpha^2 + u^2} \right\} \right]$$

One may evaluate (230) and (231) asymptotically for large $k\rho$ via the saddle point method. As before, one introduces the polar transformation

(232)
$$u = k \sin \xi \,, \quad \sqrt{k^2 - u^2} = k \cos \xi$$

and

(233)
$$x = \rho \cos \phi, \quad z = \rho \sin \phi \,.$$

The coordinates (ρ,ϕ) at the observation point are indicated in Fig. 13.

(234)

$$\Phi_I^d = -\frac{1}{2\pi i}\int_{C_\xi} e^{ik\rho\sin(\xi-\phi)}\left[i\beta(1-R_3)\left\{\frac{1}{\alpha+ik\sin\xi}+\frac{\hat{R}(k\sin\xi)}{\alpha-ik\sin\xi}\right\}\right]d\xi$$

The contour C_ξ in the complex ξ plane is deformed into the steepest descent path, and the integral is then evaluated via the saddle point method to obtain

(235a)

$$\Phi_I^d \sim -\frac{i\beta(1-R_3)A_0}{\sqrt{2i\pi k}}\left\{\frac{1}{\alpha+ik\cos\phi}+\frac{\hat{R}(k\cos\phi)}{\alpha-ik\cos\phi}\right\}\frac{e^{ik\rho}}{\sqrt{\rho}};\quad -\pi/2<\phi<0$$

Similarly, the saddle point result for Φ_{II}^d is

(235b)

$$\Phi_{II}^d \sim \frac{i\beta(1-R_3)}{\sqrt{2i\pi k}}\cdot\frac{2\alpha}{\alpha^2+k^2\cos^2\phi}\frac{e^{ik\rho}}{\sqrt{\rho}};\quad 0<\phi<\pi/2$$

The constant A_0 is introduced so that $\Phi_I^d(\Phi=0) = \phi_{II}^d(=0)$; there is no other analytical justification for its presence. The quantity R_3 in (235a) and (235b) is evaluated from (226b). Clearly, the quantities which multiply the $e^{ik\rho}/\sqrt{\rho}$ factor in (235a) and (235b) correspond to the surface wave diffraction coefficient for the regions $-\pi/2 < -\phi < 0$, and $0 < \phi < \pi/2$, respectively; this surface wave diffraction coefficient which is based on the variational solution is denoted by D_3.

(236)

$$D_3 \equiv \begin{cases} \dfrac{-i\beta(1-R_3)A_0}{\sqrt{2i\pi k}}\left\{\dfrac{1}{\alpha+ik\cos\phi}+\dfrac{\hat{R}(k\cos\phi)}{\alpha-ik\cos\phi}\right\}; & -\pi/2<\phi<0 \\ \dfrac{i\beta(1-R_3)}{\sqrt{2i\pi k}}\dfrac{2\alpha}{\alpha^2+k^2\cos^2\phi}; & 0<\phi<\pi/2 \end{cases}$$

CHAPTER IV
RESULTS AND DISCUSSION

The TM_0 surface wave reflection and diffraction coefficients associated with the termination of the dielectric cover in Fig. 2 have been obtained in this report; these coefficients allow one to employ the GTD method to calculate the fields radiated by a configuration such as that shown in Fig. 1. The GTD method is chosen because

a) it is simple to use, and yields accurate results in high-frequency problems;

b) it provides some physical insight into the radiation and scattering mechanisms involved; and

c) it can be used to treat problems for which exact analytical solutions are unavailable.

Furthermore, the GTD method has been employed successfully in the past to calculate the radiation from a dielectric covered slot in a finite ground plane in which the dielectric completely covers the ground plane [14], thereby providing an added confidence in the method.

In the GTD method, the total field at P is obtained via a superposition of the geometrical optics field along the ray s_0, and the diffracted field at P which arrives via the ray paths s_1 and s_2, as illustrated in Fig. 1. As in Chapters II and III the y-directed magnetic field is denoted by u. Let the geometrical optics field be denoted by $u_{g.o.}$, and the diffracted field from the terminations A and B by u_A^d and u_B^d, respectively. $u_{g.o.}$ corresponds to the direct radiation from the slot to P given by

$$u_{g.o.} = C_o \frac{e^{iks_o}}{\sqrt{s_o}} \tag{237}$$

The slot also excites surface waves which diffract from the terminations A and B. The surface wave excited by the slot is denoted by u_{sw}, where

$$u_{sw} = K_o e^{\pm i\beta z} e^{-\alpha x}, \text{ for } z \gtrless 0 \tag{238}$$

in which α and β are the surface wave attenuation and propagation constants discussed previously in Chapters II and III. The quantities C_o and K_o are deduced from the solution for the fields of a narrow slot radiating through a dielectric covered plane of infinite extent, as shown in Fig. 14. The quantities C_o and K_o will not be derived here since they may be obtained via techniques similar to those outlined in [8] for an electric line source excitation of a grounded dielectric slab. Only the final results for C_o and K_o are presented below.

(239)
$$C_o = \frac{i\omega\varepsilon_o M_o \cos\phi\, e^{-i\frac{\pi}{4}}}{\sqrt{2\pi k}\left\{\sqrt{\varepsilon_r-\sin^2\phi}\,\sin k\sqrt{\varepsilon_r-\sin^2\phi}\,b + i\varepsilon_r\cos\phi\,\cos k\sqrt{\varepsilon_r-\sin^2\phi}\,b\right\}}$$

and

(240)
$$K_o = \frac{-\omega\varepsilon_o k_x \alpha M_o}{\alpha\beta(1+\varepsilon_r\alpha b)\sin k_x b + k_x\beta(\alpha b+\varepsilon_r)\cos k_x b}$$

The quantities k_x^2 and b correspond to $(\varepsilon_r k^2 - \beta^2)$, and the dielectric slab thickness (in meters), respectively. The quantity M_o in (239) and (240) refers to the strength of the equivalent magnetic line source associated with the electric field in the aperture of the narrow axial slot. The total field radiated at P by the configuration in Fig. 1 is obtained by superposing the geometrical optics contribution in (237) and the diffracted fields u_A^d and u_B^d, respectively, where

(241a)
$$u_A^d(P) = \frac{K_o\, e^{i\beta\ell_o}}{1-R\, e^{i2\beta\ell_o}}\, D(\phi_A)\, \frac{e^{iks_1}}{\sqrt{s_1}}$$

and

(241b)
$$u_B^d(P) = \frac{K_o\, e^{i\beta\ell_o}}{1-R\, e^{i2\beta\ell_o}}\, D(\phi_B)\, \frac{e^{iks_2}}{\sqrt{s_2}}$$

for the case when the narrow axial slot is equidistant from the terminations at A and B (the distance being ℓ_o); the corresponding expression for the case when the slot is not equidistant from A and B is not presented here, but it can be derived in a straightforward manner. In Eqs. (241a) and (241b) the contributions from all surface waves multiply reflected between terminations A and B have been included. The quantities R and D in (241a,b) refer to the TM_o surface wave reflection and diffraction coefficients associated

with the terminations at A and B, respectively. Thus, the total field, u(P) at P is

$$u(P) = u_{g.o.} + u_A^d + u_B^d \tag{242}$$

where $u_{g.o.}$, u_A^d and u_B^d are given in (237) and (241a,b). Although examples of this type are two dimensional, the patterns obtained are identical with those of a related three-dimensional problem, in a plane of symmetry perpendicular to the axis of the slot.

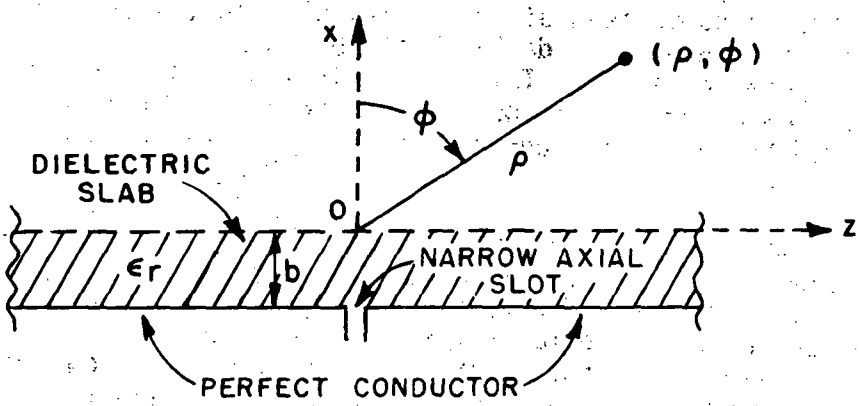

Fig. 14 -- Narrow axial slot in an infinite ground plane covered with a dielectric slab of infinite extent in the z direction.

As indicated in the introduction, the quantities R and D in (241a,b) are derived by three different methods, namely:

(1) An exact solution to the canonical problem of Fig. 2 based on the GSMT; the details of this solution are given in Chapter III. The expressions for R and D obtained by this method are denoted by R_2 and D_2, respectively. R_2 is given in (195) and D_2 is given in (186);

(2) An approximate solution to the canonical problem of Fig. 2 obtained by the variational method; the details of this solution are given in Chapter III. The expressions for R and D obtained by this method are denoted by R_3 and D_3, respectively. R_3 is given in (226b) and D_3 is given in (236);

(3) an exact solution of the problem pertaining to the approximate physical configuration of Fig. 3 in which a reactive surface approximates the dielectric cover of the exact configuration of Fig. 2; the details of this solution are given in Chapter II, and the expressions for R and D obtained by this method are denoted by R_1 and D_1, respectively. R_1 is given in (53) and D_1 is given in (60).

The numerical results for the TM_0 surface wave reflection and diffraction coefficients R and D, respectively, which are calculated by the three different methods are presented in this chapter. A comparison of the numerical results based on the different methods is made to estimate the accuracy of the approximate solutions. The numerical results for the TM_0 surface wave reflection coefficient are given first; these are followed by calculated curves for the TM_0 surface wave diffraction coefficient.

We wish to compare the reflection and diffraction coefficients of the terminated surface reactance model with those of terminated dielectric slab structure of Fig. 2. This is made possible by the relationship between X_S and b for a given ε_r, see Eqs. (2) and (5). Thus, in the following R_1 and D_1 are given both as functions of X_S and b (for a fixed ε_r). Calculated values of the surface wave reflection coefficient R_1 are listed in Table I as a function of the normal surface reactance. The thickness of the grounded dielectric cover with the same normalized surface reactance is listed in column two. The values of $|R_1|$ given in Table I are in agreement with those obtained from Kay's solution [3] to the problem in Fig. 3; however, the phase of the reflection coefficient in Kay's solution is not in a form tractable for numerical computations, and therefore it cannot be compared with the phase of R_1 presented in Table I. As mentioned previously it appears that the only reference which contains a solution from which phase calculations are tractable is that of Weinstein [5]. However, the results in [5] have an error in the final form; the error is corrected fairly easily and the numerical values for the reflection coefficient based on the corrected results are included for comparison. Both the magnitude and the phase of the reflection coefficient calculated from [5] are also given in Table I; it is seen from there that the values calculated from the corrected results in [5] agree well with the values of R_1. The magnitudes are in complete agreement; only the phase of the reflection coefficients calculated by these two methods differ slightly. Thus, we have a valuable mutual check between the solution given in Chapter II, and the one in [5] obtained by a different factorization method.

TABLE I

Reflection Coefficient R_1 (based on the exact solution to the approximate configuration of Fig. 3)
$\varepsilon_r = 2.49$, f = 8.9 GHz; free space wavelength $\lambda_o = 0.0337$ meters

Surface reactance = x_s (normalized to free space impedance)	Thickness of the dielectric cover = b (meters	Magnitude of R_1	Magnitude via Weinstein's result (corrected)	Phase of R_1 (degrees)	Phase via Weinstein's result (corrected) (degrees)
0.1128	.001	.0063	.0063	-4.156	-4.103
0.2307	.002	.0256	.0256	-8.375	-8.318
0.3581	.003	.0585	.0585	-12.660	-12.712
0.4929	.004	.1030	.1030	-16.774	-17.108
0.6245	.005	.1518	.1518	-20.344	-21.10
0.7398	.006	.1961	.1961	-23.088	-24.34
0.8328	.007	.2315	.2315	-25.070	-26.8
0.9047	.008	.2584	.2584	-26.463	-28.58
0.9598	.009	.2785	.2785	-27.452	-29.8
1.002	.010	.2937	.2937	-28.170	-30.88
1.035	.011	.3053	.3053	-28.718	-31.62
1.061	.012	.3144	.3144	-29.122	-32.20
1.083	.013	.3215	.3215	-29.451	-32.66

The value of the reflection coefficient R_2 obtained by the formally exact GSMT solution for the configuration of Fig. 2 are given in Table II. These values are also presented graphically in Fig. 15. The GSMT result for R_2 involves infinite order matrices which are truncated to finite orders for numerical calculations; it is found that accurate computations are possible with only moderate size matrices because the results converge rapidly with an increase in matrix size. In these numerical calculations, the largest matrix inverted is 5 x 5; in fact, for all practical purposes, most of the results obtained here are found to converge with only a 3 x 3 matrix. In some cases, an even smaller matrix is adequate. The convergence of R_2 as a function of the matrix size is shown in Table III for several cases.

TABLE II

Reflection Coefficient R_2 (for the problem in Fig. 2)
Based on the GSMT Solution
$\varepsilon_r = 2.49$, f = 8.9 GHz,
free space wavelength $\lambda_0 = 0.0337$ meters

Thickness of the dielectric cover, b (meters)	Magnitude of R_2	Phase of R_2 (degrees)
.001	.01545	-8.8990
.002	.06955	-15.878
.003	.18441	-20.758
.004	.38495	-20.978
.005	.62913	-15.309
.006	.80077	- 8.643
.007	.88505	- 4.674
.008	.9260	- 2.734
.009	.9483	- 1.747

(Note: A plot of the values in Table II is shown in Fig. 15).

Values of the surface wave reflection coefficient R_3 calculated from an approximate solution by the variational method for the exact canonical configuration of Fig. 2 are listed in Table IV. It is seen from Tables II and IV that the values of $|R_3|$ calculated by the variational method are consistently lower than the corresponding values of $|R_2|$ which are based on the exact solution. Similarly, Hwang [17] has found that a variational solution for the problem illustrated in Fig. 3 also gives numerical values for the magnitude

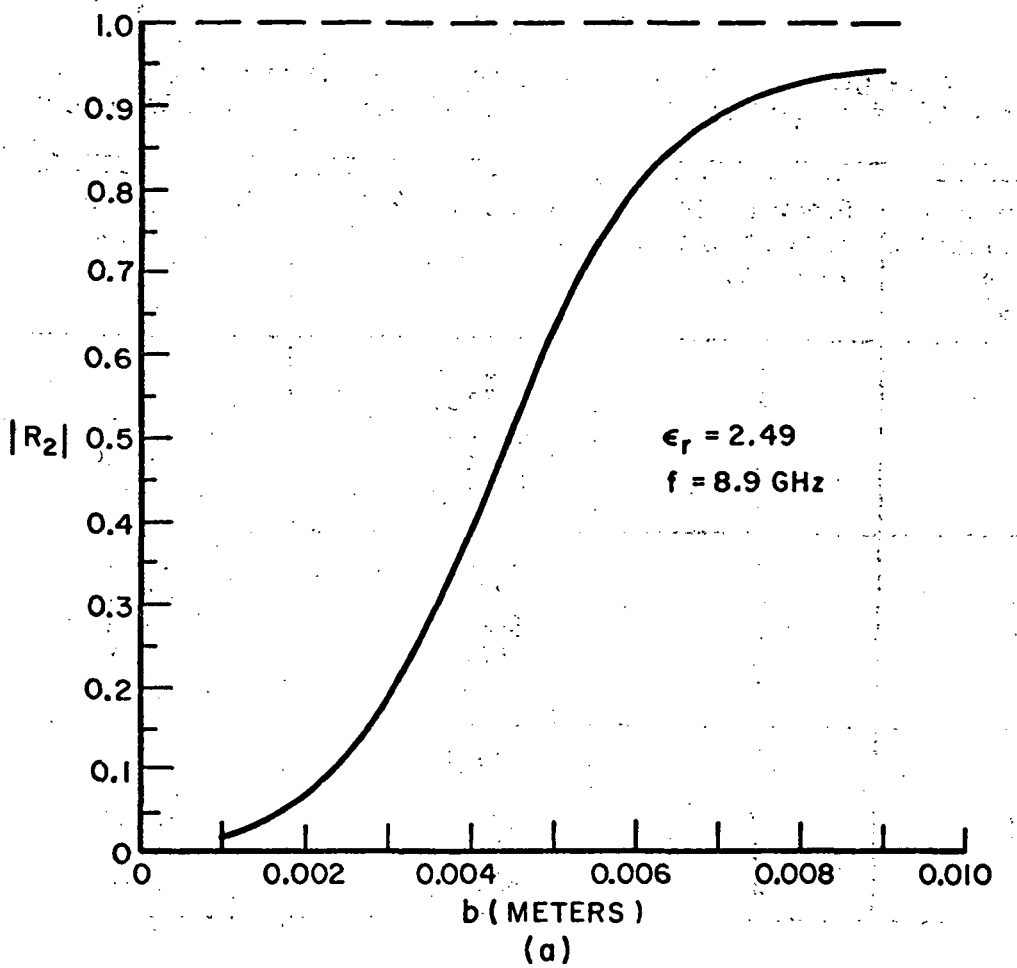

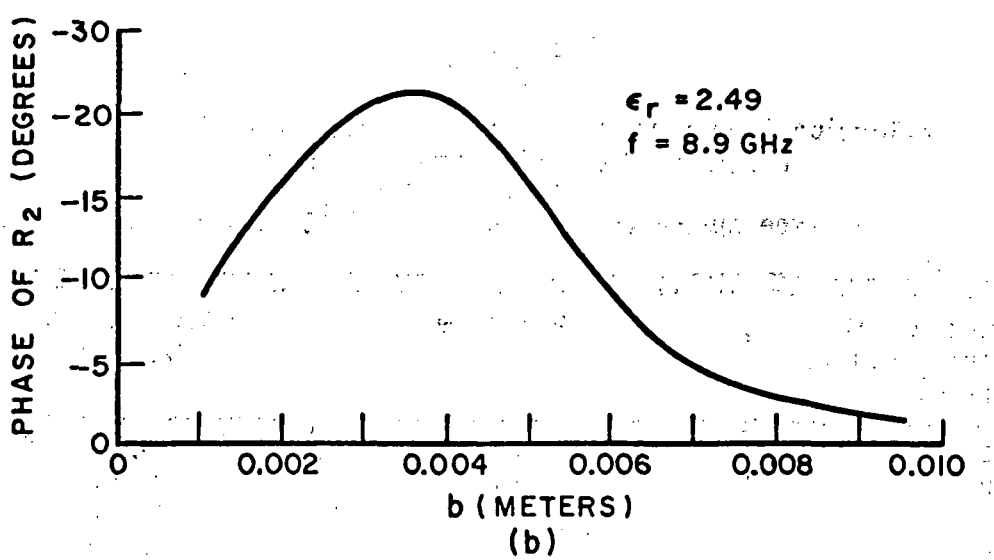

Fig. 15--Magnitude and phase of R_2 based on GSMT solution.

TABLE III

Convergence of R_2 as a Function of the Matrix Size
$\varepsilon_r = 2.49$, $f = 8.9$ GHz, free space wavelength $\lambda_o = 0.0337$ meters

Thickness of the dielectric cover b (meters)	Order of the largest matrix inverted N	Magnitude of R_2	Phase of R_2 (degrees)
.001	1	.015362	-8.5226
	2	.015430	-8.8028
	3	.015444	-8.8678
	4	.015449	-8.8946
	5	.015450	-8.8990
.004	1	.3468	-23.926
	2	.3777	-21.478
	3	.3824	-21.138
	4	.3841	-21.028
	5	.38495	-20.978
.007	1	.83465	-15.899
	2	.87939	- 6.188
	3	.88319	- 5.148
	4	.88445	- 4.821
	5	.88505	- 4.674

TABLE IV

Reflection Coefficient R_3 (for the problem in Fig. 2)
based on the variational solution
$\varepsilon_r = 2.49$, $f = 8.9$ GHz,
free space wavelength $\lambda_o = 0.0337$ meters

Thickness of the dielectric cover, b (meters)	Magnitude of R_3	Phase of R_3 (degrees)
.001	.0072	-19.02
.002	.0349	-30.80
.004	.2061	-37.37
.006	.4320	-23.93
.007	.4812	-18.76
.009	.5105	-13.76

of the reflection coefficient which are consistently lower than the corresponding values of $|R_1|$; a graphical comparison of the values of $|R_1|$ with the variational calculations of Hwang is made in Fig. 16.

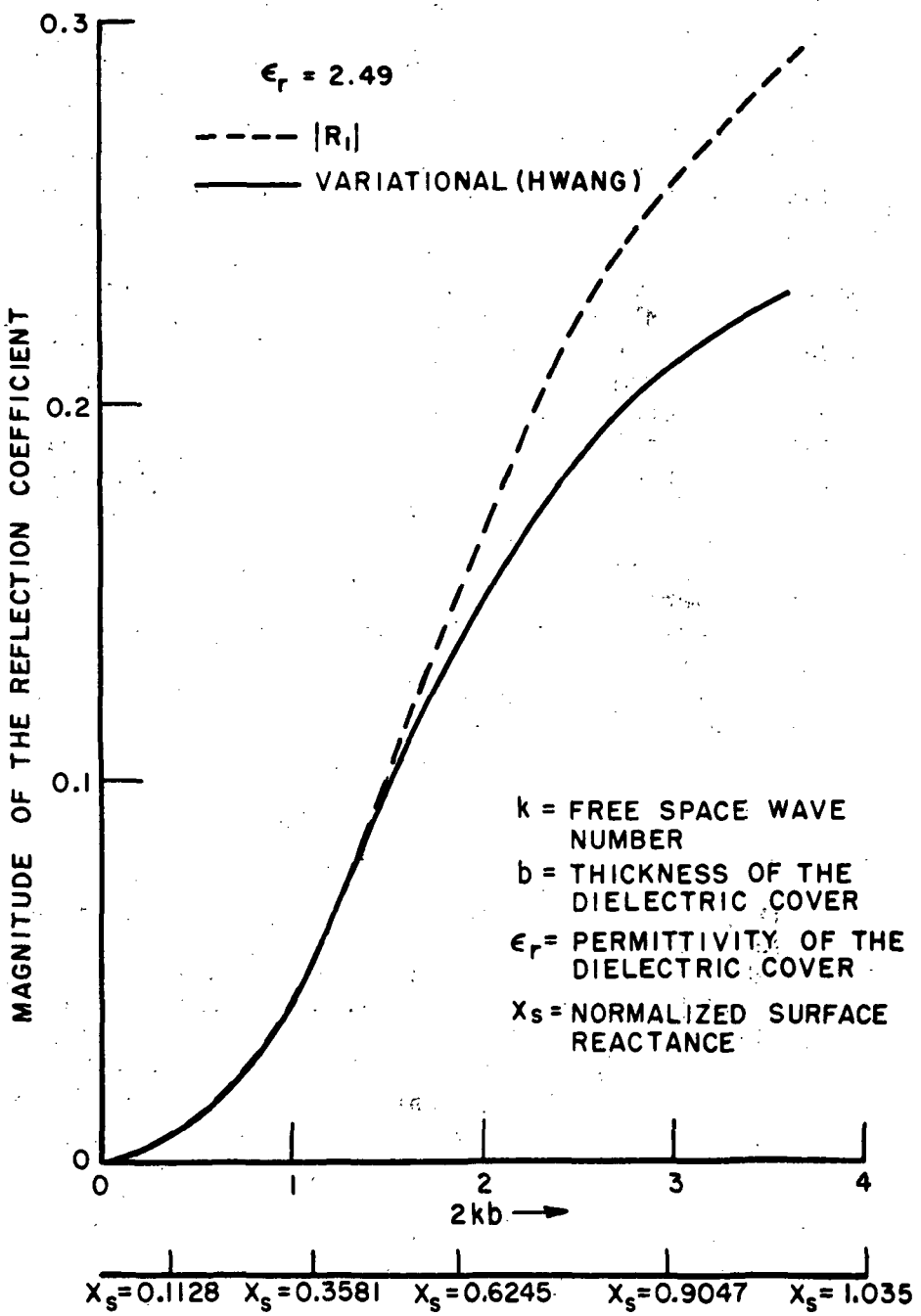

Fig. 16-- A comparison of the variational and exact calculations for the reflection coefficient pertaining to Fig. 3.

The numerical results for the TM_0 surface wave diffraction coefficients are given next. The magnitude of D_1 for the configuration in Fig. 3 is plotted in Fig. 17a as a function of the aspect angle ϕ, and for different thicknesses of the dielectric cover (or equivalent surface reactance). Corresponding numerical results for the phase of D_1 are shown in Fig. 17b. The values of $|D_1|$ agree with the corresponding values which are calculated from Kay's result [3] for the surface wave diffraction coefficient; however, the expression for the phase of the diffraction coefficient in [3] is in a form intractable for numerical calculation and hence cannot be compared with the values of the phase of D_1 (shown in Fig. 17b).

The numerical values of the surface wave diffraction coefficient, D_2 calculated by the GSMT for the configuration of Fig. 2 are shown in Figs. 18 through 22. These values are normalized such that 0 dB corresponds to the maximum value of the quantity $20 \log_{10} \sqrt{\pi k}|D_2|$ for the thinnest dielectric cover considered; namely for the dielectric cover whose thickness, $b = 0.001$ m. Also, the 0 dB level in Fig. 17a is identical to that in Figs. 18-22. Curves for the phase of D_2 as a function of aspect are plotted in Figs. 23 through 26. The formal result for D_2 which is based on the GSMT solution also involves infinite order matrices which must be truncated to finite orders for numerical calculations. Figures 20, 22 and 25 show the convergence of the calculated values of D_2 as a function of the size of the matrix being inverted; indeed, it is seen from these results that the convergence is very rapid. The R_2 and D_2 calculations require an increasing matrix size whenever the thickness and/or the permittivity of the dielectric cover increases.

It is noted that the calculation of the field in the neighborhood of the edge ($x = 0$, $z = 0$ in Fig. 2) requires an increasing number of modes, i.e., an increasing matrix size; in fact the proper edge behavior can result only if one includes an infinite number of modes (i.e., if one uses infinite order matrices) as indicated in [10]. Fortunately, in this problem, one is interested only in the far-zone radiation field, and the reflected surface wave; both of which are evaluated sufficiently far from the edge.

Figures 27, 28 and 29 give a comparison of the numerical values of $|D_1|$, $|D_2|$ and $|D_3|$ for a fixed thickness of the dielectric cover. It is seen from Figs. 27, 28, and 29 that the values of $|D_1|$ and $|D_3|$ agree well with the values of $|D_2|$ in the forward aspects defined by $0 < \phi < \pi/2$, which is also the region of higher field levels; the differences between $|D_2|$ and $|D_1|$ are approximately 6 to 10 dB in the backward region of space defined by $-\pi/2 < \phi < 0$. It is seen that the agreement between $|D_3|$ and $|D_2|$ improves as the thickness of the dielectric cover increases; this occurs because the diffracted field along the aperture ($z = 0$, $x > 0$ in Fig. 13) becomes weaker with an increase in the thickness

of the dielectric cover, thereby making the trial field in the variational solution correspondingly more accurate for pattern calculations. The strength of the diffracted field becomes weaker with an increase in the thickness of the dielectric cover because the surface wave is now more tightly bound to the dielectric-air interface, thereby increasing the magnitude of the reflection coefficient; this in turn results in a corresponding decrease in the energy diffracted by the termination.

It is seen that the diffraction coefficient D_3 is more accurate than the diffraction coefficient D_1 when the latter is used to approximate D_2. The surface wave diffraction coefficient is proportional to the radiation pattern function, and hence Figs. 18-22 describe the radiation patterns associated with the diffraction of a surface wave by the termination of the dielectric cover. The nature of the radiation pattern is intimately connected with the value of the reflection coefficient of the surface wave reflected by the termination; this may be explained as follows. The radiation pattern may be considered as being produced by an equivalent magnetic current distribution located at $x = 0$ and for $z \leq 0$. This current distribution is well-approximated by the incident and reflected surface wave fields at $x = 0$ and $z \leq 0$. One may therefore consider the equivalent current to be proportional to $e^{i\beta z} + R\, e^{-i\beta z}$ for $z \leq 0$ where R is the surface wave reflection coefficient. The radiation pattern in the forward region is primarily produced by the termination of the incident surface wave at $z = 0$; whereas, the radiation pattern in the back region is primarily produced by the excitation of the reflected surface wave at $z = 0$. When $R \ll 1$, the radiation pattern is expected to be much higher in the forward region than in the back region; whereas, when $R \to 1$, the pattern levels are expected to be nearly equal in the two regions. This viewpoint is supported by the curves in Figs. 15 and 18-22. From the values in Tables I, II and IV, it is apparent that the surface wave reflection coefficients R_3 and R_1 are not in close agreement with the values of R_2. The variational solution is expected to be somewhat inaccurate because the present trial field cannot properly account for the significant diffraction effects, especially in the vicinity of the truncation of the dielectric slab; one notes that the present choice of the trial field in the aperture is equivalent to the commonly used Kirchhoff approximation (this approximation is also used by Angulo [6] in his variational solution for the problem in Fig. 4). One would expect the variational solution to be improved by incorporating a correction term to the surface wave fields in the aperture so as to provide some information on the fields scattered by the edge ($x=0$, $z=0$ in Fig. 2) along the aperture. Although the nature of this correction term is not known apriori, it could be based on the high frequency diffracted field in the aperture together with a modification which would provide the proper behavior in the vicinity of the edge.

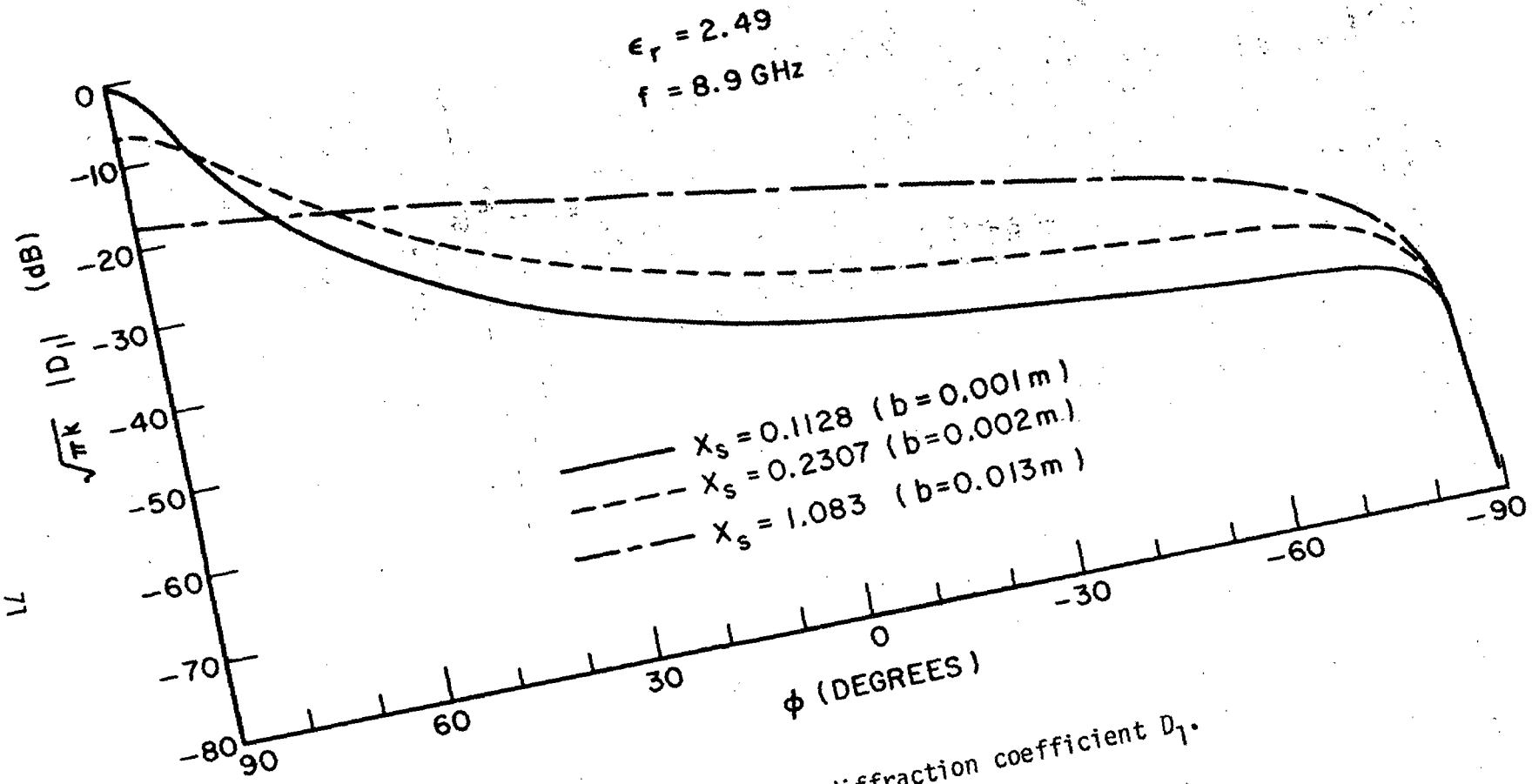

Fig. 17a-- Magnitude of the diffraction coefficient D_1.

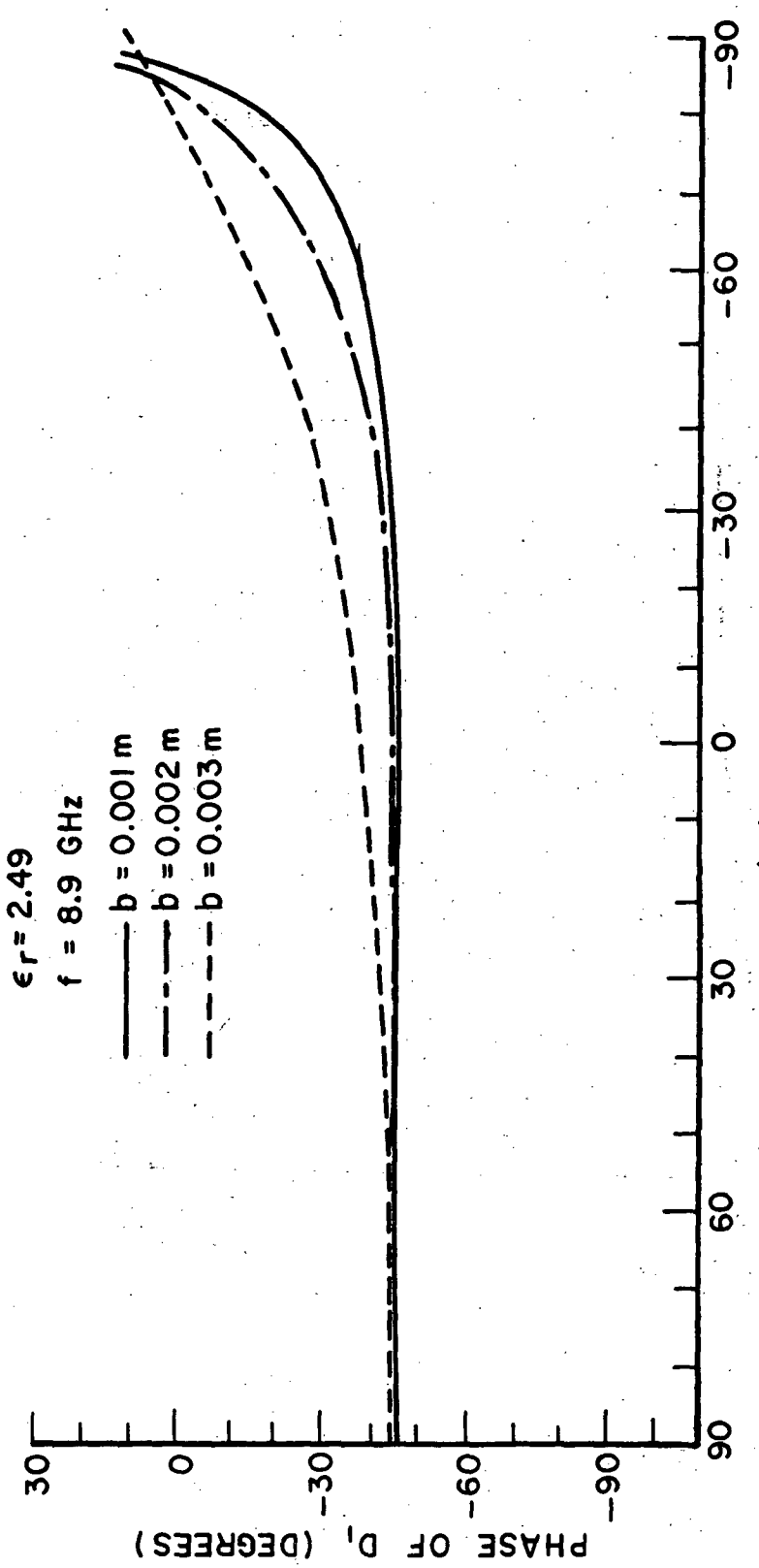

Fig. 17b-- Phase of the diffraction coefficient D_1.

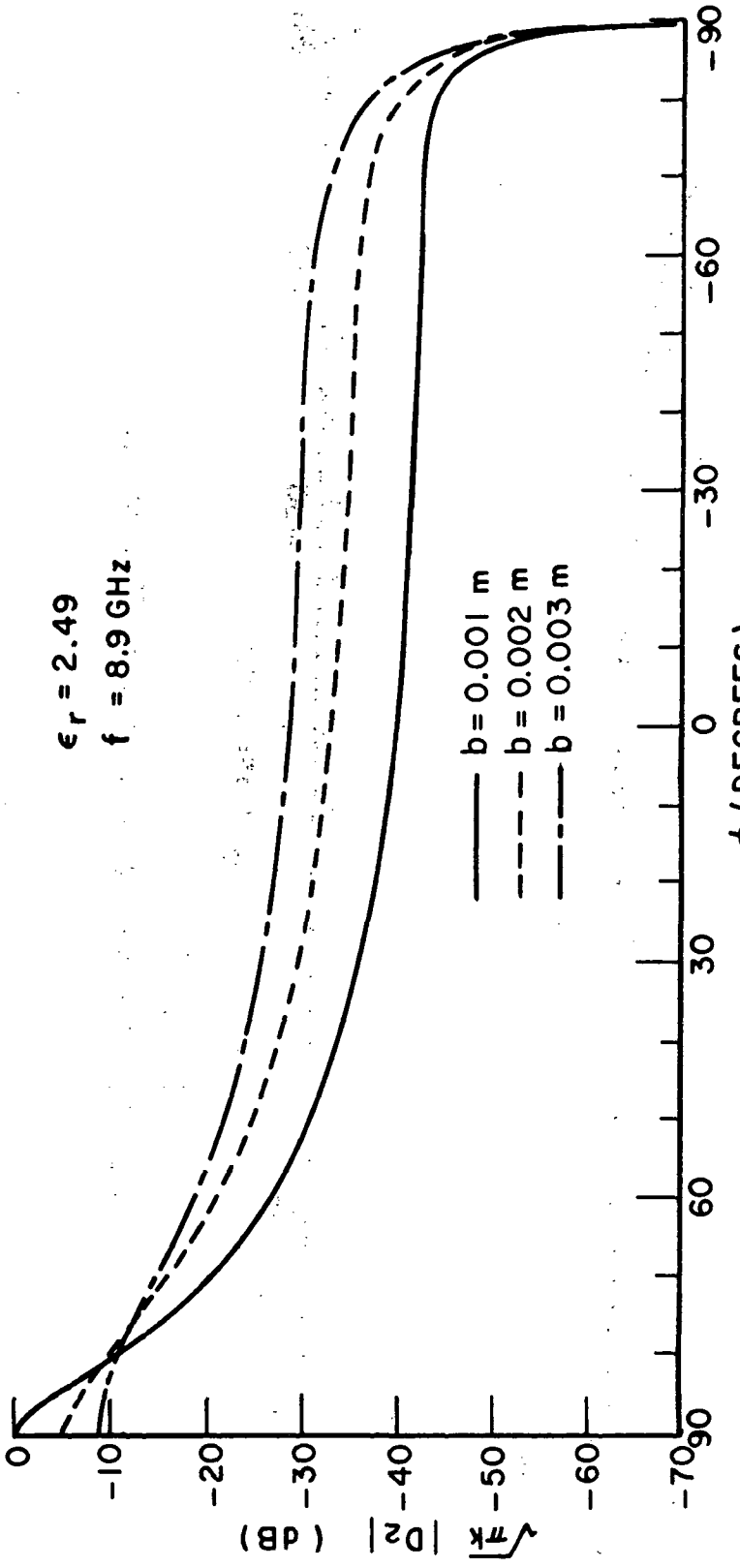

Fig. 18 -- Magnitude of the diffraction coefficient D_2.

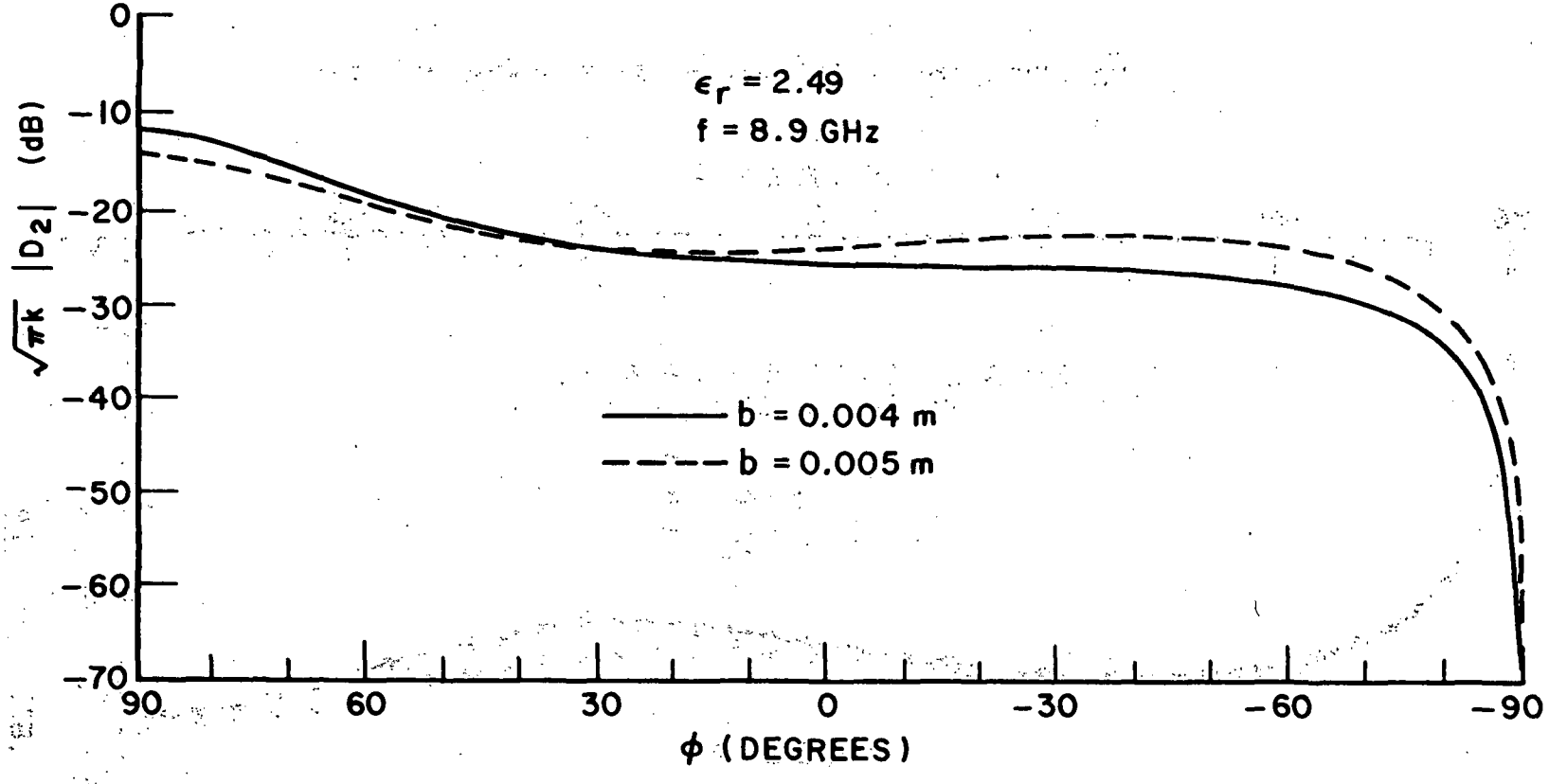

Fig. 19-- Magnitude of the diffraction coefficient D_2.

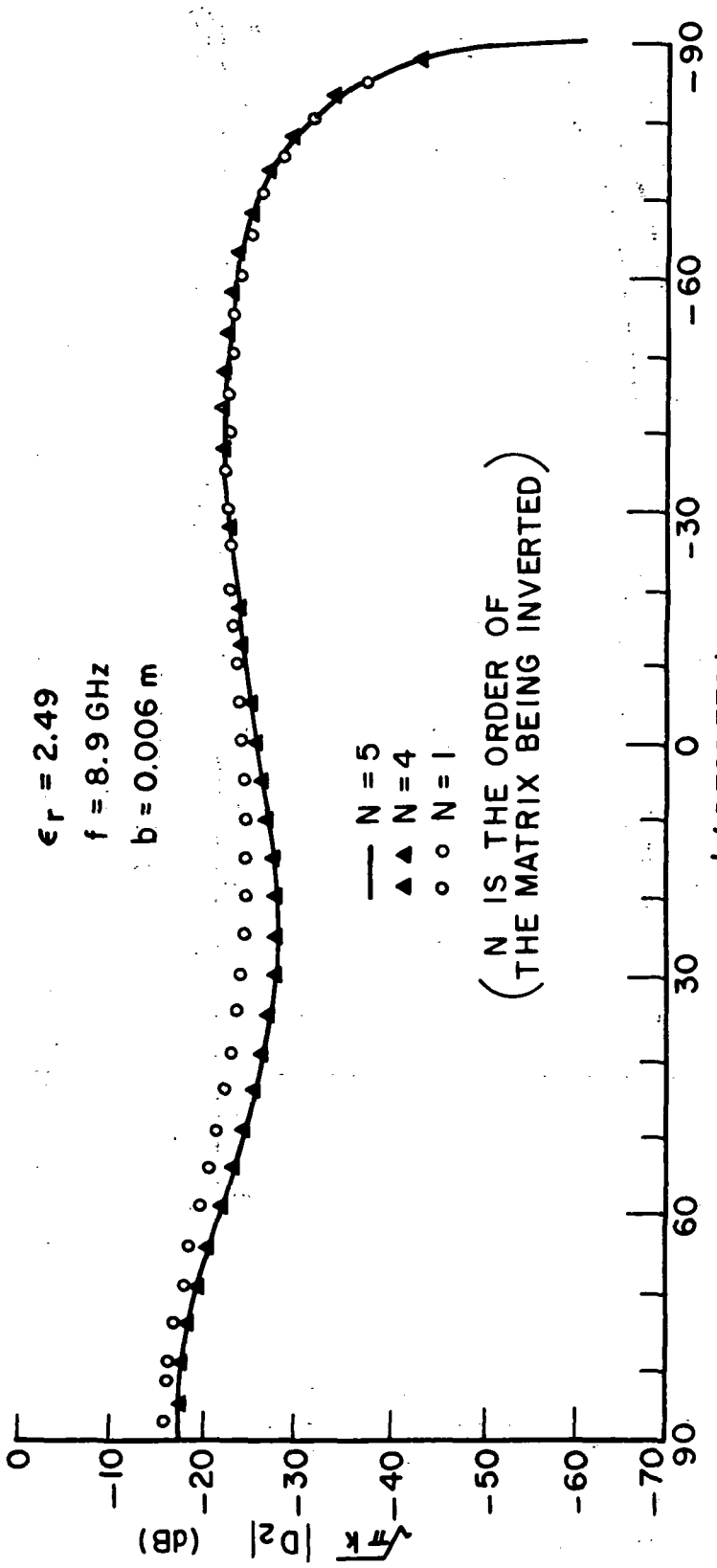

Fig. 20-- Magnitude of the diffraction coefficient D_2.

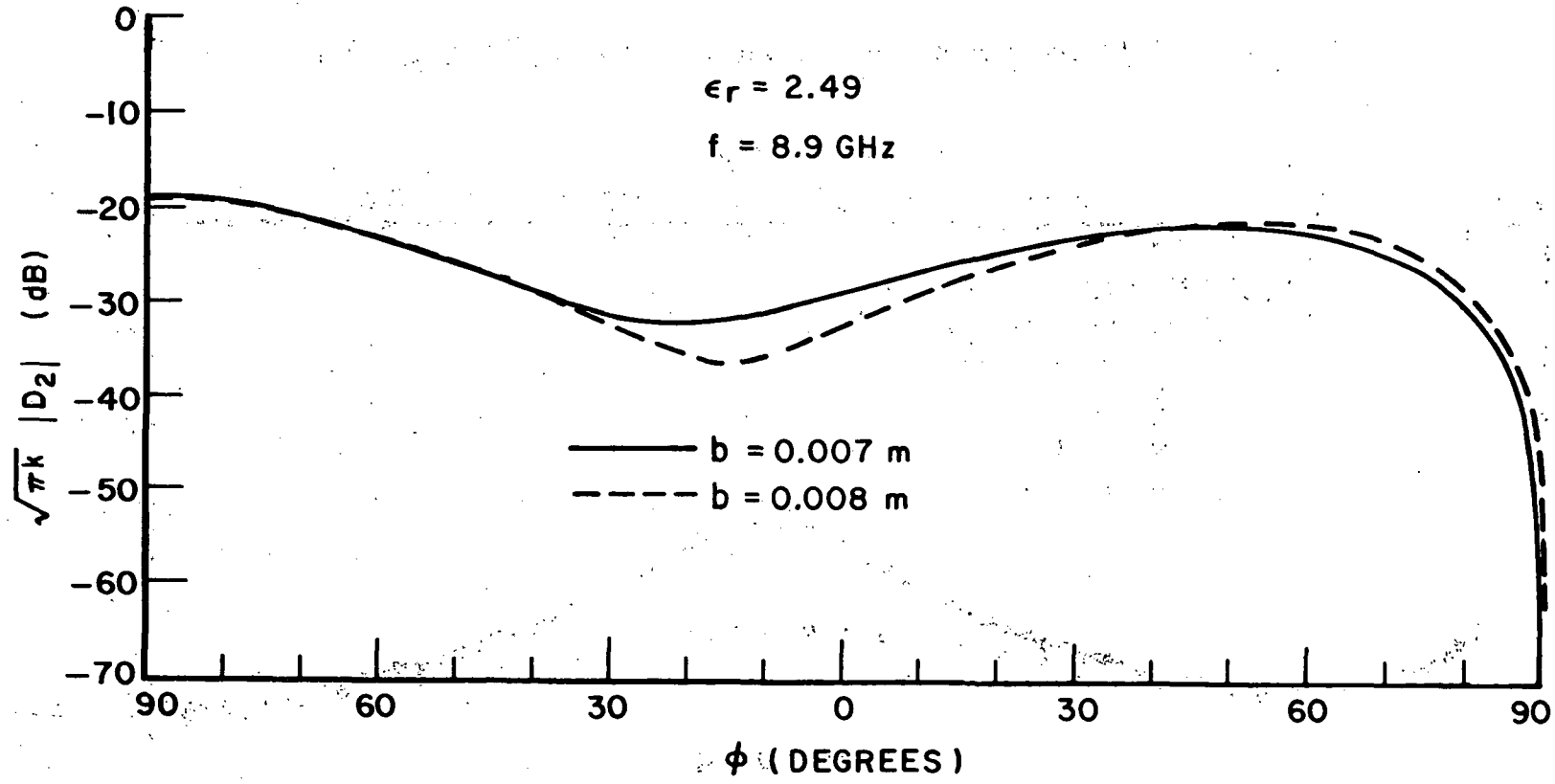

Fig. 21-- Magnitude of the diffraction coefficient D_2.

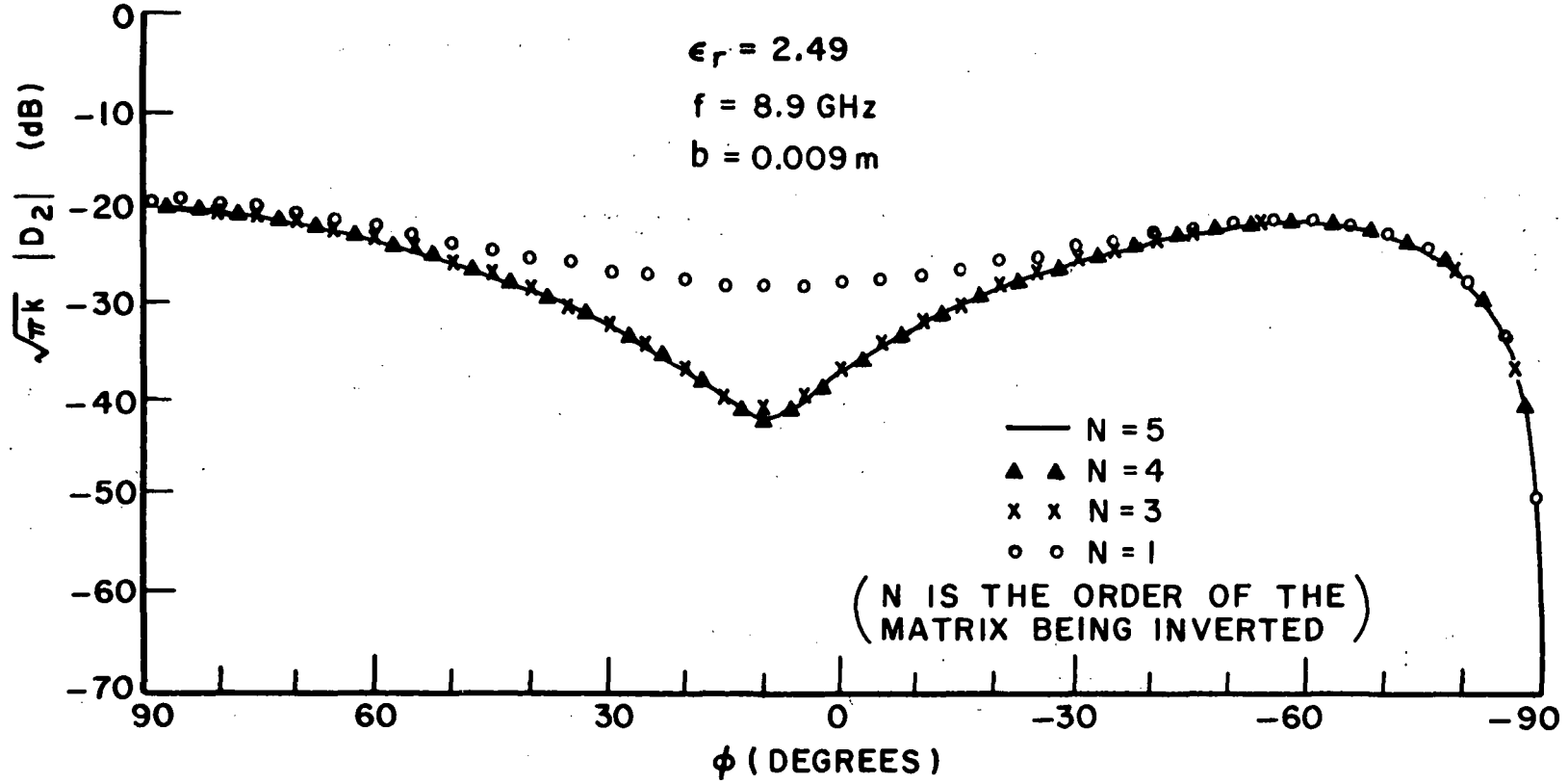

Fig. 22-- Magnitude of the diffraction coefficient D_2.

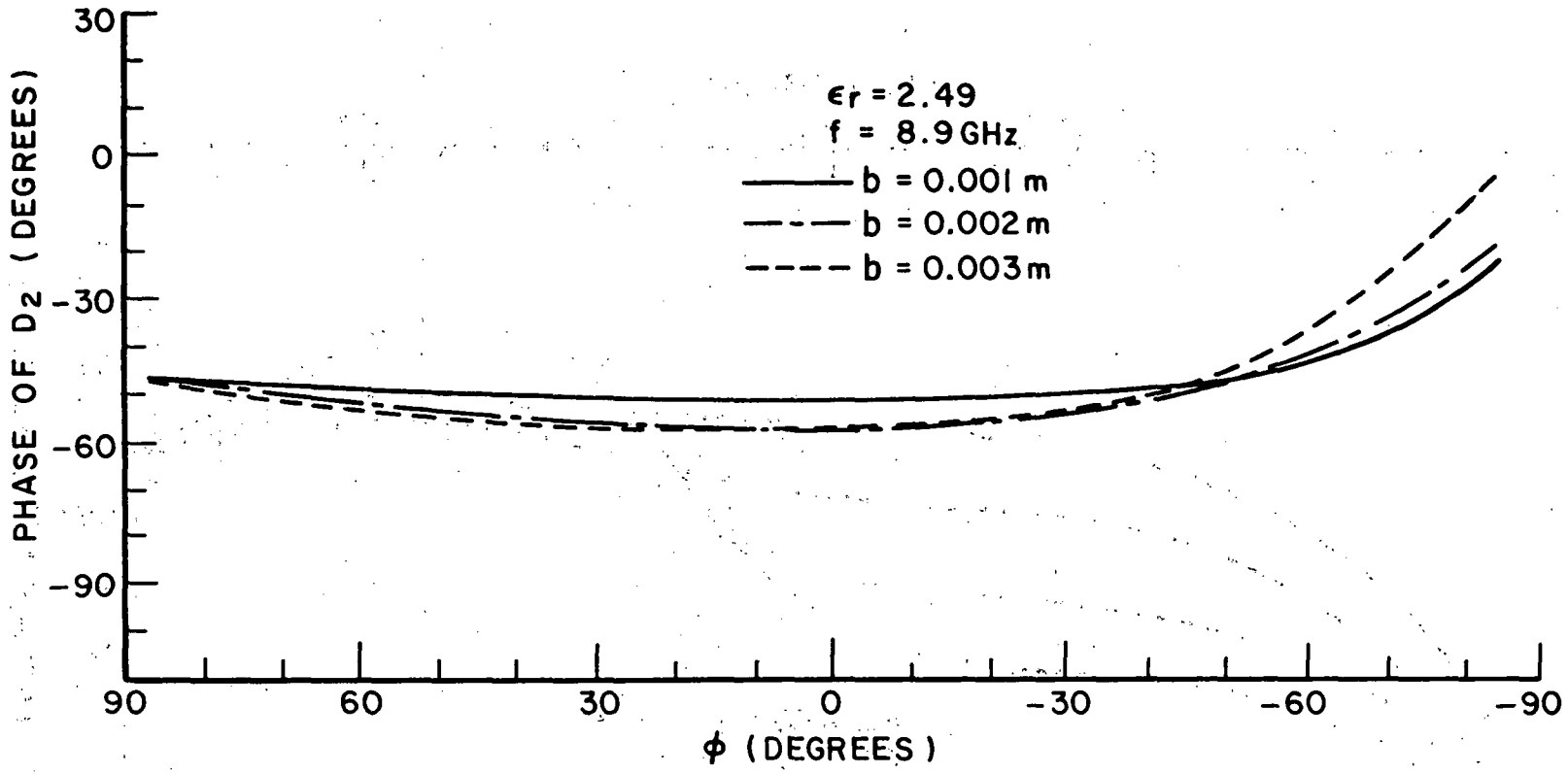

Fig. 23-- Phase of the diffraction coefficient D_2.

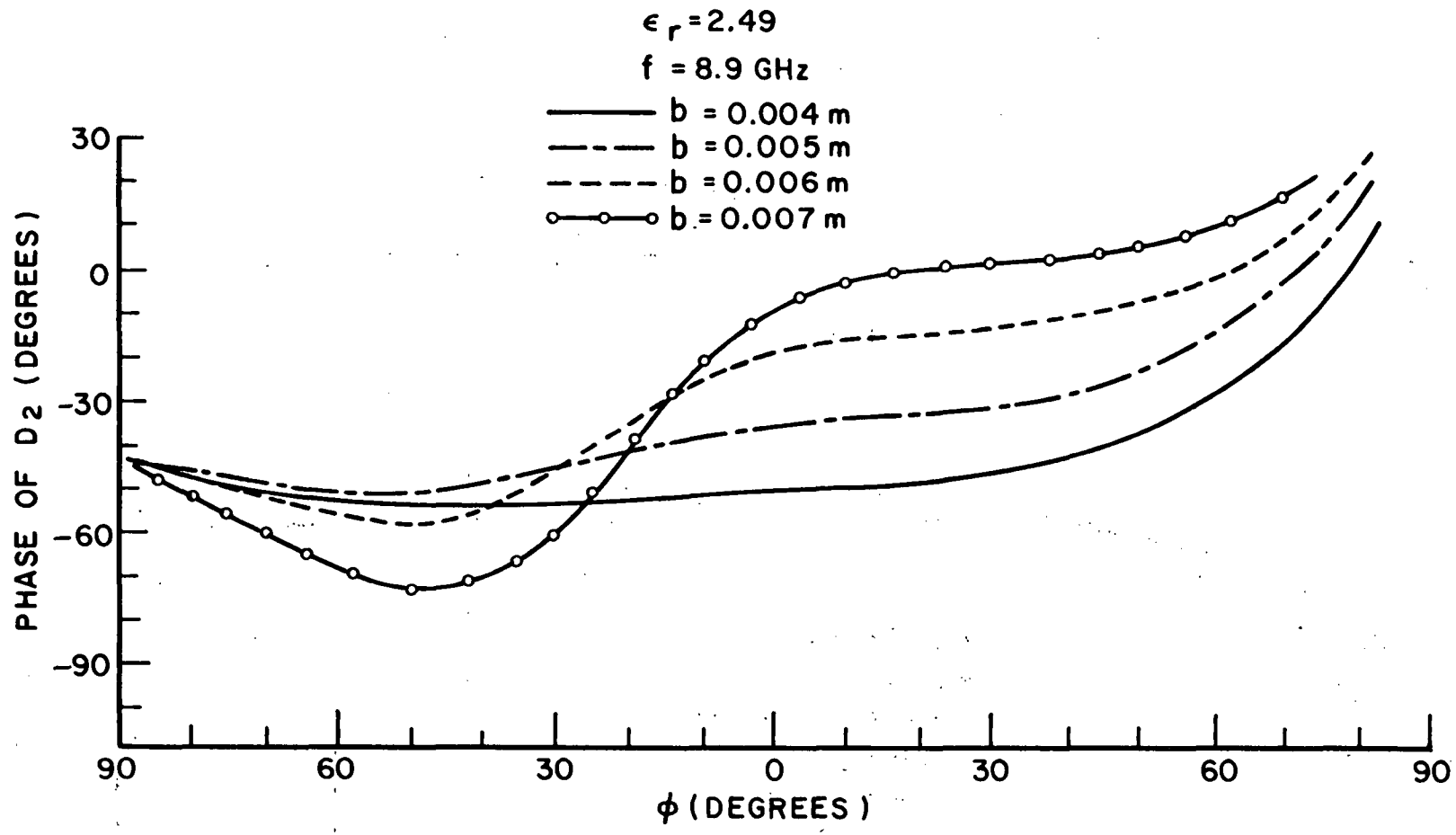

Fig. 24-- Phase of the diffraction coefficient D_2.

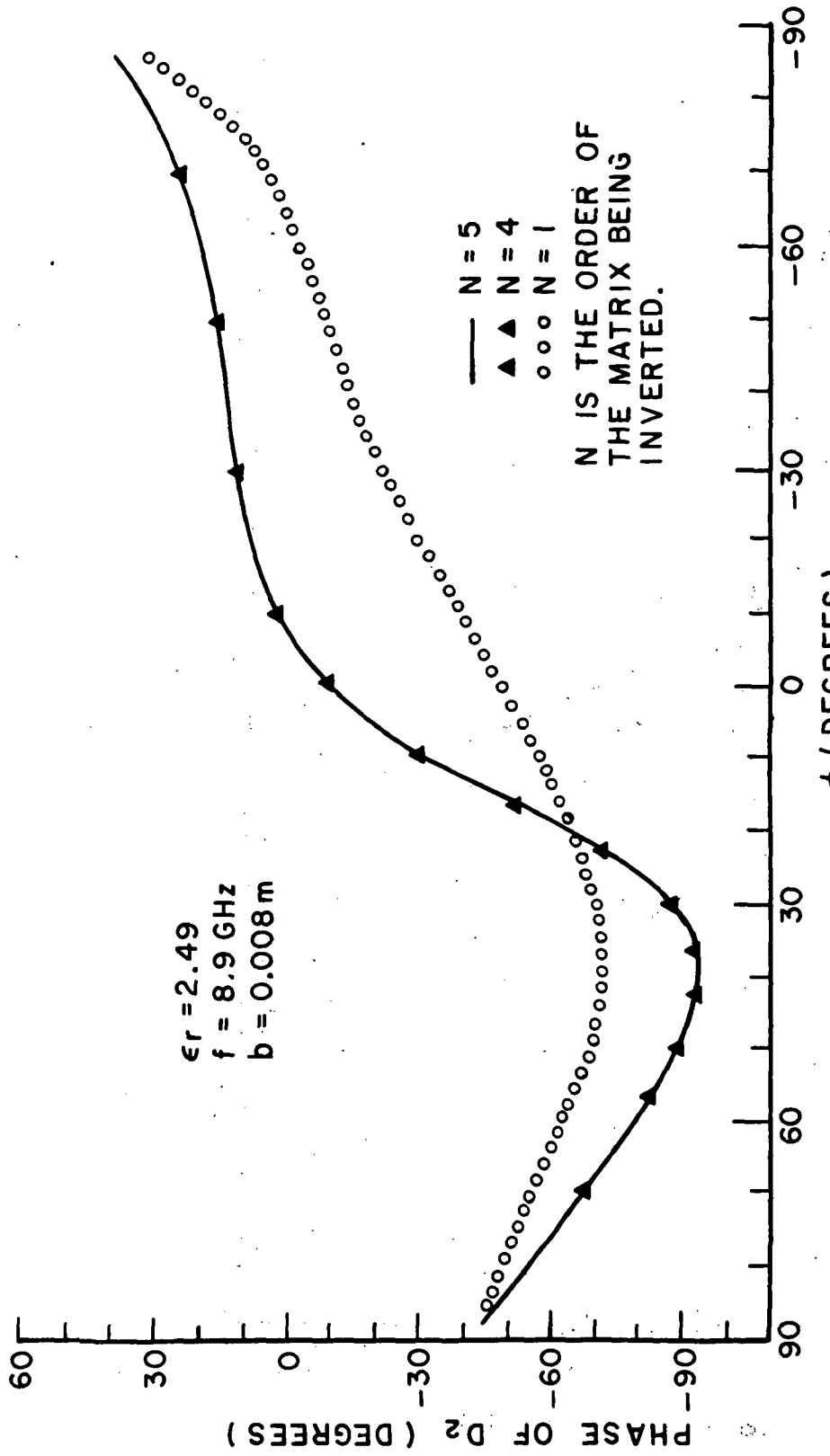

Fig. 25-- Phase of the diffraction coefficient D_2.

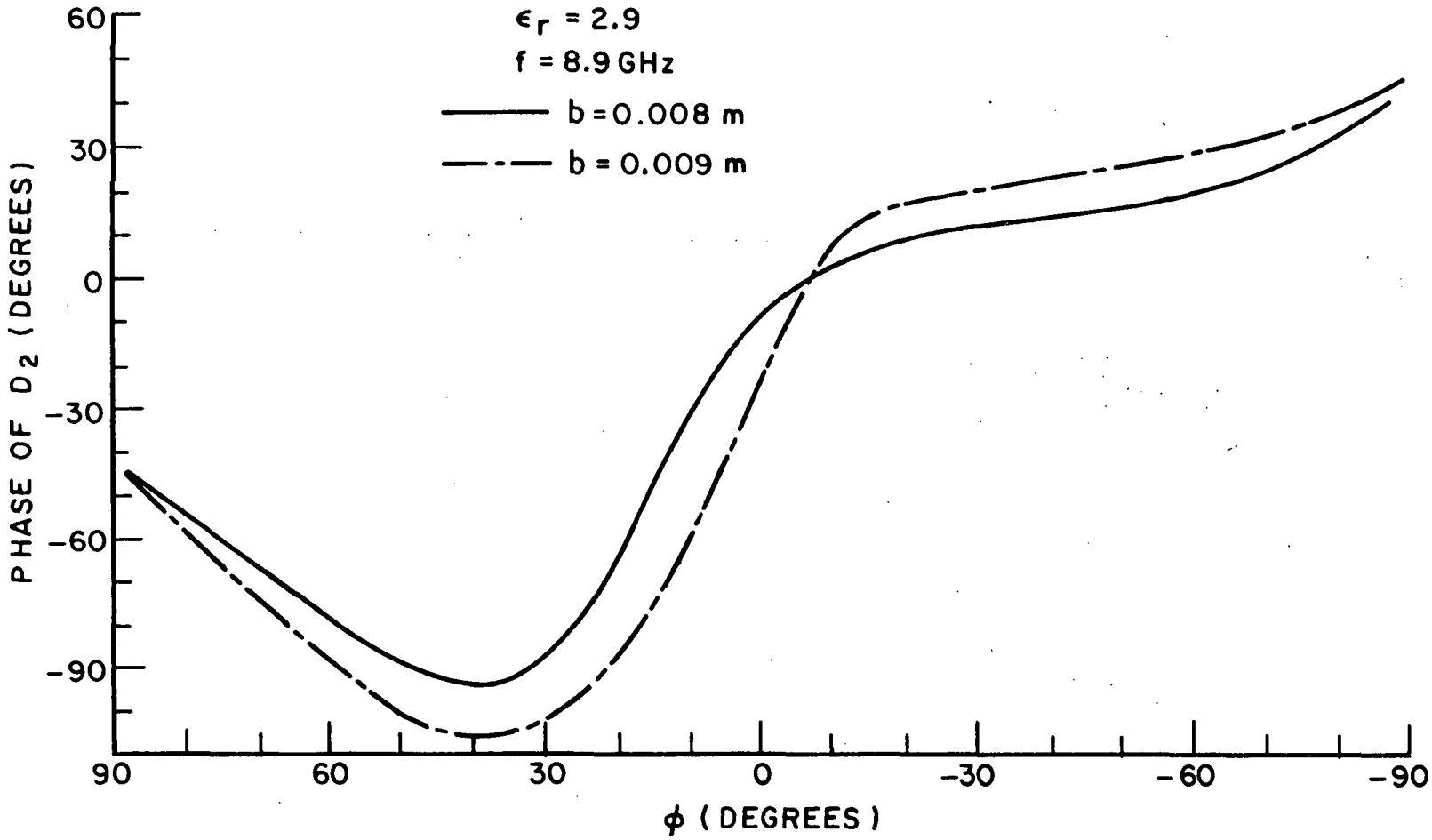

Fig. 26 -- Phase of the diffraction coefficient D_2.

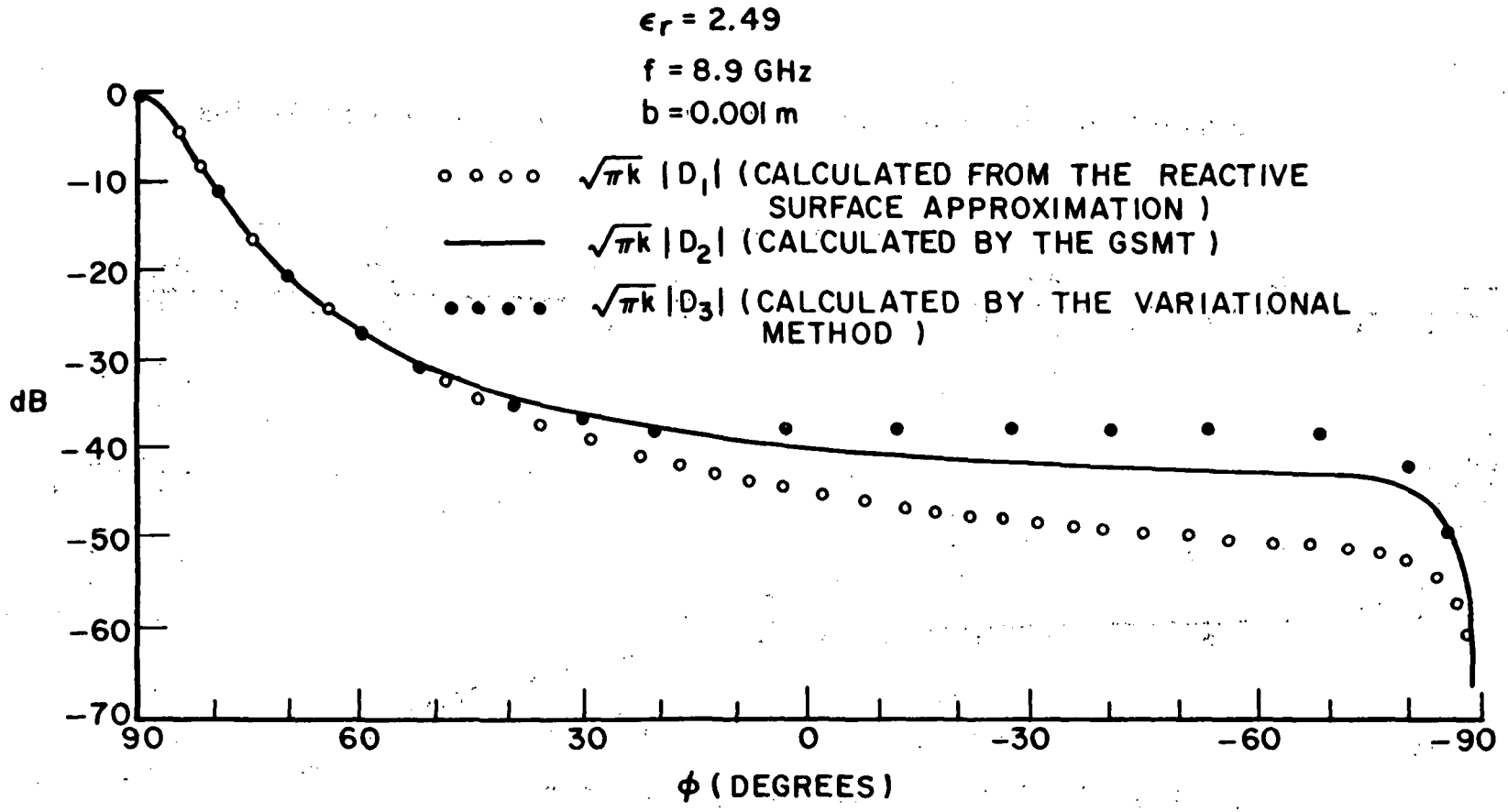

Fig. 27 -- A comparison of the diffraction coefficients D_1 and D_3 with D_2.

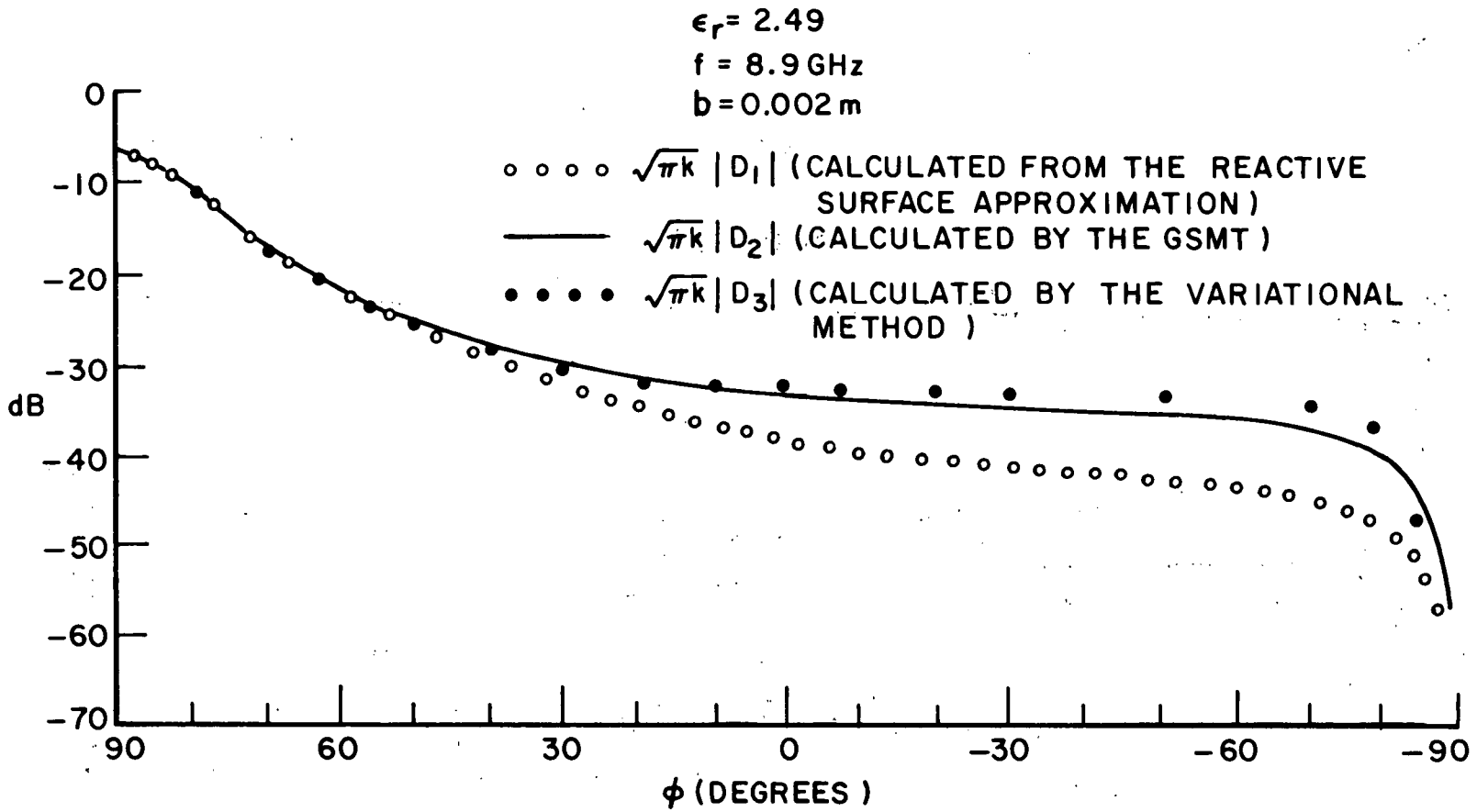

Fig. 28 -- A comparison of the diffraction coefficients D_1 and D_3 with D_2.

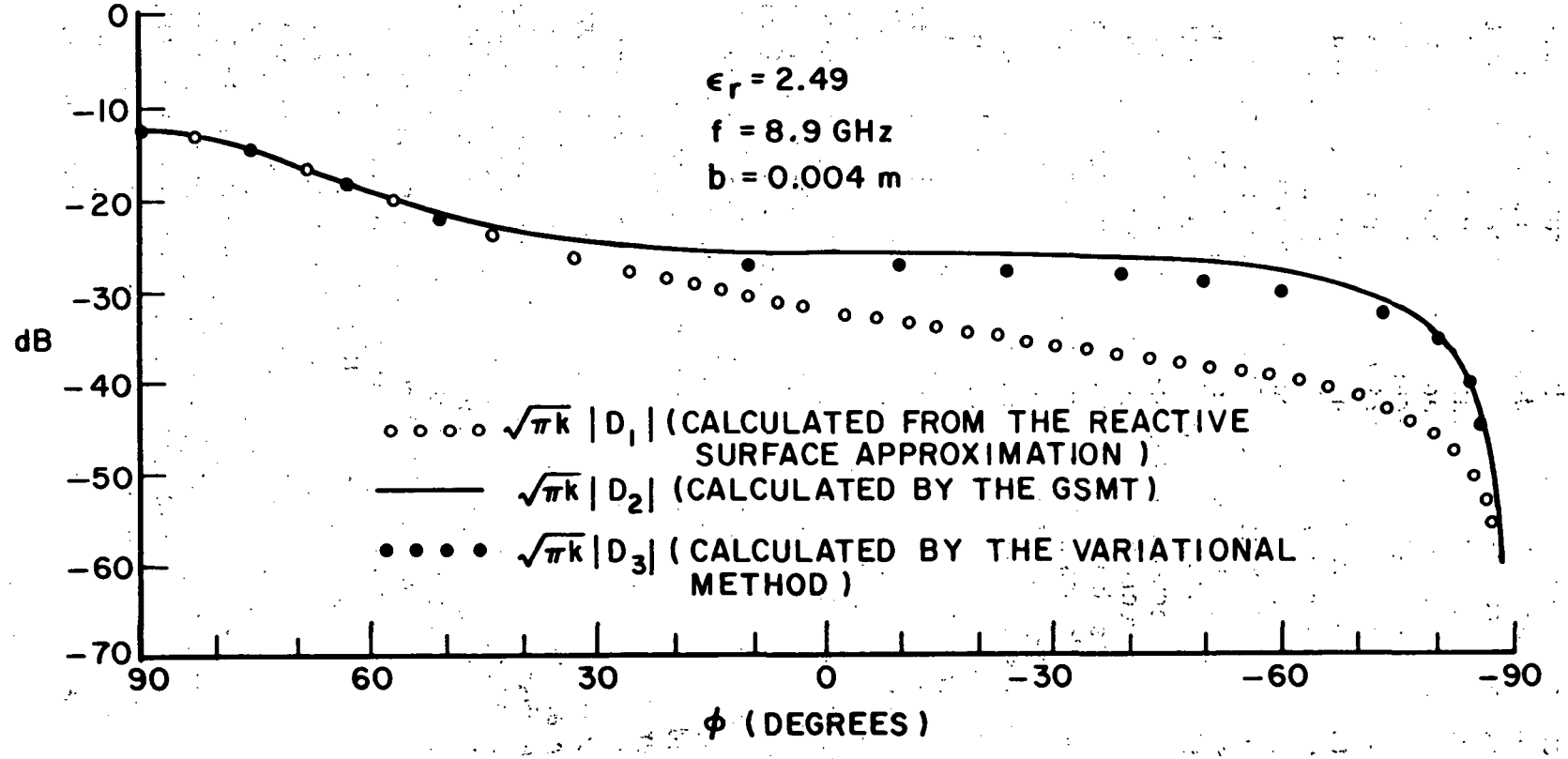

Fig. 29-- A comparison of the diffraction coefficients D_1 and D_3 with D_2.

The inaccuracy in the values of D_1 and R_1 for the surface reactance approximation to the grounded dielectric cover of Fig. 2, appears to be due largely to the fact that it does not properly account for the effect of the conducting step at z=0 and $0 < x < b$ in Fig. 2. As mentioned in the introduction, the surface reactance approximation indicated in Fig. 3 also serves to approximately describe the diffraction of a surface wave by the complementary structure of Fig. 4. It is conjectured that the terminated surface reactance model of Fig. 3 approximates the configuration of Fig. 4 better than it approximates the configuration of Fig. 2, because the latter structure has an additional discontinuity in the form of the step in the ground plane; as mentioned previously, this is evident by noting that the former structure reduces to the smooth ground plane as $\varepsilon_r \to 1$, whereas the latter structure has a residual step present. The importance of this residual step on the radiation properties of the junction may be demonstrated as follows. If one maintains the effective surface reactance of the grounded dielectric cover constant while decreasing the thickness of the slab for the configuration of Fig. 2, one tends to reduce the effect of the step without changing the discontinuity in surface reactance. The time average power ratio of the fields outside the dielectric to the fields inside the dielectric increases rapidly as the step size is decreased, while maintaining the surface reactance fixed thereby substantiating the argument that the effect of the step is reduced as the step size is decreased. Under these conditions one would expect the results for the configuration in Fig. 2 to approach those corresponding to the surface reactance configuration of Fig. 3. Indeed, this is found to be the case as shown in Figs. 30(a) and 31(a), where it is seen that $|R_2|$ approaches $|R_1|$ for a given surface reactance, X_s, as the step size decreases. One notes that the relative permittivity, ε_r of the dielectric cover increases with diminishing step size in order to keep the equivalent surface reactance a constant. The phase of R_2 also approaches the phase of R_1 until a certain minimum step size b_o is reached, see Figs. 30 and 31; however, for any further decrease in the step size, the phase of R_2 tends to deviate from the phase of R_1. This anomalous behavior for the phase of R_2 is not indicated in Figs. 30(a) and 31(a); it may result from several factors which are considered next. The phase anomaly occurs whenever the permittivity (ε_r) of the dielectric slab increases most rapidly with decrease in the thickness, b of the dielectric slab. It is seen that ε_r increases extremely rapidly with only a slight change in b for $0 < b < b_o$. One reason for the phase anomaly may be the possible existence of undetected numerical inaccuracies in the computer programs for evaluating the Wiener-Hopf factors of G(s) of (94) whenever ε_r becomes very large (the factors of G(s) and their numerical evaluation is discussed in Appendix II). Another factor contributing to the phase anomaly may arise from the following possibility. It is found that as

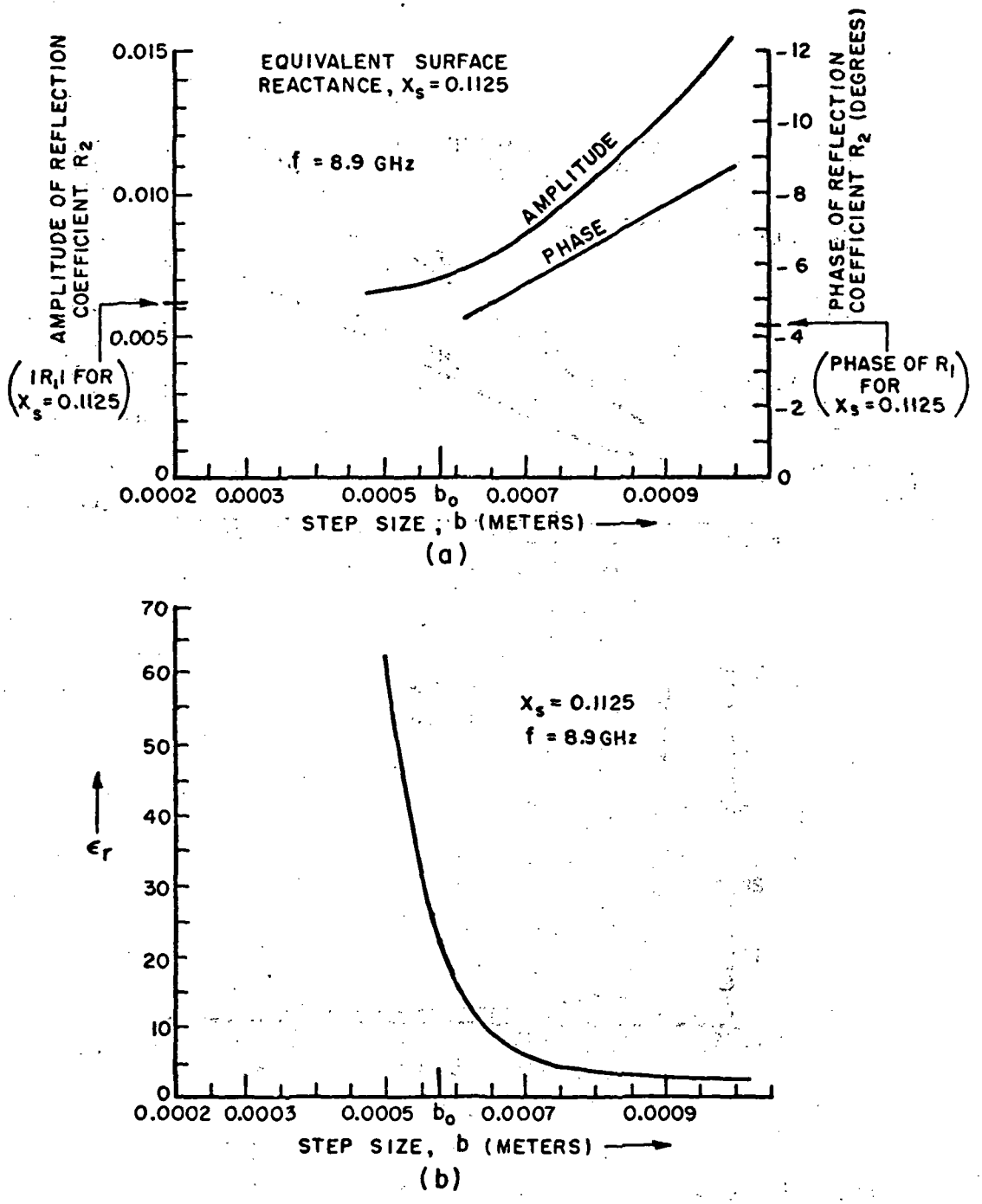

Fig. 30--Behavior of the reflection coefficient R_2 as a function of b, for $X_s = 0.1125$.

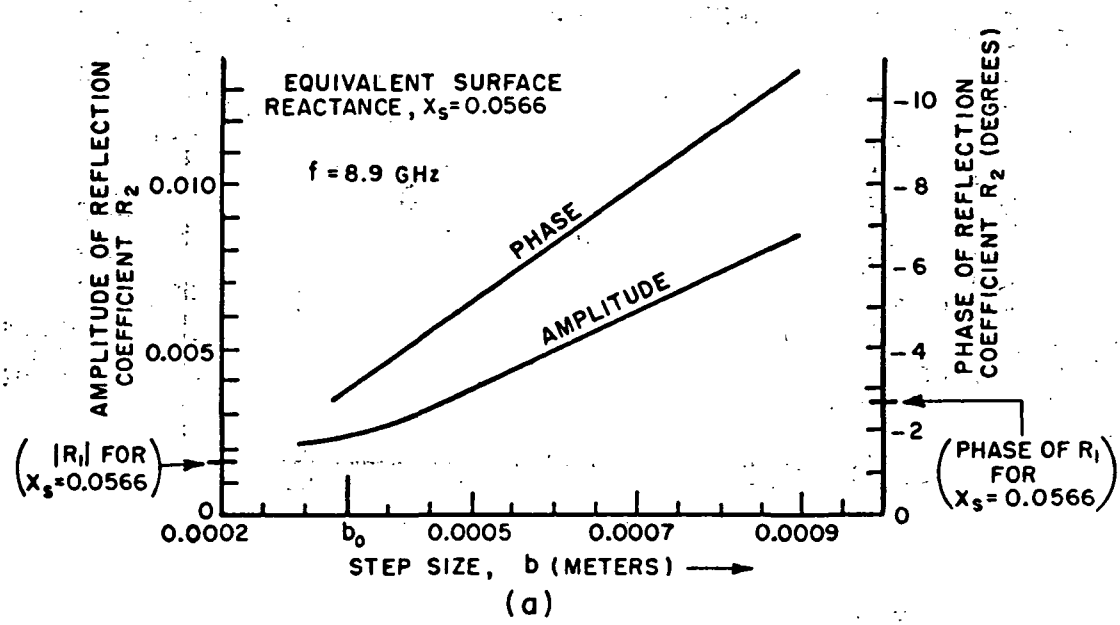

(a)

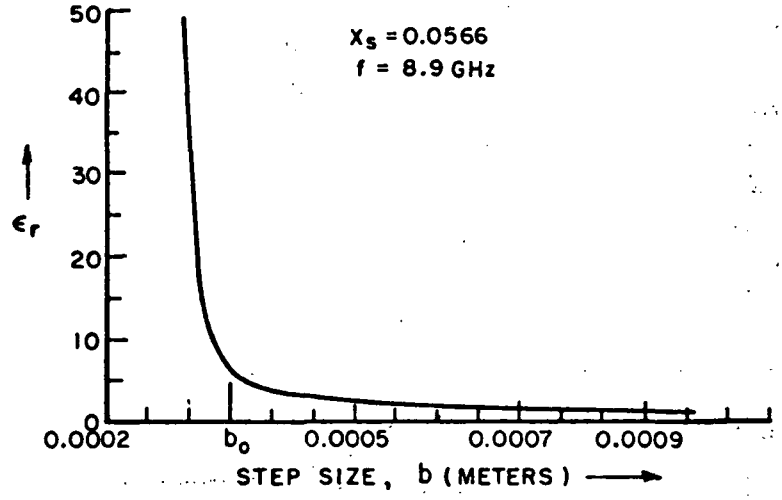

(b)

Fig. 31--Behavior of the reflection coefficient R_2 as a function of b, for X_s = 0.0566.

the height b of the step is decreased, the electrical thickness of the dielectric slab decreases only slightly and then actually increases; this increase in the electrical thickness becomes most rapid where ε_r begins to increase most rapidly. It is possible that when the electrical thickness of the step increases rapidly, one may not be able to isolate the junction effects into those which are assumed to arise independently from the discontinuity in surface reactance and from the presence of the step.

In summary, it is seen that approximations based on the surface reactance model and the variational solution, where the trial function consists of only the surface wave fields, do not yield accurate values of the reflection coefficient for the canonical problem shown in Fig. 2. On the other hand, these approximations do predict the radiation pattern in the forward region with reasonable accuracy, but they fail to yield accurate patterns for the backward region. As noted, the former is just another example of the success of a Kirchhoff-type approximation in predicting the main beam of a radiation pattern, whereas the failure to predict the patterns in the rearward region is largely the result of errors in the reflection coefficient resulting from these approximations.

We conclude the chapter with some remarks concerning the technological relevance of the research described in this report. It has already been noted that the results of this study are of importance in the analysis of slot arrays radiating in the presence of a dielectric cover. As a matter of fact, it was pointed out in the first chapter that this motivated our research; in particular, we wished to assess the effect of the termination of the cover on the performance of the antenna.

A dielectric cover is generally used for the purpose of impedance matching of the array (since the presence of the dielectric introduces an additional parameter into the problem thereby providing a means to improve the scanning capability of the array by adjusting and optimizing the parameters), and/or as a protective cover for the array, i.e., as a flush mounted radome. The dielectric cover is of course intended to have a minimal effect on the pattern of the array. However, the work of Wu, Galindo, Lechtreck, Allen[18, 19,20] and others have shown that if a surface wave is strongly excited in the cover, the energy radiated by the array can drop sharply thereby modifying the radiation pattern substantially. This condition is referred to as the forced surface wave resonance. Also, the use of dielectric cover for impedance matching may increase the frequency sensitivity of the array. Furthermore when the surface wave reaches the termination of the dielectric cover it radiates contributing to the pattern in a manner not intended in the original design. Using the diffraction coefficient derived here, a calculation of this effect can be made. If the surface wave is strongly

reflected from the terminations of the dielectric cover (see Fig. 1), a large standing wave is created in the cover; this can have an undesirable effect on the input impedance and bandwidth of the array. This standing wave can be found from the surface wave reflection coefficient given here.

The results of this study are also important to the design of surface wave antennas; a good review of the subject is given in Reference [21]. It is pointed out there that a surface wave guided along a uniform structure can radiate only at points of discontinuity, so that the terminal and feed radiation patterns are of interest. The configuration shown in Fig. 2 can be regarded as the termination of a flush mounted surface wave antenna, and the surface wave reflection and diffraction coefficients (which characterize the discontinuity in Fig. 2) may be used to advantage for analyzing the effect of the termination. It is seen from the results in this chapter that the magnitude of the surface wave reflection coefficient can be made small by decreasing the thickness of the dielectric panel; this in turn increases the level of the radiation field in the forward region. In the case of a thicker dielectric cover, it may be desirable to gradually taper the dielectric slab near its termination to reduce the magnitude of the surface wave reflected by the termination; this in turn improves the forward radiation characteristics of the end-fire surface wave antenna.

APPENDIX I
A WIENER-HOPF FACTORIZATION PROCEDURE

I. In this section, a method is discussed for factorizing the function $L(s)$ into $L_+(s)$ and $L_-(s)$ which are respectively analytic in the U.H.P. and the L.H.P. As before, $s = \sigma + i\tau$ and L.H.P. refers to the region in the complex s plane for which $\tau < \tau_-$ (where τ_- is taken to be positive for convenience), whereas, U.H.P. corresponds to the region in the s-plane for which $\tau > \tau_+$ (τ_+ is taken to be negative for convenience). $L(s)$ has the properties

(A-1) $L(s) = L(-s)$

(A-2) $L(s)$ is analytic and zonzero in the strip $\tau_+ < \tau < \tau_-$

(A-3) $L(s) \sim C_A s^{\nu}$, when $s \to \infty$ in the strip $\tau_+ < \tau < \tau_-$

C_A and ν are real constants.

(A-4) Outside the strip of analyticity, $L(s)$ may have simple poles, simple zeros, and branch points.

As a consequence of (A-1), the poles, zeros and branch points occur in pairs, symmetrically with respect to the origin. For example in the case of the branch points $s = \pm k$ ($k = k_1 + ik_2$; $k_2 << k_1$ and $k_1 > 0$, $k_2 > 0$).

The factorization of $L(s)$ is achieved via a limiting operation on a related function $K(s,a)$ which has only simple poles and simple zeros; the factorization of $K(s,a)$ is usually trivial. Specifically, $K(s,a)$ is chosen such that

(A-5) $$L(s) = \lim_{a \to \infty} K(s,a).$$

$K(s,a)$ need not be unique, even though its limit as $a \to \infty$ is unique and equal to $L(s)$. This technique of factorizing a function $L(s)$ with branch points at $s = \pm k$ through a limiting operation on a related function $K(s,a)$ which has no branch points, was first developed by Bates and Mittra [2]; they treated specific problems by this technique. Such a factorization technique generally leads to factors which are convenient for numerical calculation. More recently, Bates and Mittra[9,16] generalized their results in [2] to factorize a class of functions denoted here by $L_o(s)$ which

asymptotically behave as $C_A s^{\nu} e^{-bs}$ for large s; C_A, ν and b are real constants. $L_o(s)$ also satisfies the conditions indicated in (A-1), (A-2) and (A-4) for L(s). An integral representation for the Wiener-Hopf factors of $L_o(s)$ is initially conjectured by the authors in [16]; their conjecture is based on the form of the factors obtained earlier in [2]. In [16] the authors demonstrate their integral representation to be consistent with all the requirements on their factors, which lends credance to their factorization method. In this appendix, a derivation for the Wiener-Hopf factors of the function L(s) (with an asymptotic behavior indicated by (A-3)) is presented without requiring that the form of the factors be assumed as an initial step. The present development unlike that in [9,16] requires the introduction of a related factorization function K(s,a) as defined in (A-5); however, the final result for the factors is independent of K(s,a) even though the development of this factorization formula is based on initially introducing K(s,a) and later carrying out the limiting operation on the factors of K(s,a) as $a \to \infty$. In addition to (A-5), K(s,a) must be chosen such that it satisfies the following conditions;

(A-6) $K(s) = K(-s)$

(A-7) K(s) is analytic and non-zero in $\tau_+ < \tau < \tau_-$; elsewhere it has simple zeros and simple poles.

(A-8) $K(s) \sim C_B s^{\nu}$, where C_B is a constant.

(A-9) $\lim_{a\to\infty} K(s,a) \to L(s)$, regularly in s

(A-10) $\lim_{a\to\infty} K'(s,a) \quad L'(s)$, regularly in s

where the primes denote differentiation with respect to s.

One may factorize K(s) into $K_+(s)$ and $K_-(s)$ where the + subscript implies analyticity in the U.H.P. and the - subscript implies analyticity in the L.H.P. as before. $K_{\pm}(s)$ are given as [22]

$$(A\text{-}11)\qquad K_+(s) = [K(0)]^{1/2}\, e^{-X_0(s)}\, \frac{\prod_{m=1}^{\infty} \left(1 + \frac{s}{p_m}\right) e^{-\frac{s}{p_m}}}{\prod_{n=1}^{\infty} \left(1 + \frac{s}{q_n}\right) e^{-\frac{s}{q_n}}}$$

where $K(s)$ has simple poles at $s = \pm q_n$ and simple zeros at $s = \pm p_m$. (Here, $n = 1,2,3 \cdots$ and $m = 1, 2, 3 \cdots$). The function $K_-(s)$ is obtained from (A-11) via

$$(A\text{-}12)\qquad K_-(s) = K_+(-s).$$

$X_0(s)$ is at present an undetermined entire function; it is chosen such that (A-8) is true.

$$(A\text{-}13)\qquad X_0(s) = -X_0(-s);$$

moreover $X_0(s)$ depends on 'a'; i.e, $X_0 = X_0(s,a)$.

The representation in (A-11) is converted to a contour integral as:

$$(A\text{-}14)\qquad K_+(s) = [K(0)]^{1/2}\, e^{-X_0(s)}\, \exp\cdot\left\{\frac{1}{2\pi i}\int_{C_{UHP}} \left[\ln\left(1 + \frac{s}{\psi}\right) - \frac{s}{\psi}\right]\frac{K'(\psi)}{K(\psi)}\, d\psi\right\}$$

The contour C_{UHP} is indicated in Fig. A-1.

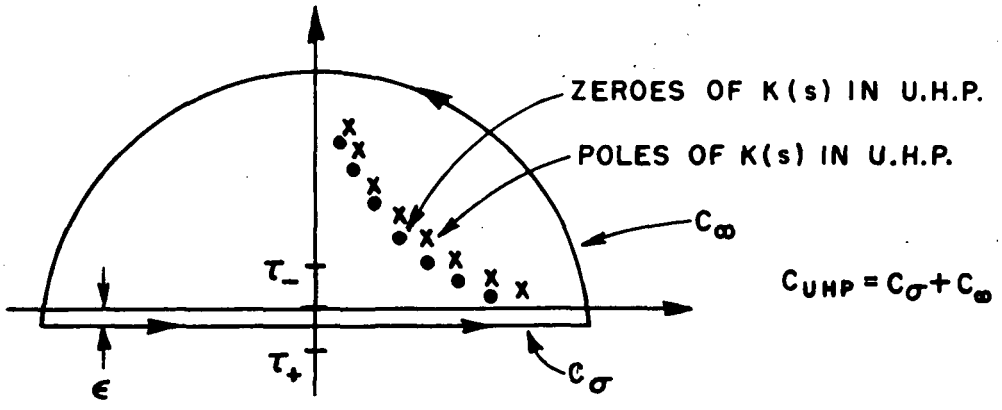

Fig. A-1 -- The contour C_{UHP} in the complex s plane.

The contribution to C_{UHP} from C_∞ vanishes so that

(A-15)

$$K_+(s) = [K(0)]^{1/2}\, e^{-X_0(s)} \exp\left\{\frac{1}{2\pi i}\int_{-\infty - i\varepsilon}^{\infty - i\varepsilon}\left[\ln\left(1+\frac{s}{\psi}\right) - \frac{s}{\psi}\right]\frac{K'(\psi)}{K(\psi)}\,d\psi\right\}.$$

Define

(A-16) $$\lim_{a\to\infty} X_0(s,a) = X(s)\ ,$$

The limit as $a\to\infty$ of (A-15) therefore leads to

(A-17) $$L_+(S) = [L(0)]^{1/2}\, e^{-X(s)} \exp\left(\frac{1}{2\pi i}\int_{-\infty - i\varepsilon}^{\infty - i\varepsilon}\left[\ln\left(1+\frac{s}{\psi}\right) - \frac{s}{\psi}\right]\frac{L'(\psi)}{L(\psi)}\,d\psi\right)$$

Let L(s) have simple zeros at $s = \pm \ell_m$ $(m = 1,2,3\cdots)$ and simple poles at $s = \pm r_n$ $(n = 1,2,3\cdots)$. In addition L(s) has branch points at $s = \pm k$ arising from the presence of $\sqrt{k^2-s^2}$ type terms. The proper branch for $\sqrt{k^2-s^2}$ is the one for which $\mathrm{Im}\sqrt{s^2-k^2} > 0$:

$$\sqrt{k^2-s^2} = i\sqrt{s^2-k^2}$$

(the above is consistent with the development in Chapters II and III). One may now close the contour in (A-17) by C_∞ in the U.H.P. (with a deformation around the branch cut) and use the Cauchy Residue Theorem to obtain

(A-18) $$L_+(s) = [L(0)]^{1/2}\, e^{-X(s)}\left\{\exp\left(-\frac{1}{2\pi i}\int_{C_{Br}}\left[\mathrm{Ln}\left(1+\frac{s}{\psi}\right) - \frac{s}{\psi}\right]\cdot\right.\right.$$

$$\left.\left.\cdot\,\frac{L'(\psi)}{L(\psi)}\,d\psi\right)\right\}\frac{\prod_{m=1}^{\infty}\left(1+\frac{s}{\ell_m}\right)e^{-\frac{s}{\ell_m}}}{\prod_{n=1}^{\infty}\left(1+\frac{s}{r_n}\right)e^{-s/r_n}}$$

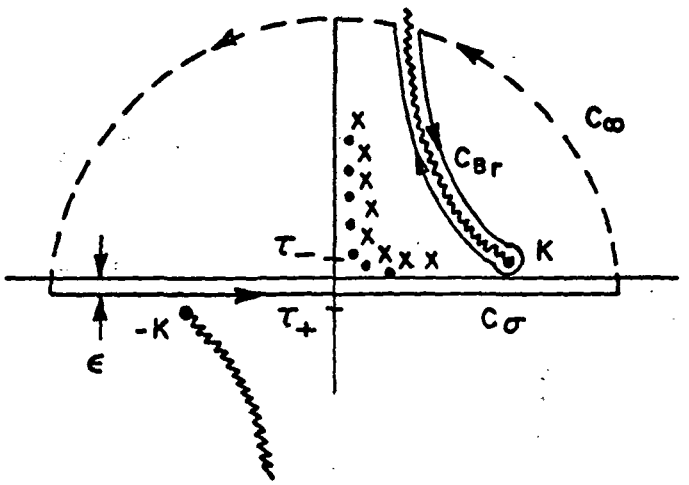

Fig. A-2 --The contour C_{Br} in the complex s plane.

The contour C_{Br} is shown in Fig. A-2. The contour $-C_{Br}$ may be mapped into the contour C_w parallel to the real axis via the usual transformation $\psi = (k^2-w^2)^{1/2}$. Without going through the details of this transformation, the final result for the integral in the complex w-plane is given below:

$$(A\text{-}19)\quad L_+(s) = \{L(0)\}^{1/2}\, e^{-X(s)}\left[\exp\left\{\frac{1}{2\pi i}\int_{C_w}\left[\ln\left(1+\frac{s}{\sqrt{k^2-w^2}}\right)-\right.\right.\right.$$

$$\left.\left.\left.-\frac{s}{\sqrt{k^2-w^2}}\right]\frac{L'(\sqrt{k^2-w^2})}{L(\sqrt{k^2-w^2})}\,dw\right]\right\}\cdot$$

$$\cdot\,\frac{\prod_{m=1}^{\infty}\left(1+\frac{s}{\ell_m}\right)e^{-\frac{s}{\ell_m}}}{\prod_{n=1}^{\infty}\left(1+\frac{s}{r_n}\right)e^{-s/r_n}}$$

The prime on $L'(\sqrt{k^2-w^2})$ now denotes differentiation w.r.t. w. The contour C_w is indicated in Fig. A-3.

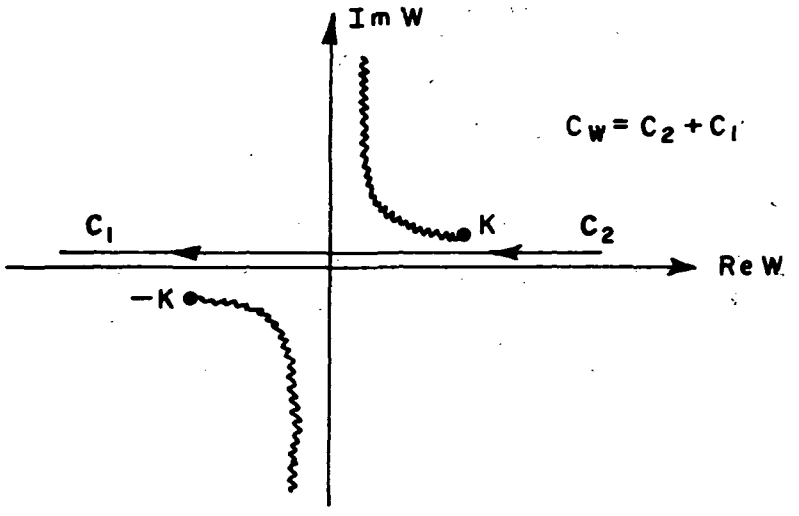

Fig. A-3-- The contour C_w in the complex w-plane.

The contour C_w may now be deformed to the real w axis. If $L(\sqrt{k^2-w^2})$ has a zero at w = 0, the contribution from w = 0, which is denoted by $(1/2)\,\nu_o$ must be included.

$$\text{(A-20)} \qquad \nu_o = \lim_{w \to 0} w \, \frac{L'(\sqrt{k^2-w^2})}{L(\sqrt{k^2-w^2})}$$

Hence (A-19) becomes

$$\text{(A-21)} \qquad L_+(s) = [L(0)]^{1/2} \, e^{-X(s)} \, e^{-\nu_o \frac{s}{2k}} \left(1 + \frac{s}{k}\right)^{\nu_o/2} \cdot$$

$$\cdot \frac{\prod_m \left(1 + \frac{s}{\ell_m}\right) e^{-\frac{s}{\ell_m}}}{\prod_n \left(1 + \frac{s}{r_n}\right) e^{-\frac{s}{r_n}}} \; \frac{1}{e^{2\pi i}} \text{P.V.} \int_{-\infty}^{\infty} \left[\ln\left(1 + \frac{s}{\sqrt{k^2-w^2}}\right) - \frac{s}{\sqrt{k^2-w^2}}\right] \cdot$$

$$\cdot \frac{L'(\sqrt{k^2-w^2})}{L(\sqrt{k^2-w^2})} \, dw$$

The P.V. indicates that 1/2 (residues) of any other zeros of $L(\sqrt{k^2-w^2})$ encountered along the real axis must be included. The infinite integral in (A-21) may be re-expressed as a semi-infinite integral:

(A-22)

$$L_+(s) = [L(0)]^{1/2}\, e^{-X(s)} \cdot \frac{\nu_0 s}{2k} \left(1+\frac{s}{k}\right)^{\frac{\nu_0}{2}} \prod_m \left(1+\frac{s}{\ell_m}\right) e^{-\frac{s}{\ell_m}} \Big/ \prod_n \left(1+\frac{s}{r_n}\right) e^{-s/r_n} \cdot$$

$$\cdot \exp\left\{\frac{-1}{2\pi i}\, P.V. \int_0^\infty \left[\ln\left(1+\frac{s}{\sqrt{k^2-w^2}}\right) - \frac{s}{\sqrt{k^2-w^2}}\right]\{\mathcal{L}(w)+\mathcal{L}(-w)\}dw\right\}$$

where

(A-23)

$$\mathcal{L}(w) \equiv \frac{\frac{d}{dw} L(\sqrt{k^2-w^2})}{L(\sqrt{k^2-w^2})}$$

X(s) in (A-22) must be chosen such that $L_+(s)$ has the proper asymptotic behavior as indicated in (A-3). For specific problems, X(s) may be determined from a knowledge of the asymptotic behavior of the infinite products and of the integral

$$\frac{1}{2\pi i}\, P.V. \int_0^\infty \left[\ln\left(1+\frac{s}{\sqrt{k^2-w^2}}\right)\right]\{\mathcal{L}(w)+\mathcal{L}(-w)\}\, dw$$

which occur in (A-22); a typical procedure for the asymptotic evaluation of these terms as $s\to\infty$ in the strip $\tau_+ < \tau < \tau_-$ is indicated in Sections II and III of this appendix. (Also see [2].) It is noted that the final form of the factors $L_\pm(s)$ indicated in (A-22) is not dependent on the choice of an appropriate closed region function K(s,a); one may therefore proceed directly to the expression in (A-22) for $L_\pm(s)$ without ever specifying a closed region function K(s,a). One notes however, that K(s,a) was introduced in order to arrive at the final expression for $L_\pm(s)$. In some cases it may be difficult to evaluate X(s) in the expression for $L_\pm(s)$ directly from the asymptotic behavior of the terms in (A-22); when this happens to be the case, it may be worthwhile to specify an appropriate closed region function K(s,a) for the problem in order that one may now obtain X(s) from the operation $X(s) = \lim_{a\to\infty} X_0(s,a)$. The function $X_0(s,a)$ appearing in (A-11) can usually be determined quite readily.

II. Application of (A-22) to the Factorization of $\sqrt{k^2-s^2}(\sqrt{k^2-s^2} - i\alpha)^{-1}$

The function L(s) to be factored is

$$(A\text{-}24) \quad L(s) = \frac{\sqrt{k^2-s^2}}{\sqrt{k^2-s^2} - i\alpha} ,$$

where α is a real constant. This function is encountered in the solution of the problem illustrated in Fig. 3. If one places a conducting boundary at x = a in Fig. 3, the function to be factorized becomes

$$(A\text{-}25) \quad K(s,a) = \frac{\sqrt{k^2-s^2}\,\sin\sqrt{k^2-s^2}\,a}{\sqrt{k^2-s^2}\,\sin\sqrt{k^2-s^2}\,a + \alpha\cos\sqrt{k^2-s^2}\,a}$$

Clearly $\lim_{a\to\infty} K(s,a) = L(s)$ which is also seen from physical considerations (i.e. moving the conducting boundary at x=a to ∞ yields back the original problem of Fig. 3). K(s,a) has no branch points in the s-plane. Both L(s) and K(s,a) satisfy the requirements indicated in Section I. Without re-deriving all the details in going from $K_{\pm}(s,a)$ to $L_{\pm}(s)$, one proceeds directly with (A-22). $\mathcal{L}(w)$ for this problem is

$$(A\text{-}26) \quad \mathcal{L}(w) = \frac{\frac{d}{dw}\,L(\sqrt{k^2-w^2})}{L(\sqrt{k^2-w^2})} = \frac{-i\alpha}{w(w-i\alpha)}$$

Also

$$(A\text{-}27) \quad \nu_0 = \lim_{w\to 0} w\,\mathcal{L}(w) = 1$$

and

$$(A\text{-}28) \quad \mathcal{L}(w) + \mathcal{L}(-w) = -\frac{2i\alpha}{w^2 + \alpha^2}$$

L(s) has no zeros; it has poles at $s = \pm\beta$ (where $k^2-\beta^2=-\alpha^2$) and branch points at $s = \pm k$. Hence we may write $L_+(s)$ for this problem via (A-21) as

$$(A\text{-}29)\quad L_+(s) = \left(\frac{k}{k-i\alpha}\right)^{1/2} e^{-X(s)-\frac{s}{2k}} \left(1+\frac{s}{k}\right)^{1/2} \left(1+\frac{s}{\beta}\right)^{-1}$$

$$e^{-\frac{P.V.}{2\pi i}\int_{-\infty}^{\infty}\left[\ln\left(1+\frac{s}{\sqrt{k^2-w^2}}\right)-\frac{s}{\sqrt{k^2-w^2}}\right]\frac{-i\alpha\, dw}{w(w-i\alpha)}}$$

Also,

$$(A\text{-}30)\quad L_-(s) = L_+(-s)$$

One knows from (A-24) that $L(s) \sim C_0 s^0$, where C_0 is a constant. Hence, $L_+(s) \sim C_0^{1/2}$; one may now use this condition to find X(s) in (A-29).

The P.V. $\int_{-\infty}^{\infty}$ in (A-29) may be written as

(A-31)

$$P.V.\int_{-\infty}^{\infty} = -\oint_{C_S} - \int_{\Sigma} - \int_{C_{Br}} = -2\pi i \cdot \frac{1}{2}\,(\text{Residue at } w=0) - \int_{C_{Br}}$$

The contours C_S, Σ and C_{Br} are shown in Fig. A-4. The integral over Σ gives a vanishing contribution. Only the

$$\ln(1 + s/\sqrt{k^2-w^2})$$

term in the integrand can exhibit an algebraic behavior in s for $L_+(s)$ as $s\to\infty$; hence, one considers this term first.

$$(A\text{-}32)\quad -\frac{1}{2\pi i}P.V.\int_{-\infty}^{\infty}\ln\left(1+\frac{s}{\sqrt{\quad}}\right)\cdot\mathcal{L}(w)dw = \frac{1}{2}\ln\left(1+\frac{s}{k}\right) - \int_{C_{Br}}$$

It can be shown that $\int_{C_{Br}}$ is bounded and is a constant. Hence the

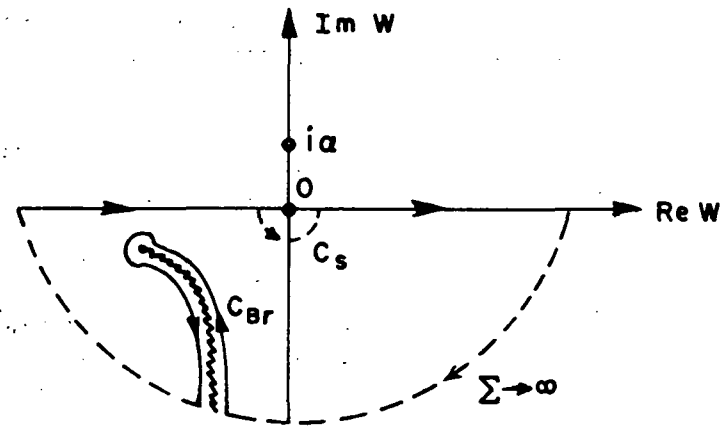

Fig. A-4 -- The contours C_s, Σ and C_{Br} in the complex w plane.

term $\frac{1}{2}\ln\left(1+\frac{s}{k}\right)$ dominates over $\int_{C_{Br}}$ as $s \to \infty$ so that

$$(A\text{-}33)\quad \exp\frac{1}{2\pi i}\,P.V.\int_{-\infty}^{\infty}\ln\left(1+\frac{s}{\sqrt{\quad}}\right)\cdot\mathcal{L}(w)dw \sim O(s^{1/2})$$

Utilizing (A-33) in the asymptotic behavior of $L_+(s)$ in (A-29), one obtains

$$(A\text{-}34)\quad L_+(s) \sim [L(0)]^{1/2}\, e^{-X(s)-s/2k}\exp\frac{-1}{2\pi i}\,P.V.\int_{-\infty}^{\infty}\frac{s}{\sqrt{k^2-w^2}}\cdot\mathcal{L}(w)\,dw$$

(since the $\left(1+\frac{s}{k}\right)^{1/2}$ factor in (A-29) behaves as $s^{1/2}$ whereas $\left(1+\frac{s}{\beta}\right)^{-1}$ behaves as s^{-1}).
Clearly the proper choice of $X(s)$ such that $L_+(s) \sim$ constant as $s\to\infty$, is

$$(A\text{-}35)\quad X(s) = -\frac{s}{2k} - \frac{s}{2\pi i}\,P.V.\int_{-\infty}^{\infty}\frac{\mathcal{L}(w)}{\sqrt{k^2-w^2}}\,dw\,.$$

Incorporating the above result in (A-29) and converting the infinite integral representation of (A-29) to a semi-infinite integral representation given in (A-22) gives the final form for $L_+(s)$ as

$$(A\text{-}36)\quad L_+(s) = \left(\frac{k}{k - i\alpha}\right)^{1/2} \frac{\left(1 + \frac{s}{k}\right)^{1/2}}{\left(1 + \frac{s}{\beta}\right)} e^{\frac{1}{\pi} P.V. \int_0^\infty \ln\left(1 + \frac{s}{\sqrt{k^2 - w^2}}\right) \frac{\alpha}{w^2 + \alpha^2} dw}$$

$L_-(s)$ may be deduced from (A-36) via (A-30); alternatively, $L_-(s)$ may be obtained from the relation

$$(A\text{-}37)\quad L_-(s) = L(s)/L_+(s).$$

The numerical evaluation of the integral for $L_+(s)$ is carried out using a ten point Gaussian quadrature.

III. Application to the Factorization of $G(s) = (\gamma\gamma_1 \sinh \gamma_1 b) \cdot (\gamma_1 \sinh \gamma_1 b + \varepsilon_r \gamma \cosh \gamma_1 b)^{-1}$

The factorization of $G(s) = (\gamma\gamma_1 \sinh \gamma_1 b)(\gamma_1 \sinh \gamma_1 b + \varepsilon_r \gamma \cosh \gamma_1 b)^{-1}$ is essential to the solution of the problem discussed in Chapter III. As before, $\gamma = \sqrt{s^2 - k^2}$, and $\gamma_1 = \sqrt{s^2 - k_d^2}$. In this section, the factorization of G(s) will be carried out by proceeding directly to the expression for $L_\pm(s)$ in (A-22) without specifying an appropriate closed region function K(s,a). Here, G(s) corresponds to L(s) of Section I, and $\mathcal{G}(w)$ will be defined to correspond to $\mathcal{L}(w)$ of Section I. Since the details for the factorization of G(s) are lengthy, only the important results leading to $G_+(s)$ will be given. Let

$$(A\text{-}38)\quad w' = \sqrt{-k^2 + k_d^2 + w^2}, \text{ where k and } k_d \text{ are given in Chapter III.}$$

One May write $\mathcal{G}(w)$ as

$$(A\text{-}39)\quad \mathcal{G}(w) \equiv \frac{\frac{d}{dw} G(\sqrt{k^2 - w^2})}{G(\sqrt{k^2 - w^2})} = \frac{d}{dw} \ln G(\sqrt{k^2 - w^2})$$

where

$$(A\text{-}40)\quad G(\sqrt{k^2 - w^2}) = \frac{iww' \sin w'b}{-w' \sin w'b - i\varepsilon_r w \cos w'b}$$

Hence, $\mathcal{J}(w)$ is given by

$$(A\text{-}41)\quad \mathcal{J}(w) = \frac{w'^4 \sin^2 w'b + i\varepsilon_r b w^3 w'^2 + i\varepsilon_r w^3 w' \sin w'b \cos w'b}{w[w'^4 \sin^2 w'b + i\varepsilon_r w w'^3 \sin w'b \cos w'b]}$$

Also

$$(A\text{-}42)\quad \mathcal{J}(w) + \mathcal{J}(-w) = 2i\left\{\frac{\varepsilon_r w^2 b + \left(\frac{w^2}{w'} - w'\right)\varepsilon_r \sin w'b \cos w'b}{w'^2 \sin^2 w'b + \varepsilon_r^2 w^2 \cos^2 w'b}\right\}$$

It is easily verified that $\nu_o = 1$, since

$$(A\text{-}43)\quad \nu_o = \lim_{w\to 0} w\,\mathcal{J}(w) = 1$$

One may write $G_+(s)$ in terms of the above results via (A-22) as

$$(A\text{-}44)\quad G_+(s) = \{G(0)\}^{1/2}\, e^{-X(s) - \frac{s}{2k}} \cdot \frac{\left(1 + \frac{s}{k}\right)^{1/2} \prod_{m=1}^{\infty} \left(1 + \frac{s}{\beta_m}\right) e^{-\frac{s}{\beta_m}} \left(1 + \frac{s}{k_d}\right)}{\left(1 + \frac{s}{\beta}\right)} \cdot \exp\left\{-\frac{1}{2\pi i}\,\mathrm{P.V.} \int_0^{\infty} \left[\ln\left(1 + \frac{s}{\sqrt{k^2 - w^2}}\right) - \frac{s}{\sqrt{k^2 - w^2}}\right] \cdot \left\{\mathcal{J}(w) + \mathcal{J}(-w)\right\} dw\right\}$$

where the zeros of G(s) occur at $s = \pm\beta_m$, $m = 0, 1, 2 \cdots$ and $\beta_0 = k_d$ (see Chapter III for definition of β_m). The poles of G(s) occur at $s = \pm\beta$ (corresponding to the TM_0 surface wave poles). The choice of X(s) is such that $G_+(s)$ behaves asymptotically as $s^{1/2}$ when $s\to\infty$; the latter is a consequence of the fact that $G(s) \sim O(s)$ as $s\to\infty$ in the strip within which G(s) is analytic. The asymptotic behavior of the integral

$$\text{P.V.} \int_0^\infty \ln\left(1 + \frac{s}{\sqrt{k^2-w^2}}\right) \cdot \left\{\mathcal{G}(w) + \mathcal{G}(-w)\right\} dw$$

(or of it's alternative respresentation which involves the infinite integral

$$\text{P.V.} \int_{-\infty}^\infty \ln\left(1 + \frac{s}{\sqrt{k^2-w^2}}\right)\mathcal{G}(w)\, dw$$

occuring in the expression for $G_+(s)$ in (A-44) is ascertained in a manner identical to that in Section II of this appendix (see (A-32) and (A-33)). The infinite product,

$$\prod_{m=1}^{\infty} \left(1 + \frac{s}{\beta_m}\right) e^{-\frac{s}{\beta_m}}$$

occuring in (A-44) is replaced by

$$\prod_{n=1}^{\infty} \left(1 + \frac{s}{\beta_n}\right) e^{\frac{isb}{n\pi}}$$

so that it's asymptotic behavior is readily obtained via [9]; thus

$$\text{(A-45)} \qquad \prod_{n=1}^{\infty} \left(1 + \frac{s}{\beta_n}\right) e^{\frac{isb}{n\pi}} \sim s^{-1/2}\, e^{\frac{sb}{2}}\, e^{\frac{isb}{\pi}\left[\Gamma_o + \ln\left(\frac{sb}{\pi}\right) - 1\right]}$$

$$\arg \frac{sb}{i\pi} \neq \pm \pi.$$

One notes that changing the exponential factors in the infinite product is justified since the negative of these exponential factors must also be present in a similar representation for $G_-(s)$; these exponential factors are required to ensure the convergence of the infinite products. One notes that Γ_o in (A-45) is defined as

Euler's constant = 0.5772156649.

It is easily seen that the proper choice for X(s) which ensures an algebraic growth for $G_+(s)$ as $s \to \infty$ is

$$\text{(A-46)} \qquad X(s) = \frac{isb}{\pi}\left[\Gamma_o + \ln\left(\frac{kb}{2\pi}\right)\right] + \frac{sb}{2} + I(s) - \frac{s}{2k}$$

where

$$(A\text{-}47) \quad I(s) \equiv -s \int_0^\infty \frac{dw}{\sqrt{k^2-w^2}} \left[\frac{b}{\pi} - \frac{\mathcal{G}(w) + \mathcal{G}(-w)}{2\pi i} \right].$$

Hence $G_+(s)$ is

$$(A\text{-}48) \quad G_+(s) = G_1^{1/2}(0) \frac{(s+k)^{1/2}(s+k_d)}{\left(1 + \frac{s}{\beta}\right)} \prod_{n=1}^{\infty} \left(1 + \frac{s}{\beta_n}\right) e^{\frac{isb}{n\pi}} \cdot$$

$$\cdot e^{\int_0^\infty g(s,w) \left[-\frac{b}{\pi} + \hat{G}(w) \right] dw} e^{P(s)}$$

where

$$(A\text{-}49) \quad G_1^{1/2}(0) \equiv \left\{ \frac{i \sin k_d b}{-k_d^2 \sin k_d b - i\varepsilon_r k \, k_d \cos k_d b} \right\}^{1/2}$$

$$(A\text{-}50) \quad g(s,w) \equiv \ln\left(1 + \frac{s}{\sqrt{k^2-w^2}}\right) - \frac{s}{\sqrt{k^2-w^2}}$$

$$(A\text{-}51) \quad \hat{G}(w) \equiv \frac{b}{\pi} - \frac{1}{\pi} \frac{\varepsilon_r w^2 b + \left(\frac{w^2}{w'} - w'\right) \varepsilon_r \sin w'b \cos w'b}{w'^2 \sin^2 w'b + \varepsilon_r^2 w^2 \cos^2 w'b}$$

and

$$(A\text{-}52) \quad P(s) \equiv -\frac{isb}{\pi} \left[\Gamma_o + \ln\left(\frac{kb}{2\pi}\right) \right] - \frac{sb}{2} - I(s) .$$

Finally, $G_-(s)$ is identical to $G_+(-s)$. The representation in (A-48) is not suitable for numerical computations, because I(s) in (A-52) is not well behaved. If one consideres the contribution to I(s) over the range $w_o < w < \infty$ where w_o is an arbitrarily large number, then one may accurately approximate the integrand as follows:

$$-\frac{1}{\sqrt{k^2-w^2}}\left[\frac{b}{\pi}-\frac{\mathcal{G}(w)+\mathcal{J}(w)}{2\pi i}\right]_{\approx}^{\approx}-\frac{1}{iw}\frac{b}{\pi}\left(1-\frac{\varepsilon_r}{1+(\varepsilon_r^2-1)\cos^2 wb}\right)$$

The integration of the above from w_o to ∞ would converge if the term

$$\left(1-\frac{\varepsilon_r}{1+(\varepsilon_r^2-1)\cos^2 wb}\right)$$

was purely oscillatory (i.e., behaved as sin w); however, the

$$\frac{\varepsilon_r}{1+(\varepsilon_r^2-1)\cos^2 wb}$$

term in the brackets oscillates about a non-zero mean value equal to

$$\frac{\varepsilon_r^2+1}{2\varepsilon_r}$$

(which will equal unity only if $\varepsilon_r=1$), thereby implying that the integral I(s) of (A-47) is non-convergent for $\varepsilon_r\neq 1$. There are no other terms in $G_+(s)$ which can compensate for the divergent behavior of I(s), thereby making the above representation for $G_+(s)$ unsuitable for numerical computations. This factorization procedure has been applied to a number of examples in the past without difficulty; hence, the present result is unexpected. In this sense it is a peculiar case. In Appendix II we find $G_+(s)$ by a formal factorization procedure.

APPENDIX II
EVALUATION OF THE WIENER-HOPF FACTORS OF G(s) VIA THE FORMAL FACTORIZATION PROCEDURE

I. It was indicated in Section III of Appendix I that the limiting type factorization procedure of Appendix I although ordinarily preferred over a formal factorization procedure for convenience in calculating the factors, strangely leads to a representation for the factors of G(s) which fail to converge. Therefore, the factorization of G(s) is carried out via the formal factorization scheme described in this appendix. Since the well known texts on the subject of Wiener-Hopf methods such as those by Noble[19] and Mittra and Lee[9] deal with the development of formal factorization formulae, only a summary of the results will be given and then applied to the factorization of G(s).

Consider the complex function F(s) of the complex variable s with the following requirements:

(A-53) F(s) is analytic, regular and non-zero in the strip $\tau_+ < \tau < \tau_-$ (where $\tau = \text{Im } s$; $s = \sigma + i\tau$). Figure 10 indicates the strip of analyticity for F(s).

(A-54) $F(s) \to 1$ uniformly as $|\sigma| \to \infty$ in the strip $\tau_+ < \tau < \tau_-$.

It can be shown that F(s) may be factorized in the folliwing manner:

$$F(s) = F_+(s)\, F_-(s) \tag{A-55}$$

where

$$F_+(s) = \exp\left[\frac{1}{2\pi i}\int_{-\infty+i\tau_a}^{\infty+i\tau_a} \frac{\ln F(z)}{z-s}\, dz\right]_{\tau_- > \text{Im } s > \tau_a > \tau_+} \tag{A-56}$$

and

$$F_-(s) = \exp\left[\frac{1}{2\pi i}\int_{-\infty+i\tau_b}^{\infty+i\tau_b} dz \frac{\ln F(z)}{z-s}\right]_{\tau_+ < \text{Im } s < \tau_b < \tau_-} \tag{A-57}$$

The contours of integration for the integrals in (A-56) and (A-57) are shown in Fig. A-5(a). $F_+(s)$ is regular and non-zero in the upper half s plane defined by $\tau > \tau_+$, whereas $F_-(s)$ is regular and non-zero in the lower half s-plane defined by $\tau < \tau_-$. It is possible to evaluate $F_+(s)$ for Im $s < \tau_a$ and $F_-(s)$ for Im $s > \tau_b$ by deforming the contours of integration in Fig. A-5(a) to enclose the point s as indicated in Fig. A-5(b) (for $s = s_1$ with Im $s_1 > \tau_b$ and for $s = s_2$ with Im $s_2 < \tau_a$).

G(s) of (94) may be factorized via the formulae of (A-56) and (A-57). G(s) is re-written below for convenience.

$$(A\text{-}58) \qquad G(s) = (\gamma\gamma_1 \sinh \gamma_1 b)(\gamma_1 \sinh \gamma_1 b + \varepsilon_r \gamma \cosh \gamma_1 b)^{-1}$$

where

$$(A\text{-}59a,b) \qquad \gamma = \sqrt{s^2-k^2} = -i\sqrt{k^2-s^2}, \quad \gamma_1 = \sqrt{s^2-k_d^2}, \text{ and}$$

k and k_d appearing in (A-59a,b) correspond to the wave numbers in free space and in the dielectric slab (of thickness b), respectively. The zeroes of $\gamma_1 \sin h \gamma_1 b$ in (A-58) occur at $s = \pm k_d$ and at $s = \pm i|\beta_n|$ (where $n = 1,2,3,\cdots$). Since the problem is restricted so that only the TM_0 surface wave propagates, the only zeroes of $(\gamma_1 \sinh \gamma_1 b + \varepsilon_r \gamma \cosh \gamma_1 b)$ in (A-58) are at $s = \pm\beta$. The branch points of G(s) occur at $s = \pm k$ and at infinity. The branch points, zeroes, and poles of G(s) are indicated in Fig. A-6. For convenience of analysis, k and k_d are made complex by allowing them to possess small imaginary values (this corresponds to introducing a slight loss in the medium as indicated in Chapter III) so that

$$k = k_1 + ik_2 \begin{pmatrix} \text{with } k_2 << k_1 \\ \text{and } k_1,\ k_2 > 0 \end{pmatrix} \text{ and } k_d = k_3 + ik_4 \begin{pmatrix} \text{with } k_4 << k_3 \\ \text{and } k_3, k_4 > 0 \end{pmatrix};$$

this allows G(s) to be analytic and non-zero within the strip, defined by $\tau_+ < \tau < \tau_-$, and $|\sigma| < \infty$, in the complex s plane. $\tau_+ = -\min(k_2,k_4)$ and $\tau_- = \min(k_2,k_4)$; $\tau_\pm \to 0$ as k_2 and k_4 both approach zero. Figure A-7 indicates the locations of the poles, zeroes and branch points of G(s) when k and k_d are allowed to be complex. Since $G(s) \sim O(s)$ as $|s| \to \infty$ in the strip, it is not possible to factorize G(s) directly via (A-56) and (A-57) since the condition in (A-54) is violated. It is therefore necessary to re-express G(s) as

$$(A\text{-}60) \qquad G(s) = G_1(s)\, G_2(s)\, G_3(s)$$

where

$$(A\text{-}61) \qquad G_1(s) \equiv \sqrt{s^2-k^2} = -i\sqrt{k^2-s^2}$$

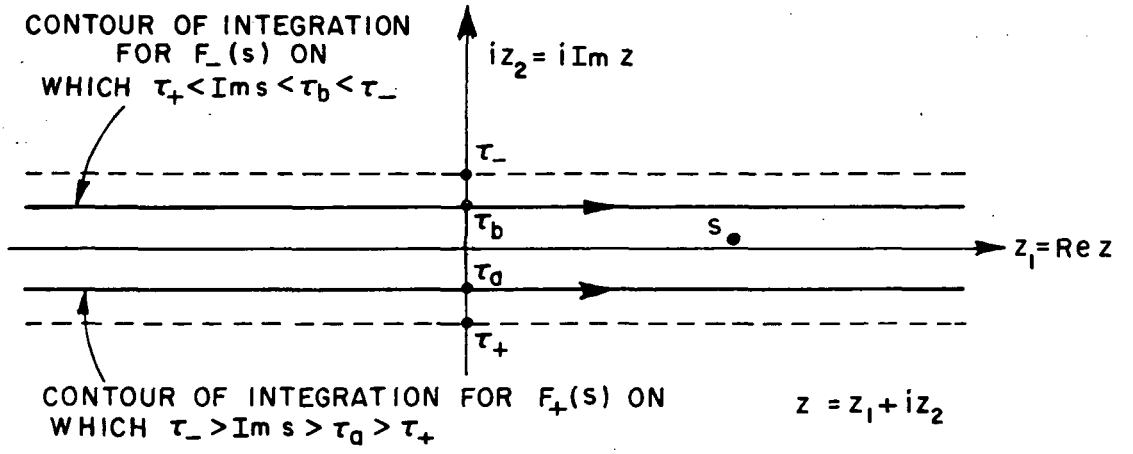

(a)

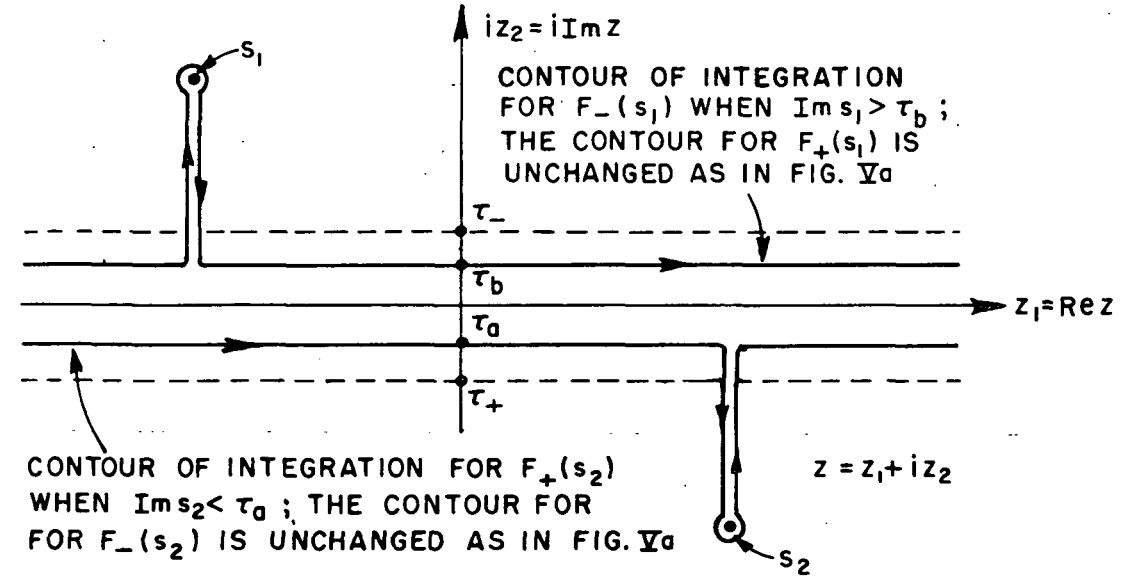

(b)

Fig. A-5-- Contours of integration for the Wiener-Hopf factors.

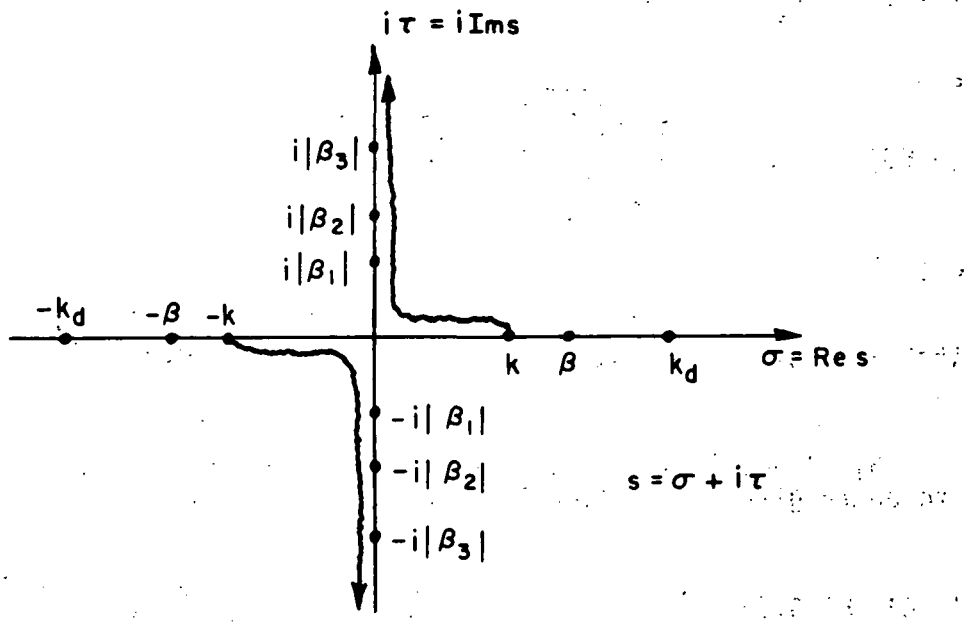

Fig. A-6 --Poles, zeros and branch points of G(s) in the complex s plane.

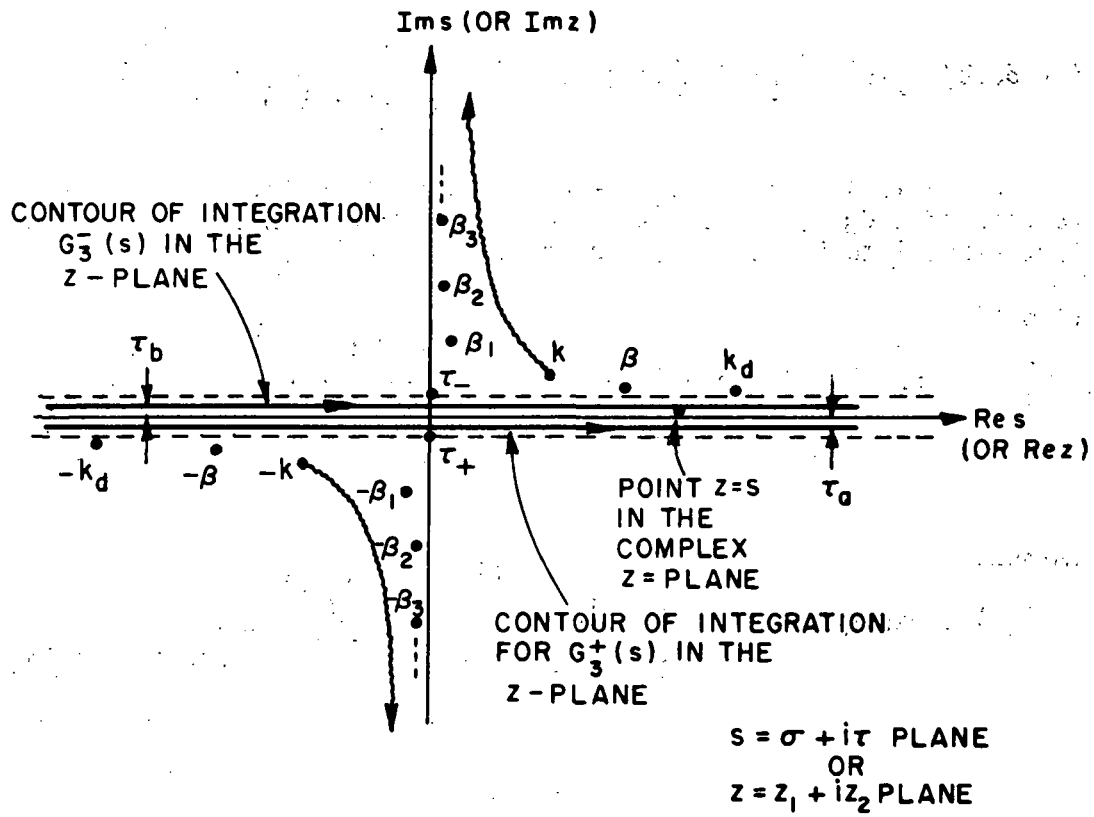

Fig. A-7 --Zeros and singularities of G(s) when k and k_d are complex, and the contours of integration for $G_3^{\pm}(s)$ in the z plane.

(A-62) $$G_2(s) \equiv (s^2-k_d^2)/(s^2-\beta^2)$$

and

(A-63) $$G_3(s) \equiv \frac{\sinh\sqrt{s^2-k_d^2}b}{\sqrt{s^2-k_d^2}} \cdot \frac{s^2-\beta^2}{g(s)}$$

with

(A-64) $$g(s) \equiv \sqrt{s^2-k_d^2}\sinh\sqrt{s^2-k_d^2}b + \varepsilon_r\sqrt{s^2-k^2}\cosh\sqrt{s^2-k_d^2}b$$

$G_1(s)$ and $G_2(s)$ may be factorized by inspection, or via the procedure given in Section I of Appendix I. Thus,

(A-64a,b) $$G_1(s) = G_1^+(s)\,G_1^-(s); \quad G_1^+(s) = (-ik)^{1/2}\left(1+\frac{s}{k}\right)^{1/2} = G_1^-(-s)$$

and

(A-65a,b) $$G_2(s) = G_2^+(s)\,G_2^-(s); \quad G_2^+(s) = \frac{k_d}{\beta}\frac{\left(1+\frac{s}{k_d}\right)}{\left(1+\frac{s}{\beta}\right)} = G_2^-(-s)$$

$G_3(s)$ is analytic and non-zero in the strip $(\tau_+<\tau<\tau_-;\ |\sigma|\to\infty)$; furthermore, $G_3(s)\to 1$ as $|s|\to\infty$ in the strip. Thus, $G_3(s)$ may be factorized into $G_3^+(s)\,G_3^-(s)$ via (A-56) and (A-57).

(A-66a)
$$G_3^+(s) \equiv \exp k_+(s) = \exp\left\{\frac{1}{2\pi i}\int_{-\infty+i\tau_a}^{\infty+i\tau_a}\frac{\ln G_3(z)}{z-s}\,dz\right\}_{\tau_-<\mathrm{Im}\ s<\tau_a<\tau_+}$$

(A-66b)
$$G_3^-(s) \equiv \exp k_-(s) = \exp\left\{-\frac{1}{2\pi i}\int_{-\infty+i\tau_b}^{\infty+i\tau_b}\frac{\ln G_3(z)}{z-s}\,dz\right\}_{\tau_+<\mathrm{Im}\ s<\tau_b<\tau_-}$$

The quantities $k_+(s)$ and $k_-(s)$ are the terms which appear inside the brackets on the R.H.S. of (A-66a) and (A-66b), respectively. The contours of integration and the location of $z = s$ in the complex z plane for (A-66a,b) are indicated in Fig. A-7. One may express $k_+(s)$ as

$$(A\text{-}67) \qquad k_+(s) = \frac{1}{2\pi i}\left[\int_{0+i\tau_a}^{\infty+i\tau_a} dz\,\frac{\ln G_3(z)}{z-s} - \int_{0-i\tau_a}^{\infty-i\tau_a} \frac{\ln G_3(z)}{z+s}\,dz\right]$$

One now lets k_2 and k_4 approach zero (reducing the loss in the medium to zero); this allows one to express $k_+(s)$ above as

$$(A\text{-}68) \qquad k_+(s) = \frac{s}{i\pi}\int_{C_+} \frac{\ln G_3(z)}{z^2 - s^2}\,dz$$

where the contour of integration C_+ is indicated in Fig. A-8(a) whenever s is real and positive. A similar representation for $k_-(s)$ when k_2 and k_4 are set to zero (i.e., when the strip of analyticity for $G_3(s)$ shrinks to the real z-axis, except for the singularities at $z = k$ and $z = s$) is given by

$$(A\text{-}69) \qquad k_-(s) = -\frac{s}{i\pi}\int_{C_-} \frac{\ln G_3(z)}{z^2 - s^2}\,dz$$

where the contour C_- is depicted in Fig. A-8(b) for positive real s.

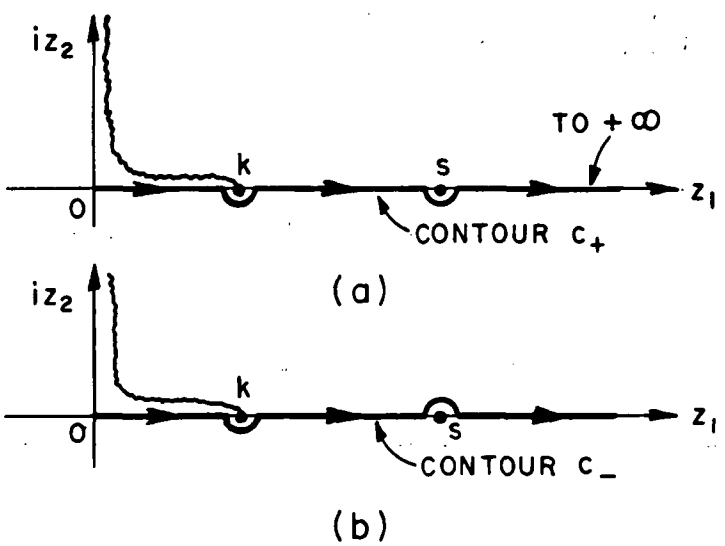

Fig. A-8 -- Contours C_+ and C_- associated with $G_3^+(s)$ and $G_3^-(s)$ for real s

It can be shown that the contribution to the integrals in (A-68) and (A-69) arising from the branch point at $z = k$ is vanishingly small; hence, these integrals may be expressed as principal value (P.V.) integrals over a semi-infinite range along the real z axis after taking into consideration the effect of the pole at $z = s$ (by including one half of the residue arising from this pole). Therefore,

$$(A\text{-}70) \qquad k_+(s) = \frac{s}{i\pi}\ \text{P.V.} \int_0^\infty \frac{\ln G_3(z)}{z^2 - s^2}\, dz + \frac{1}{2} \ln G_3(s);\ \text{for } s>0$$

and

$$(A\text{-}71) \qquad k_-(s) = \frac{-s}{i\pi}\ \text{P.V.} \int_0^\infty \frac{\ln G_3(z)}{z^2 - s^2}\, dz + \frac{1}{2} \ln G_3(s);\ \text{for } s>0$$

Thus, one may factorize $G(s)$ into $G_+(s)\ G_-(s)$ where

$$(A\text{-}72a) \qquad G_+(s) = G_1^+(s)\ G_2^+(s)\ G_3^+(s)$$

and

$$(A\text{-}72b) \qquad G_-(s) = G_1^-(s)\ G_2^-(s)\ G_3^-(s)$$

with $G_1^\pm(s)$ and $G_2^\pm(s)$ indicated in (A-64b) and (A-65b). $G_3^\pm(s)$ in (A-72a,b) are defined in (A-66a,b) with $k_+(s)$ and $k_-(s)$ given by (A-70) and (A-71), respectively. Equations (A-70) and (A-71) are valid for $s>0$; when $s<0$ (i.e., $s=-|s|$) one may employ the relations

$$(A\text{-}73a,b) \qquad k_+(-|s|) = k_-(|s|);\ k_-(-|s|) = k_+(|s|).$$

The relations indicated in (A-73a,b) follow from the fact that $G_3(-|s|) = G_3(|s|)$. Clearly,

$$(A\text{-}74a,b) \qquad G_3^+(|s|) = G_3^-(-|s|),\ \text{and}\ \ G_3^+(-|s|) = G_3^-(|s|)\ ,$$

whenever (A-73a,b) are valid; therefore, it follows via (A-72a,b) that

$$(A\text{-}75) \qquad G_+(|s|) = G_-(-|s|).$$

The factors of $G_3(s)$ when s is complex may be evaluated directly via the formulae in (A-58) and (A-57) with the corresponding contours of integration indicated in Fig. A-5. The relationships

$$G_3^+(s) = G_3^-(-s) \tag{A-76}$$

and

$$G_+(s) = G_-(-s) \tag{A-77}$$

are valid even for complex values of s.

Specifically, one needs to evaluate $G_+(s)$ at $s = \beta$, $s = k_d$, $s = \beta_n$ $(= i|\beta_n|$, $n = 1,2,3 \cdots)$ and $s = k \sin \phi$ (with $|\phi| < \pi/2$), in order to construct the surface wave reflection and diffraction coefficients pertaining to the configuration of Fig. 2; however, before proceeding to these cases, it is desirable to re-write (A-70) and (A-71) in a form suitable for the numerical evaluation of the integrals.

The quantity

$$\pm \frac{s}{i\pi} \text{ P.V.} \int_0^\infty \frac{\ln G_3(z)}{z^2 - s^2} \, dz$$

in (A-70) and (A-71) may be re-expressed for the purposes of numerical computations as

$$\pm \frac{s}{i\pi} \text{ P.V.} \int_0^\infty = \begin{cases} \pm \frac{s}{i\pi} \left[\lim_{\varepsilon \to 0} \left\{ \int_0^{k-\varepsilon} + \int_{k+\varepsilon}^{s-\delta} + \int_{s-\delta}^{s-\varepsilon} + \int_{s+\varepsilon}^{s+\delta} + \int_{s+\delta}^{\infty} \right\} \right], & \text{for } s>k>0 \\ \pm \frac{s}{i\pi} \left[\lim_{\varepsilon \to 0} \left\{ \int_0^{s-\delta} + \int_{s-\delta}^{s-\varepsilon} + \int_{s+\varepsilon}^{s+\delta} + \int_{s+\delta}^{k-\varepsilon} + \int_{k+\varepsilon}^{\infty} \right\} \right], & \text{for } 0<s<k \end{cases} \tag{A-78}$$

One notes that the integrand in (A-78) is real whenever $z>k$ and s is real. It is desirable to split the integral as shown above since it allows one to substantially reduce any numerical roundoff errors arising from the numerical evaluation of the integral in the neighborhood of the pole at $z = s$; the integral in the deleted neighborhood of the pole is then evaluated very accurately in closed form as discussed below.

$G_3(z)$ is analytic at $z = s$ as well as for all positive real values of z excluding the point $z = k$; hence, $\ln G_3(z)$ in the integrand of (A-78) may be accurately approximated in the immediate neighborhood of $z = s$ by it's two term Taylor Expansion as

$$\text{(A-79)} \qquad \ln G_3(z) \approx \ln G_3(s) + \left[\frac{1}{G_3(z)} \frac{d}{dz} G_3(z)\right]_{z=s} (z - s)$$

$$= \ln G_3(s) + \frac{G_3'(s)}{G_3(s)} \quad (z-s).$$

The integral from $z = s-\delta$ to $z = s + \delta$ excluding the point $z = s$ which occurs in (A-78) may be written via (A-79) as

$$\text{(A-80)} \qquad \pm \frac{s}{i\pi} \lim_{\varepsilon \to 0} \left[\int_{s-\delta}^{s-\varepsilon} \frac{\ln G_3(z)}{z^2 - s^2} dz + \int_{s+\varepsilon}^{s+\delta} dz \frac{\ln G_3(z)}{z^2 - s^2} \right]$$

$$= \pm \frac{s}{i\pi} \lim_{\varepsilon \to 0} \left[\ln G_3(s) \left\{ \int_{s-\delta}^{s-\varepsilon} \frac{dz}{z^2 - s^2} + \int_{s+\varepsilon}^{s+\delta} \frac{dz}{z^2 - s^2} \right\} + \right.$$

$$\left. + \frac{G_3'(s)}{G_3(s)} \left\{ \int_{s-\delta}^{s-\varepsilon} \frac{dz}{z + s} + \int_{s+\varepsilon}^{s+\delta} \frac{dz}{z + s} \right\} \right]$$

The extent of the interval 2δ about $z = s$ is chosen such that the R.H.S. of (A-79) is a sufficiently accurate representation for $\ln G_3(z)$ within the interval. After some straightforward manipulations (A-80) becomes

$$\text{(A-81)} \qquad \pm \frac{s}{i\pi} \lim_{\varepsilon \to 0} \left[\int_{s-\delta}^{s-\varepsilon} \frac{\ln G_3(z)}{z^2 - s^2} dz + \int_{s+\varepsilon}^{s+\delta} \frac{\ln G_3(z)}{z^2 - s^2} dz \right]$$

$$= \pm \frac{s}{i\pi} \lim_{\varepsilon \to 0} \left[- \frac{\ln G_3(s)}{2s^2} (\delta-\varepsilon) + \frac{G_3'(s)}{sG_3(s)} (\delta-\varepsilon) \right]$$

$$= \pm \frac{1}{i\pi} \left[- \frac{\ln G_3(s)}{2s} + \frac{G_3'(s)}{G_3(s)} \right] \delta .$$

Incorporating (A-81) in (A-78) yields

$$(A\text{-}82)\qquad \pm\frac{s}{i\pi}\,P.V.\int_0^\infty \frac{\ln G_3(z)}{z^2-s^2}\,dz =$$

$$=\begin{cases} \pm\dfrac{s}{i\pi}\left[\lim\limits_{\varepsilon\to 0}\left\{\int_0^{k-\varepsilon}+\int_{k+\varepsilon}^{s-\delta}+\int_{s+\delta}^{\infty}\right\}\right]_{s>k} \pm\dfrac{1}{i\pi}\left[-\dfrac{\ln G_3(s)}{2s}+\dfrac{G_3'(s)}{G_3(s)}\right]\delta, \\ \text{or} \\ \pm\dfrac{s}{i\pi}\left[\lim\limits_{\varepsilon\to 0}\left\{\int_0^{s-\delta}+\int_{s+\delta}^{k-\varepsilon}+\int_{k+\varepsilon}^{\infty}\right\}\right]_{\substack{s<k\\ s>0}} \pm\dfrac{1}{i\pi}\left[-\dfrac{\ln G_3(s)}{2s}+\dfrac{G_s'(s)}{G_3(s)}\right]\delta \end{cases}$$

The result given in (A-82) may be directly employed in the integrals on the R.H.S. of (A-70) and (A-71) to evaluate $K_+(s)$ and $K_-(s)$, respectively when s is real. When s has a non-zero imaginary part (s is complex), the representation for $k_+(s)$ and $k_-(s)$ is taken directly from (A-56) and (A-57) respectively, together with the corresponding contours of integration indicated in Fig. A-5.

II. Evaluation of $G_3^+(\beta)$: The factors of G_3 for $s=\beta$ where $\beta>k>0$ are obtained via (A-70) and (A-82); in particular, $G_3^+(\beta)$ equals $e^{k_+(\beta)}$ where

$$(A\text{-}83)\qquad k_+(\beta)=\frac{\beta}{i\pi}\left[\lim_{\varepsilon\to 0}\left\{\int_0^{k-\varepsilon}\frac{\ln G_3(z)}{z^2-\beta^2}\,dz+\int_{\kappa+\varepsilon}^{\beta-\delta}\frac{\ln G_3(z)}{z^2-\beta^2}\,dz+\right.\right.$$

$$\left.\left.+\int_{\beta+\delta}^{\infty}\frac{\ln G_3(z)}{z^2-\beta^2}\,dz\right\}\right]+\frac{1}{i\pi}\left\{-\frac{\ln G_3(\beta)}{2\beta}+\frac{G_3'(\beta)}{G_3(\beta)}\right\}\delta+$$

$$+\frac{1}{2}\ln G_3(\beta)$$

The term, $\ln G_3(\beta)$ appearing in (A-83) is calculated via

$$(A\text{-}84)\qquad \ln G_3(\beta)=\ln\left[\lim_{z\to\beta}G_3(z)\right]=\ln\left(\frac{2\beta\mathcal{R}_0}{(\beta^2-k_d^2)\sqrt{\beta^2-k^2}}\right)$$

where $\mathcal{R}_0$ is the residue defined by $\lim\limits_{z\to\beta}(z-\beta)G(z)$ which was introduced in (113). The quantity $G_3'(\beta)$ in (A-83) is presented later in (A-88).

One notes that the ratio $(z^2-\beta^2)/g(z)$ occuring in the expression for $G_3(z)$ (see (A-63)) is sensitive to any slight inaccuracy involved in the numerical evaluation of β whenever z is in the neighborhood of β. Thus, it is apparent that the numerator and the denominator of $G_3(z)$ may not simultaneously attain a zero value at $z=\beta$ if a sufficiently precise value of β is not available. In order to make the integral in (A-83) less sensitive to any small errors in β, the integral from $k+\varepsilon$ to $\beta-\delta$ and also from $\beta+\delta$ to ∞ are further split as follows

$$(A\text{-}85) \qquad \int_{k+\varepsilon}^{\beta-\delta} + \int_{\beta+\delta}^{\infty} = \int_{k+\varepsilon}^{\beta-T} + \int_{\beta-T}^{\beta-\delta} + \int_{\beta+\delta}^{\beta+T} + \int_{\beta+T}^{\infty} \quad ,$$

and the term $g(z)$ which appears in $G_3(z)$ for the integrals over $\beta-T$ to $\beta-\delta$, and over $\beta+\delta$ to $\beta+T$, is replaced by it's four-term Taylor expansion about $z=\beta$. The interval 2T about $z=\beta$ is therefore chosen such that $g(z)$ is accurately represented by four terms in a Taylor expansion for $g(z)$ about $z=\beta$. In the interval $\beta-T < z < \beta+T$, $g(z)$ is therefore given by

$$(A\text{-}86) \qquad g(z) \approx g(\beta) + g'(\beta)(z-\beta) + \frac{1}{2} g''(\beta)(z-\beta)^2 + \frac{1}{6} g'''(\beta)(z-\beta)^3$$
$$= [g'(\beta) + \frac{1}{2} g''(\beta)(z-\beta) + \frac{1}{6} g'''(\beta)(z-\beta)^2](z-\beta)$$

since $g(\pm\beta) = 0$. The quantities $g'(z)$ and $g''(z)$ are given below in terms of $\gamma(\equiv\sqrt{z^2-k^2} = -i\sqrt{k^2-z^2})$ and γ_1 $(\equiv\sqrt{z^2-k_1^2})$ which have been defined earlier; these quantities are evaluated at $z=\beta$ and employed in (A-86) above.

$$(A\text{-}87a) \qquad g(z) = \gamma_1 \sinh \gamma_1 b + \varepsilon_r \gamma \cosh \gamma_1 b$$

$$(A\text{-}87b) \qquad g'(z) = \frac{z}{\gamma_1} \sinh \gamma_1 b + zb \cosh \gamma_1 b + \varepsilon_r \frac{z}{\gamma} \cosh \gamma_1 b +$$
$$+ \varepsilon_r z b \frac{\gamma}{\gamma_1} \sinh \gamma_1 b$$

$$(A\text{-}87c) \qquad g''(z) = \frac{\sinh \gamma_1 b}{\gamma_1} - \frac{z^2}{\gamma_1^3} \sinh \gamma_1 b + \frac{z^2 b}{\gamma_1^2} \cosh \gamma_1 b +$$
$$+ b \cosh \gamma_1 b + \frac{z^2 b^2}{\gamma_1} \sinh \gamma_1 b +$$

(A-87c) (Cont).
$$+\varepsilon_r \frac{\cosh \gamma_1 b}{\gamma\gamma_1} - \varepsilon_r \frac{z^2}{\gamma^3}\cosh \gamma_1 b + 2\varepsilon_r \frac{z^2 b}{\gamma\gamma_1}\sinh \gamma_1 b +$$
$$+\varepsilon_r \frac{\gamma b}{\gamma_1}\sinh \gamma_1 b + \varepsilon_r \frac{\gamma z^2 b^2}{\gamma_1^2}\cosh \gamma_1 b -$$
$$-\varepsilon_r \gamma \frac{z^2 b}{\gamma_1^3}\sinh \gamma_1 b.$$

The expression for $g'''(z)$ is rather lengthy, but can be obtained by a straightforward differentiation of $g''(z)$; hence, it will not be presented here. The quantity $G_3'(\beta)$ in (A-83) may be expressed in terms of $g'(\beta)$ and $g''(\beta)$ as

(A-88)
$$G_3'(\beta) = g'(\beta)\left[\frac{\sin\sqrt{k_d^2-\beta^2}\,b}{\sqrt{k_d^2-\beta^2}} - \frac{2\beta^2 b\cos\sqrt{k_d^2-\beta^2}\,b}{(k_d^2-\beta^2)} + \frac{2\beta^2}{(k_d^2-\beta^2)}\cdot\frac{\sin\sqrt{k_d^2-\beta^2}\,b}{\sqrt{k_d^2-\beta^2}}\right] -$$
$$- g''(\beta)\cdot\beta\frac{\sin\sqrt{k_d^2-\beta^2}\,b}{\sqrt{k^2-\beta^2}}$$
$$= \frac{}{[g'(\beta)]^2}$$

III. Evaluation of $G_3^+(k_d)$: The evaluation of $G_3^+(k_d)$ where $k_d > \beta > k$ proceeds in a manner similar to that for $G_3^+(\beta)$ discussed earlier. Specifically, $G_3^+(k_d) = \exp(k_+(k_d))$ where

(A-89)
$$k_+(k_d) = \frac{k_d}{i\pi}\left[\lim_{\varepsilon\to 0}\left\{\int_0^{k-\varepsilon}\frac{\ln G_3(z)}{z^2-k_d^2}\,dz + \int_{k+\varepsilon}^{k_d-\delta}\frac{\ln G_3(z)}{z^2-k_d^2}\,dz + \right.\right.$$
$$\left.\left. + \int_{k_d+\delta}^{\infty}\frac{\ln G_3(z)}{z^2-k_d^2}\,dz\right\}\right] + \frac{1}{i\pi}\left\{-\frac{\ln G_3(k_d)}{2k_d} + \frac{G_3'(k_d)}{G_3(k_d)}\right\}\delta +$$
$$+ \frac{1}{2}\ln G_3(k_d)$$

and

$$(A\text{-}90)\quad G_3(k_d) = \frac{b(k_d^2-\beta^2)}{\varepsilon_r\sqrt{k_d^2-k^2}}\quad ;\quad \ln G_3(k_d) = \ln\left\{\frac{b(k_d^2-\beta^2)}{\varepsilon_r\sqrt{k_d^2-k^2}}\right\}$$

Also

$$(A\text{-}91)\quad G_3'(k_d) = \frac{1}{\varepsilon_r\sqrt{k_d^2-k^2}}\left\{2k_db - 2k_db\cdot G_3(k_d) - \right.$$

$$\left. - \frac{k_db(k_d^2-\beta^2)}{(k_d^2-k^2)} - k_db^3(k_d^2-\beta^2)\right\} + \frac{k_db^2}{3}\cdot G_3(k_d).$$

Since β lies in the interval $k+\varepsilon < \beta < k_d - \delta$, it is desirable to re-express the integral over $k+\varepsilon$ to $k_d - \delta$ in (A-89) as

$$(A\text{-}92)\qquad \int_{k+\varepsilon}^{k_d-\delta} = \int_{k+\varepsilon}^{\beta-T} + \int_{\beta-T}^{\beta+T} + \int_{\beta+T}^{k_d-\delta}$$

The g(z) term in $G_3(z)$ for

$$\int_{\beta-T}^{\beta+T} \frac{\ln G_3(z)}{z^2-k_d^2}\,dz$$

of (A-92) is replaced by it's four term Taylor expansion about $z = \beta$ as indicated earlier for $G_+(\beta)$ for the purposes of making the calculation of $G_3(z)$ insensitive to any small differences which may exist between the calculated value of β and the true value of β.

IV. Evaluation of $G_3^+(i|\beta_n|)$: $G_3^+(i|\beta_n|) = \exp k_+(i|\beta_n|) = G_3^+(\beta_n)$ where

$$\beta_n = \sqrt{k_d^2 - \left(\frac{n\pi}{b}\right)^2} = i\sqrt{\left(\frac{n\pi}{b}\right)^2 - k_d^2},\ n = 1,2,3,\ \ldots,$$

as indicated in Chapter III, and

$$(A\text{-}93)\quad K_+(i|\beta_n|) = \frac{i|\beta_n|}{i\pi}\left[\lim_{\varepsilon\to 0}\left\{\int_0^{k-\varepsilon}\frac{\ln G_3(z)}{z^2+|\beta_n|^2}\,dz + \int_{k+\varepsilon}^{\beta-T}\frac{\ln G_3(z)}{z^2+|\beta_n|^2}\,dz + \right.\right.$$

$$\left.\left. + \int_{\beta-T}^{\beta+T}\frac{\ln G_3(z)}{z^2+|\beta_n|^2}\,dz + \int_{\beta+T}^{\infty}\frac{\ln G_3(z)}{z^2+|\beta_n|^2}\,dz\right\}\right]$$

The term $g(z)$ in $G_3(z)$ which occurs in the integral over $\beta-T < z < \beta+T$ in (A-93) is approximated by it's four term Taylor expansion about $z = \beta$ as done previously for $G_3^+(\beta)$ and $G_3^+(k_d)$, and for similar reasons. One notes that the integrand in (A-93) possesses pole singularities on the imaginary z-axis unlike that for $k_+(\beta)$ and $k_+(k_d)$ for which the singularities occur on the path of integration.

V. Evaluation of $G_3^+(k \sin\phi)$: Since $|\phi| < \pi/2$ (see Chapter III for details), it follows that $|k \sin\phi| < k$. Thus, $G_3^+(k\sin\phi) = \exp k_+(k\sin\phi) = \exp k_+(\pm|k\sin\phi|)$, for $\phi \gtrless 0$. It was indicated in Section I of this appendix that one can relate $k_+(-|k\sin\phi|)$ to $k_-(|k\sin\phi|)$ by the equality

$$(A\text{-}94)\quad k_+(-|k\sin\phi|) = k_-(|k\sin\phi|)\ .$$

The quantities $k_\pm(|k\sin\phi|)$ are given by

(A-95)

$$k_+(|k\sin\phi|) = \frac{|k\sin\phi|}{i\pi}\left[\lim_{\varepsilon\to 0}\left\{\int_0^{|k\sin\phi|-\delta}\frac{\ln G_3(z)dz}{z^2-|k\sin\phi|^2} + \right.\right.$$

$$+ \int_{|k\sin\phi|+\delta}^{k-\varepsilon}\frac{\ln G_3(z)\,dz}{z^2-|k\sin\phi|^2} + \int_{k+\varepsilon}^{\beta-T}\frac{\ln G_3(z)\,dz}{z^2-|k\sin\phi|^2} +$$

$$\left.\left. + \int_{\beta-T}^{\beta+T}\frac{\ln G_3(z)\,dz}{z^2-|k\sin\phi|^2}\,dz + \int_{\beta+T}^{\infty}\frac{\ln G_3(z)\,dz}{z^2-|k\sin\phi|^2}\right\}\right] +$$

(A-95) (Cont)

$$+\frac{1}{i\pi}\left\{\frac{-\ln G_3(|k\sin\phi|)}{2|k\sin\phi|}+\frac{G_3'(|k\sin\phi|)}{G_3(|k\sin\phi|)}\right\}\delta+$$

$$+\frac{1}{2}\ln G_3(|k\sin\phi|)\,,\quad \text{for } \phi>0$$

and

(A-96)

$$k_-(|k\sin\phi|)=\frac{-|k\sin\phi|}{i\pi}\left[\lim_{\varepsilon\to 0}\left\{\int_0^{|k\sin\phi|-\delta}\frac{\ln G_3(z)dz}{z^2-|k\sin\phi|^2}+\right.\right.$$

$$+\int_{|k\sin\phi|+\delta}^{k-\varepsilon}\frac{\ln G_3(z)\,dz}{z^2-|k\sin\phi|^2}+\int_{k+\varepsilon}^{\beta-T}\frac{\ln G_3(z)\,dz}{z^2-|k\sin\phi|^2}+$$

$$\left.\left.+\int_{\beta-T}^{\beta+T}\frac{\ln G_3(z)}{z^2-|k\sin\phi|^2}\,dz+\int_{\beta+T}^{\infty}\frac{\ln G_3(z)}{z^2-|k\sin\phi|^2}\,dz\right\}\right]-$$

$$-\frac{1}{i\pi}\left\{\frac{-\ln G_3(|k\sin\phi|)}{2|k\sin\phi|}+\frac{G_3'(|k\sin\phi|)}{G_3(|k\sin\phi|)}\right\}\delta+$$

$$+\frac{1}{2}\ln G_3(|k\sin\phi|)\,,\quad \text{for } \phi<0.$$

In order to evaluate $G_3'(|k\sin\phi|)$ one must set $z=|k\sin\phi|$ in

(A-97)

$$G_3'(z)=\frac{\sinh\gamma_1 b}{\gamma_1}\left\{\frac{(\gamma_1\sinh\gamma_1 b+\varepsilon_r\gamma\cosh\gamma_1 b)(2z)-(z^2-\beta^2)(z)\cdot}{\cdot\left(\frac{\sinh\gamma_1 b}{\gamma_1}+b\cosh\gamma_1 b+\varepsilon_r\frac{\cosh\gamma_1 b}{\gamma}+\varepsilon_r\frac{\gamma b\sinh\gamma_1 b}{\gamma_1}\right)}{(\gamma_1\sinh\gamma_1 b+\varepsilon_r\gamma\cosh\gamma_1 b)^2}\right\}+$$

(A-97)
(Cont)

$$+\frac{(z^2-\beta^2)z}{\gamma_1 \sinh \gamma_1 b + \varepsilon_r \gamma \cosh \gamma_1 b} \cdot \left\{ \frac{b \cosh \gamma_1 b - \frac{\sinh \gamma_1 b}{\gamma_1}}{\gamma_1^2} \right\}$$

Finally, the term $g(z)$ in $G_3(z)$ which occurs in the integral over β-T to β+T in (A-95) and (A-96) is approximated as in (A-86) for the purposes of making the numerical evaluation of the integral less sensitive to any small differences which may be present in the calculated value of β from it's true value.

REFERENCES

1. J.B. Keller, "Geometrical Theory of Diffraction," Journal of the Optical Society of America, Vol. 52, February 1962, pp. 116-130.

2. C.P. Bates and R. Mittra, "Waveguide Excitation of Dielectric and Plasma Slabs," Radio Science, Vol. 3 (new series), No. 3, March 1968, pp. 251-266. (Also see Ph.D. dissertation by C.P. Bates, University of Illinois, 1968.)

3. A.F. Kay, "Scattering of a Surface Wave by a Discontinuity in Reactance," IRE Transactions on Antennas and Propagation, AP-7, 1959, pp. 22-31.

4. G.D. Maliuzhinets, "The Excitation, Reflection and Emission of Surface Waves from a Wedge with Given Face Impedances," Soviet Physics, Dokl., Vol. 3, 1958, pp. 752-755.

5. L.A. Weinstein, The Theory of Diffraction and the Factorization Method, the Golem Press, Boulder, Colorado, 1969, pp. 320-326.

6. C.M. Angulo, "Diffraction of Surface Waves by a Semi-infinite Dielectric Slab," I.R.E. Trans. on Antennas and Propagation, Vol. AP-5, January 1957, pp. 100-108.

7. J. Pace and R. Mittra, "Generalized Scattering Matrix Analysis of Waveguide Discontinuity," Quasi-Optics, XIV, Polytechnic Institute of Brooklyn Press, New York, N.Y., 1964, pp. 177-197.

8. R.E. Collin, Field Theory of Guided Waves, McGraw-Hill Book Co., New York, 1960.

9. R. Mittra and S.W. Lee, Analytical Techniques in the Theory of Guided Waves, Macmillan Co., New York, Collier-Macmillan Ltd., London, 1971.

10. S.W. Lee and R. Mittra, "Diffraction by Thick Conducting Half-Plane and a Dielectric-Loaded Waveguide," IEEE Trans., AP-16, 1968, pp. 454-461.

11. S.C. Kashyap and M.A.K. Hamid, "Diffraction Characteristics of a Slit in a Thick Conducting Screen," IEEE Trans. on Antennas and Propagation, Vol. AP-19, No. 4, July 1971, pp. 499-507.

12. N. Marcuvitz. "Field Representations in Spherically Stratified Regions," The Theory of Electromagnetic Waves (a symposium), InterScience Publishers, Inc., N.Y., 1951, pp. 263-315.

13. L.B. Felsen, "Alternative Field Representations in Regions Bounded by Spheres, Cones and Planes," IRE Trans., Vol. AP-5, January 1957, pp. 109-121.

14. R.G. Kouyoumjian, P.H. Pathak, and Y.M. Hwang, "The Radiation from Slots in Truncated Dielectric Covered Surfaces," 1971 IEEE International Symposium on Antennas and Propagation Digest, pp. 93-96.

15. C.M. Angulo and W.S.C. Chang, "The Launching of Surface Waves by Parallel Plate Waveguide," IEEE Trans. on Antennas and Propagation, October 1959, p. 359.

16. C.P. Bates and R. Mittra, "A Factorization Procedure for Wiener-Hopf Kernels," Comm. to the IEEE Trans. on Antennas and Propagation, January 1969, pp. 102-103.

17. Y. M. Hwang. "Electromagnetic and Scalar Diffraction by a Right-Angled Wedge With a Uniform Surface Impedance." Tech. Rep. 3001-6 (Grant No. NGR 36-008-144), ElectroScience Lab., Ohio State Univ., Sept. 1973. (Available as NASA CR-2404, 1974.)

18. N. Amitay, V. Galindo, and C.P. Wu, Theory and Analysis of Phased Array Antennas, Wiley-Interscience publication, 1972.

19. L.W. Lechtreck, "Cumulative Coupling in Antenna Arrays," Proc. 1965 International Symposium, IEEE G-AP, pp. 144-149.

20. J.L. Allen, "On Surface Wave Coupling between Elements of Large Arrays," IEEE Transactions on Antennas and Propagation (communication), AP-13, pp. 638-639, July 1965.

21. R.E. Collin, and F.J. Zucker (editors), Antenna Theory, Part II, McGraw-Hill, 1969 (see Chapter 21).

22. E.C. Titchmarsh, Theory of Functions, (2nd ed.), New York, Oxford University Press, 1939.

23. B. Noble, Methods Based on the Wiener-Hopf Technique, Pergamon Press, Inc., New York, 1958.

☆ U.S. GOVERNMENT PRINTING OFFICE: 1974—739-160/121

NATIONAL AERONAUTICS AND SPACE ADMINISTRATION
WASHINGTON, D.C. 20546

OFFICIAL BUSINESS
PENALTY FOR PRIVATE USE $300

SPECIAL FOURTH-CLASS RATE BOOK

POSTAGE AND FEES PAID
NATIONAL AERONAUTICS AND SPACE ADMINISTRATION
451

U.S.MAIL

POSTMASTER: If Undeliverable (Section 158 Postal Manual) Do Not Return

"The aeronautical and space activities of the United States shall be conducted so as to contribute . . . to the expansion of human knowledge of phenomena in the atmosphere and space. The Administration shall provide for the widest practicable and appropriate dissemination of information concerning its activities and the results thereof."

—NATIONAL AERONAUTICS AND SPACE ACT OF 1958

NASA SCIENTIFIC AND TECHNICAL PUBLICATIONS

TECHNICAL REPORTS: Scientific and technical information considered important, complete, and a lasting contribution to existing knowledge.

TECHNICAL NOTES: Information less broad in scope but nevertheless of importance as a contribution to existing knowledge.

TECHNICAL MEMORANDUMS: Information receiving limited distribution because of preliminary data, security classification, or other reasons. Also includes conference proceedings with either limited or unlimited distribution.

CONTRACTOR REPORTS: Scientific and technical information generated under a NASA contract or grant and considered an important contribution to existing knowledge.

TECHNICAL TRANSLATIONS: Information published in a foreign language considered to merit NASA distribution in English.

SPECIAL PUBLICATIONS: Information derived from or of value to NASA activities. Publications include final reports of major projects, monographs, data compilations, handbooks, sourcebooks, and special bibliographies.

TECHNOLOGY UTILIZATION PUBLICATIONS: Information on technology used by NASA that may be of particular interest in commercial and other non-aerospace applications. Publications include Tech Briefs, Technology Utilization Reports and Technology Surveys.

Details on the availability of these publications may be obtained from:

SCIENTIFIC AND TECHNICAL INFORMATION OFFICE

NATIONAL AERONAUTICS AND SPACE ADMINISTRATION

Washington, D.C. 20546